Stratigraphic Framework, Paleoenvironments, and Indigenous Terraforming of Inshore Estuarine Subbasins in Tampa Bay, Florida, U.S.A.

Authors: Jackson, Kendal, Wang, Ping, Pluckhahn, Thomas J., Rogers, Jaime A., and Thompson, Victor D.

Source: Journal of Coastal Research, 39(5) : 779-815

Published By: Coastal Education and Research Foundation

URL: https://doi.org/10.2112/JCOASTRES-D-22-00128.1

Journal of Coastal Research	39	5	779–815	Charlotte, North Carolina	September 2023

Stratigraphic Framework, Paleoenvironments, and Indigenous Terraforming of Inshore Estuarine Subbasins in Tampa Bay, Florida, U.S.A.

Kendal Jackson[†]*, Ping Wang[‡], Thomas J. Pluckhahn[†], Jaime A. Rogers[†], and Victor D. Thompson[§]

[†]Department of Anthropology
University of South Florida
Tampa, Florida 33620, U.S.A.

[‡]School of Geosciences
University of South Florida
Tampa, Florida 33620, U.S.A.

[§]Department of Anthropology
University of Georgia
Athens, Georgia 30602, U.S.A.

www.JCRonline.org

ABSTRACT

Jackson, K.; Wang, P.; Pluckhahn, T.J.; Rogers, J.A., and Thompson, V.D., 2023. Stratigraphic framework, paleoenvironments, and Indigenous terraforming of inshore estuarine subbasins in Tampa Bay, Florida, U.S.A. *Journal of Coastal Research,* 39(5), 779–815. Charlotte (North Carolina), ISSN 0749-0208.

Tampa Bay is a karst-controlled estuary system on Florida's central peninsular Gulf of Mexico coast. Although previous work has reconstructed late-Pleistocene environments (*ca*. 20–11.5 kya) and early marine influence (*ca*. 8–5.5 kya) in deeper central portions of the bay, the estuarine development of the shallow inshore subbasins remains poorly understood. Across the late Holocene, Indigenous societies terraformed the coastal strand with large volumes of estuarine mollusk shell, and these anthropogenic landforms constitute coastal barriers that partially enclose marginal tidal bayous. This study integrates sediment coring and archaeological excavations to reconstruct the Holocene estuarine evolution of four inshore subbasins within Tampa Bay. This study synthesizes sedimentological, macrofossil, and archaeological data to describe and differentiate seven sedimentary facies and 18 subfacies representing weathered Miocene limestone at the base, overlain by late-Pleistocene freshwater wetland deposits, followed by Holocene estuarine sediments and late-Holocene shell-terraformed settlements. Four stratigraphic cross-sections and >100 radiocarbon assays are utilized to interpret the sequences of inshore estuary development, situate ancient shell-bearing Native settlements within a geologic and paleoenvironmental framework, and resolve elements of mid- and late-Holocene sea-level history.

ADDITIONAL INDEX WORDS: *Historical ecology, archaeology, depositional system, estuaries, sea-level rise.*

INTRODUCTION

Estuaries are semienclosed coastal water bodies where seawater and freshwater mix to support characteristic habitats and biota (Pritchard, 1967; Whitfield and Elliott, 2011). Geologically, estuaries are dynamic and short-lived features that form in drowned depressions along coastal margins, exhibiting geomorphologies and associated sedimentary facies formed by marine (tides and waves) and terrestrial (riverine) processes (Dalrymple, Zaitlin, and Boyd, 1992). As "transitional waters" (McLusky and Elliot, 2007), estuaries link continental and marine biomes and facilitate exchanges of nutrients, organic matter, biota, and sediments (Baird and Ulanowicz, 1993; Elliott and Whitfield, 2011). Extant estuaries have formed over the past 8000 years in response to reduced rates of sea-level rise during the middle to late Holocene (Cronin *et al*., 2007; Punwong, Selby, and Marchant, 2018; Tanabe, Nakashima, and Mizuno, 2022). Across subsequent millennia, human societies inhabiting transgressing estuarine zones developed coastal lifeways marked by population aggregation, sedentism, and sociopolitical stratification (Bailey and Milner, 2003; Gamble, 2017; Grier, 2014; Pluckhahn and Thompson, 2018; Riddick *et al*., 2022). During the late Holocene (*ca*. 3–0.5 kya), estuaries and adjacent coastal strands came to support cosmopolitan human populations that intensively managed coastal resources (Cáceres *et al*., 2018; Giaime *et al*., 2022; Kennett and Kennett, 2006; LaViolette and Fleisher, 2009). Subsequent centuries of Euro-colonial mercantile expansion and industrialization proceeded through the dismantling of Indigenous management systems, the commodification and overexploitation of resources, pollution, and the physical alteration of estuarine ecosystems (Brush, 2009; Jackson *et al*., 2001; Kirby, 2004; Lotze *et al*., 2006; Thompson *et al*., 2020). Compounding these stresses, the unfolding impacts and imminent threats of global warming and sea-level rise will significantly affect estuaries—which support most of the world's major cities and ports (Pinto *et al*., 2010; Zedler and Kercher, 2005). Given this context, and the pressing need to maintain and restore estuarine ecosystems worldwide, it is imperative to improve and integrate the geological, ecological, and cultural histories of estuaries.

For this study, an interdisciplinary research team collected 65 sediment cores and conducted 38 archaeological excavations with the goal of developing a holistic understanding of Holocene estuary evolution in Tampa Bay—a karst-controlled, sediment-starved estuarine system on the central peninsular Gulf Coast of Florida. The study is focused on the history of Tampa Bay's inshore subbasins, including the construction and modification (*i.e*. terraforming, *sensu* Grier, Angelbeck, and McLay, 2017) of coastal landforms by ancestral Native American societies. Specific questions addressed include (1) what major sedimentary facies are preserved within Tampa

DOI: 10.2112/JCOASTRES-D-22-00128.1 received 22 December 2022; accepted in revision 25 March 2023; corrected proofs received 15 May 2023; published pre-print online 5 June 2023.
*Corresponding author: kendalj@usf.edu

Bay's inshore subbasins? (2) What can these sedimentary records and their chronostratigraphic organization tell us about Holocene marine transgression and the development of shallow inshore estuarine systems? and (3) How are ancient terraformed Indigenous settlements situated within the geologic and paleoenvironmental framework?

Study Area

Tampa Bay is a large (1000 km^2), shallow (4 m average depth) microtidal estuary system on Florida's central peninsular Gulf Coast (Figure 1). The region lies at the center of the Florida carbonate platform (Scott, 2011) and is situated near the northern extent of the West Central Barrier Island Chain—a mixed-energy barrier island–inlet system that extends from the Anclote River to Cape Romano (Davis, 1994, 2011; Hine *et al*., 2003; Wang and Beck, 2022). The karst-controlled paleogeomorphology and sedimentary characteristics of Tampa Bay, and Charlotte Harbor to the south, are unlike incised river valley estuaries (Dalrymple, Zaitlin, and Boyd, 1992; Li *et al*., 2002). Building on decades of previous work (Brooks and Doyle, 1998; Duncan *et al*., 2003; Stahl, 1970; Suthard, 2005; Willis, 1984), Hine *et al*. (2009) mapped the early-Miocene seismic basement beneath Middle and Lower Tampa Bay, demonstrating that the basin was formed by deep-seated karst dissolution during Neogene sea-level oscillations—producing a large complex of nested sinkholes restricted by domes, pinnacles, or ridges of more durable limestone.

The karst influence on Tampa Bay's geomorphology has created a series of complex sedimentary subbasins (Brooks, 2011). Sedimentary facies within Tampa Bay representing terrestrial, transitional, and estuarine sediments deposited since the Last Glacial Maximum (LGM) have been described by Brooks *et al*. (2004), Larson, Brooks, and Edgar (2004), and Larson *et al*. (2006). Studies of the bay's extant and historical tidal wetland systems (*e.g*., mangrove swamp, marsh, salt prairie, seagrass meadow, oyster reef) have described and differentiated their physical and biological characteristics (Gerlach *et al*., 2017; Hesterberg, Jackson, and Bell, 2022; Jackson, Brooks, and Larson, 2021; Radabaugh *et al*., 2018, 2021). Sedimentary facies of the inner continental shelf and the barrier island–lagoon systems seaward of Tampa Bay have been described by Brooks *et al*. (2003) and Davis *et al*. (2003), respectively. Sedimentological work by Brooks and Doyle (1998) and others (Brooks *et al*., 1991, Cronin *et al*., 2007; Doyle *et al*., 1989) revealed that karst depressions in Middle Tampa Bay, lower Hillsborough Bay, and western Old Tampa Bay (Figure 1) contain stratified siliciclastic and organic sediments that accumulated from the LGM to the present. Paleoecological work on sediment cores from bathymetric depressions in Middle Tampa Bay (Willard *et al*., 2007) and Lower Hillsborough Bay (van Soelen *et al*., 2010) has reconstructed major environmental transitions from *ca*. 20–11.5 kya and *ca*. 8.2–5.4 kya, respectively. From the LGM through the Younger Dryas (*ca*. 12.3–11.5 kya), a deep karst basin underlying Middle Tampa Bay contained a large freshwater paleolake system ("Paleolake Edgar") likely flanked by freshwater wetland mosaics. Marine influence becomes apparent in Lower Hillsborough Bay cores between 7 and 6 kya. Sedimentary, biomarker, and microfossil data suggest that estuarine conditions were established by 5.5 kya, forming "a series of restricted lagoons, related to karst depressions, with limited water circulation" (van Soelen *et al*., 2010:222). Erosion of early- and middle-Holocene units from the Middle Tampa Bay sediment record and coarsely resolved geochronology in the lower Hillsborough Bay record after *ca*. 5.5 kya leave much of Tampa Bay's Holocene estuarine development unresolved. This is particularly true of the bay's numerous inshore subbasins, which, until now, have not produced well-resolved sedimentary records.

Although geologic and paleoecologic work on the Florida peninsula has historically excluded Indigenous peoples from reconstructions of late-Pleistocene and Holocene environmental history, recent research by geoarchaeologists (*e.g*., McFadden, 2016) and multidisciplinary teams (*e.g*., Thompson *et al*., 2016) has begun to investigate ancestral Native societies as geological agents. Indigenous peoples were present (and likely widely distributed) on the Florida peninsula by *ca*. 14.5 kya (Halligan, 2022; Halligan *et al*., 2016), and research from the greater Southeastern Coastal Plain indicates that terminal-Pleistocene human populations altered fire regimes and vegetation communities (Delcourt and Delcourt, 2004). The Tampa Bay watershed has yielded relatively high concentrations of Pleistocene-age projectile points (Daniel and Wisenbaker, 1987; Faught and Pevny, 2019; Goodyear *et al*., 1983). Given the persistence of freshwater wetlands in Tampa Bay's karst depressions across arid climate intervals (*e.g*., the Older Dryas, Inter-Allerød, and Younger Dryas) when the encompassing peninsula was dominated by xeric scrubby savannah (Grimm *et al*., 2006; Watts, 1980; Willard *et al*., 2007), pre-estuarine Tampa Bay may have been an inland oasis for human groups (Purdy and Hine, 2021; Thulman, 2009).

By the mid-Holocene, peninsular Gulf Coast peoples had developed maritime lifeways and began constructing large rings, mounds, and ridges from mollusk shell, vertebrate faunal remains, discarded artifacts, and quartz sand (Russo and Quitmyer, 2008; Saunders and Russo, 2011). Late-Holocene Native societies intensified these practices, and by *ca*. 1000 calibrated (cal) years before present (YBP) the peninsula's western coastline was dotted with shell-bearing sites, some measuring more than 0.5 km^2 in area and raised more than 10 m above surrounding terrains (Austin, Mitchem, and Weisman, 2014; Pluckhahn, Jackson, and Rogers, 2021; Sassaman *et al*., 2017; Schwadron, 2017; Thompson *et al*., 2018). In Tampa Bay, as elsewhere along Florida's Gulf and Atlantic coasts, shell-terraformed Native settlements are situated conspicuously on the seascape, commonly on prominent points or along major tidal creeks, and sometimes forming islands or peninsulas that partially enclose tidal bayous (Pluckhahn, Jackson, and Rogers, 2022).

METHODS

Four study areas were selected, representing major inshore subbasins of Tampa Bay that were not heavily altered by 20^{th}-century dredge-and-fill operations; these include Upper Tampa Bay (UTB), Weedon Island (WI), Cockroach Bay (CRB), and Bishop Harbor (BH) (Figure 1). In each study area, shallow estuarine basins and tidal wetlands are partially blocked by

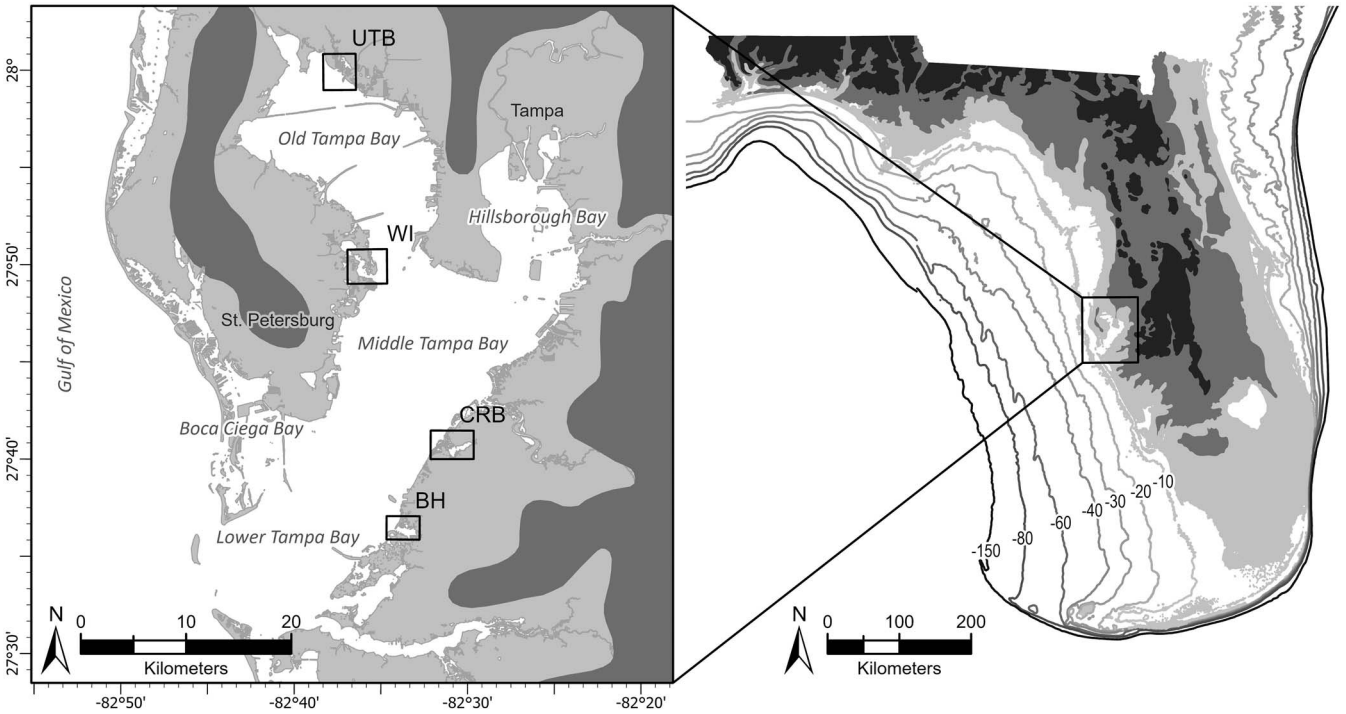

Figure 1. Right panel: Map of Florida with bathymetric contours on the continental shelf in meters and relic marine terraces displayed in greyscale. Light grey regions are less than +10.5 m and include the Silver Bluff and Palmico terraces; medium grey regions are greater than +10.5 m and less than +30.5 m and include the Talbot, Penholoway, and Wicomico terraces; dark grey regions include upland terraces above +30.5 m. Left panel: Map of Tampa Bay estuary depicting the four inshore subbasins sampled for this study: UTB = Upper Tampa Bay, WI = Weedon Island, CRB = Cockroach Bay, BH = Bishop Harbor.

seaward islands or peninsulas associated with Indigenous shell-bearing settlements.

Field Data Collection

Field sampling involved collecting sediment cores and excavating small archaeological test units (measuring up to 1×1 m in plan). Most sampling was oriented along cross-shore transects, with additional testing conforming to the morphologies of archaeological features (Figures 2–5; Supplemental Data).

A total of 23 vibration cores were collected at shallow subtidal locations along cross-shore transects. Vibracoring protocol followed standard methods (Lanesky *et al*., 1979) using 7.6-cm-diameter aluminum pipes. Vibracore depth ranged from 0.5 m to 7.3 m, with most cores measuring longer than 4 m. A total of 38 percussion cores were collected using 7.6-cm-diameter aluminum pipes at inter- and supratidal locations along the cross-shore transects and opportunistically from archaeological features. Penetration depths for these cores ranged from 1.2 m to 2.0 m. A total of four multisection percussion cores were collected from shell-platform mounds at Cockroach Key (8HI2, CRB study area) and Harbor Key (8MA13, BH study area) using a JMC subsurface probe and 3-cm-diameter core tubes, reaching 4.5 m in depth.

A total of 38 test units were excavated across seven shell-bearing archaeological sites. Thirty-six of these units measured 0.5×0.5 m in plan and were excavated to tidal water level (typically *ca*. 1 m in depth). Two larger test units, measuring 1×1 m in plan, were excavated at sites within the UTB study area (8HI6698 and 8HI996). All test units were excavated in levels measuring $\leq$10 cm within observed strata. When possible, test units were extended by percussion core or auger probe to determine stratigraphy and collect samples below the limit of open excavation. Excavated sediments were processed through 3.2-mm mesh in the field. In addition to all vertebrate faunal remains and artifacts (*e.g*., ceramics and tools of animal bone, stone, and shell), field crews collected robust samples of mollusk shell, enabling precise estimations of minimum number of individuals (MNI) for mollusk taxa. Bulk sediment samples were collected from each of the observed shellwork strata within test units for physical sedimentological analyses.

Laboratory Analyses

Sediment samples were analyzed to produce grain size distribution data. Samples were dispersed into a sodium hexametaphosphate solution (50 g/L). After a 12-hour soaking period, samples were wet-sieved through 63-μm (4 phi) mesh, separating coarse (sand and gravel) and fine (mud) fractions. Coarse fractions were dried and analyzed using standard sieves to yield percent composition values for sand-sized particles at 0.25-phi intervals. Mean grain size and sorting statistics were calculated by moment method following Balsillie (1995). Total organic matter (TOM) and carbonate content

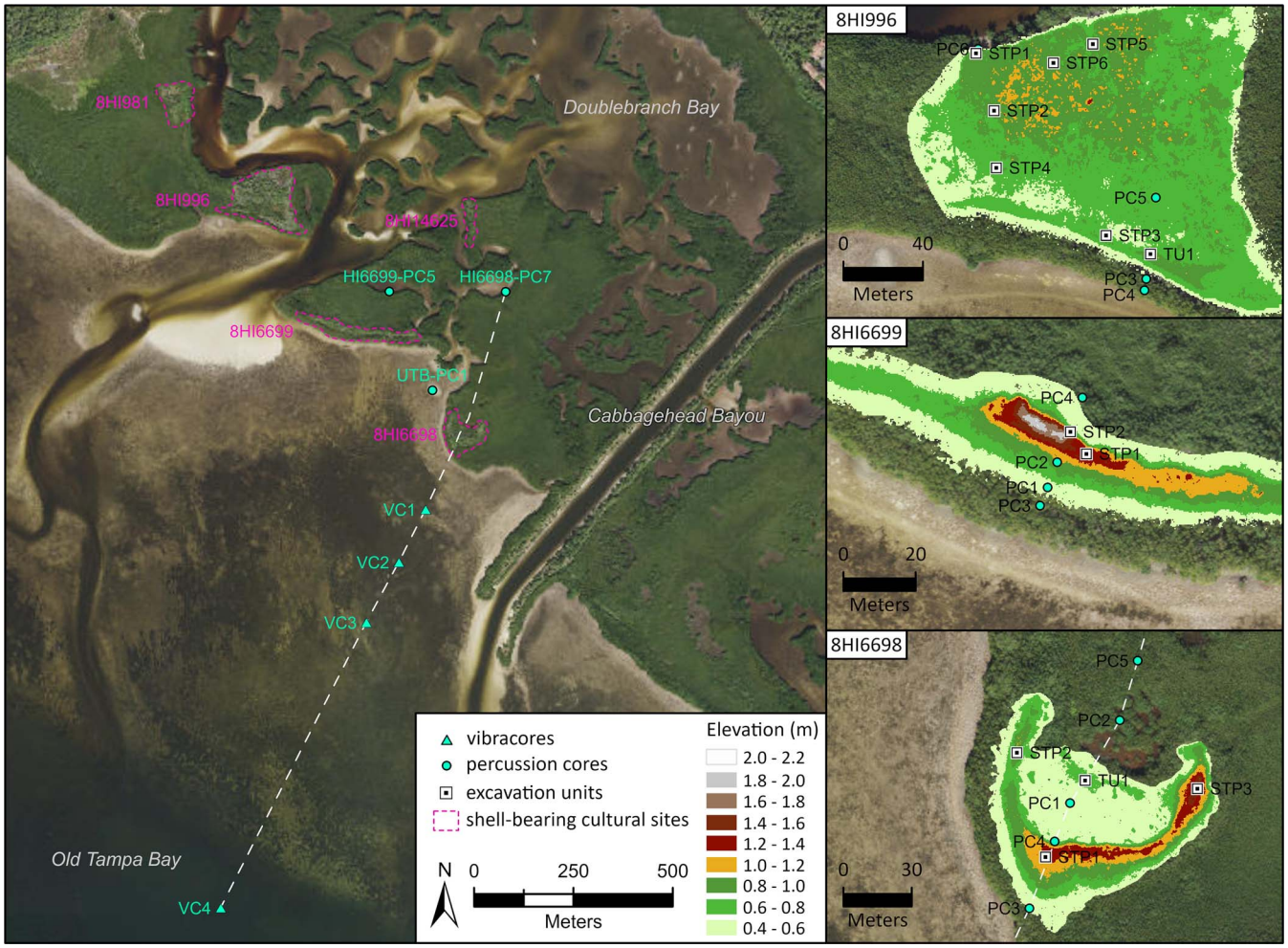

Figure 2. Left panel: Orthoimagery of Upper Tampa Bay (UTB) study area displaying vibracore and percussion core locations. Dashed white line indicates the stratigraphic cross-section depicted in Figure 7. Right panel: Maps of archaeological sampling across UTB archaeological sites (8HI996, 8HI6699, and 8HI6698) atop light detection and ranging (LIDAR)-derived digital elevation models (*ca*. 2019).

($CaCO_3$) were derived by sequential loss on ignition on 1.5-cm^3 sample volumes following established methods (Dean, 1974).

Analyses of archaeological mollusk shell followed established protocols (Reitz and Wing, 2008) and identified all collected shell (>3.2 mm) to the lowest possible taxonomy. Intact and fragmentary shells were analyzed to estimate MNI for each taxon within an assemblage on the basis of the identification of nonrepeating shell features (Mason, Peterson, and Tiffany, 1998). MNI data were utilized to calculate mollusk taxonomic diversity using the Shannon–Weaver index (*i.e*. Shannon's *H*) (Shannon and Weaver, 1949). Equability of mollusk assemblages was calculated using the Sheldon index (Sheldon, 1969). Macrofossil analyses of stratigraphic sediment samples from vibracores focused on sediment fractions >500 μm and produced presence–absence and qualitative data for mollusk and vertebrate inclusions. Finer sediment fractions from these samples (125–500 μm) were scanned for foraminifera under low-power magnification.

A total of 130 plant macrofossil and organic sediment samples were analyzed at the Center for Applied Isotope Studies at the University of Georgia to produce accelerator mass spectrometry (AMS) ^{14}C assays. Raw ^{14}C dates were calibrated in OxCal version 4.4. (Bronk Ramsey, 2009) using IntCal20 to derive probability distributions for calendar ages (Reimer *et al*., 2020).

RESULTS

This interdisciplinary work produced large sedimentary and archaeological data sets that extend from the terminal Pleistocene to the present and represent a substantial spatial extent of Tampa Bay's inshore zone. These data enable the description and differentiation of sedimentary facies, the reconstruction of Holocene inshore estuarine flooding sequences, and the chronostratigraphic contextualization of Indigenous shell mound sites. Detailed results of radiocarbon analyses are

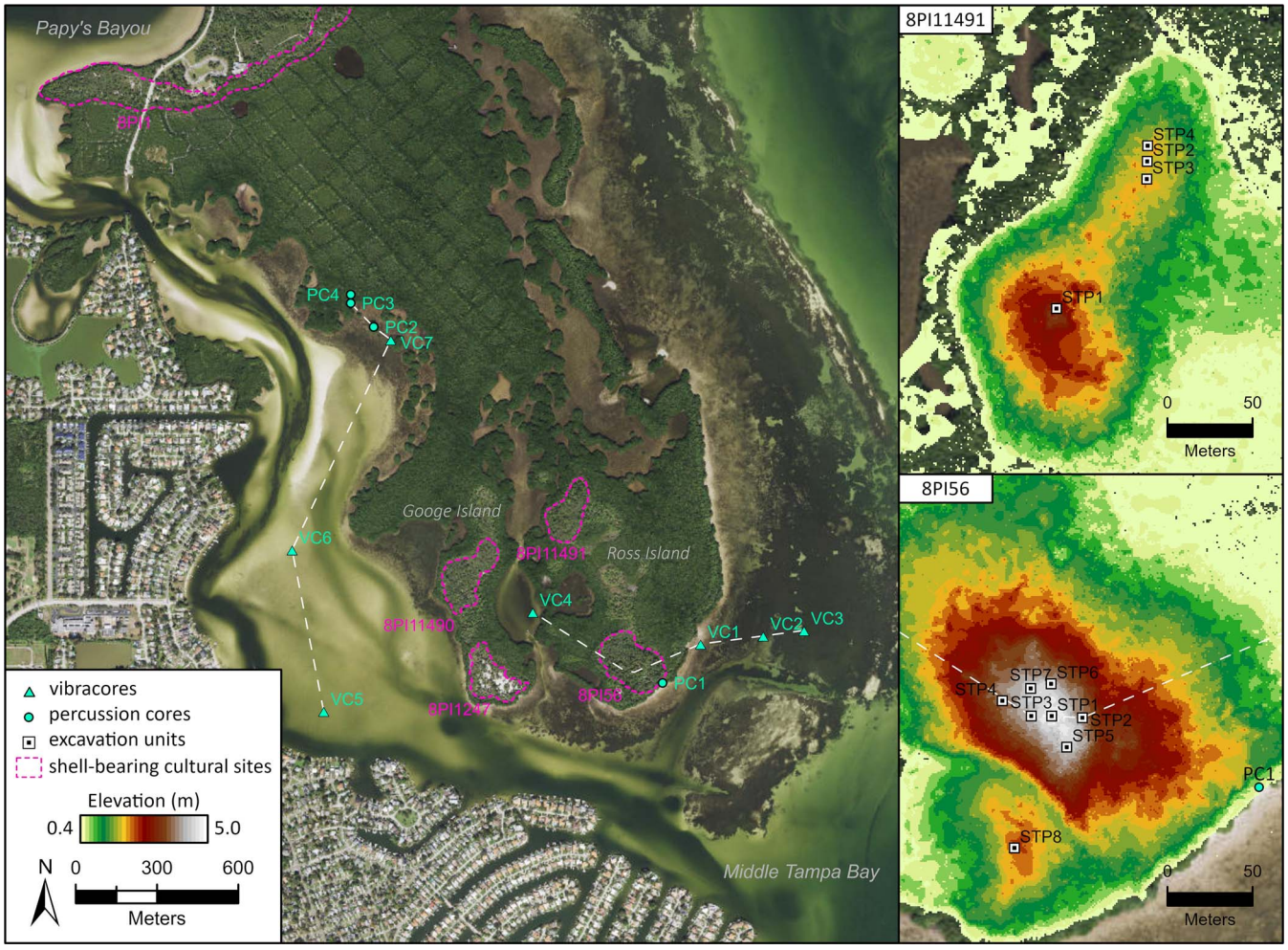

Figure 3. Left panel: Orthoimagery of Weedon Island (WI) study area displaying vibracore and percussion core locations. Dashed white line indicates the stratigraphic cross-sections depicted in Figure 8 (seaward) and in Supplementary Figure 4 (landward). Right panel: Maps of archaeological sampling of WI archaeological sites (8PI56 and 8PI11491) atop light detection and ranging (LIDAR)-derived digital elevation models (*ca*. 2019).

provided in Appendix Table 4. Reported elevation values are corrected to NAVD88.

Sedimentary Facies

Physical–sedimentological, macrofossil, archaeological, and chronometric data sets were synthesized to differentiate seven sedimentary facies and 18 subfacies, described below that represent depositional environments and ancient cultural features preserved within Tampa Bay's inshore basins (Figure 6; Appendix Tables 1–3; Supplementary Data).

Sedimentary Facies 1: Weathered Miocene Limestones (Hawthorn Group)

Weathered limestones were encountered at the base of cores from UTB, CRB, and BH. Karst weathering is apparent where limestone or limestone residuum was encountered. This facies represents the weathered surface of the rock unit upon which the unconsolidated strata were developed.

Blue-Green Clay Residuum Subfacies. This subfacies was encountered at UTB and BH, where it frequently constituted vibracore refusal (UTB-VC2, VC3, VC4, BH-VC3, and VC6). Upper contacts were encountered from −3 to −6 m elevation. Maximum recovery was approximately 1 m, but maximum thickness is unknown. Sediments are dense grey-blue to greenish-blue mud (16–73%) with no discernable macrofossils; upper portions of the unit tend to be sandier with lenses of yellowish oxidation (Figure 6a). This subfacies was described by Davis *et al*. (2003) and Brooks *et al*. (2003) beneath the inner shelf and barrier island systems near the mouth of Tampa Bay, where Sr isotope dating indicated a Miocene age.

Phosphatic Limestone Residuum Subfacies. This subfacies was encountered at the base of vibracores in CRB (CRB-VC1, VC2, VC3, VC5, and VC6) and BH (BH-VC1, VC3, VC4, VC5, and VC6), where it invariably constituted refusal. The upper surface is uneven, typically occurring between −3.5 and −5.5 m

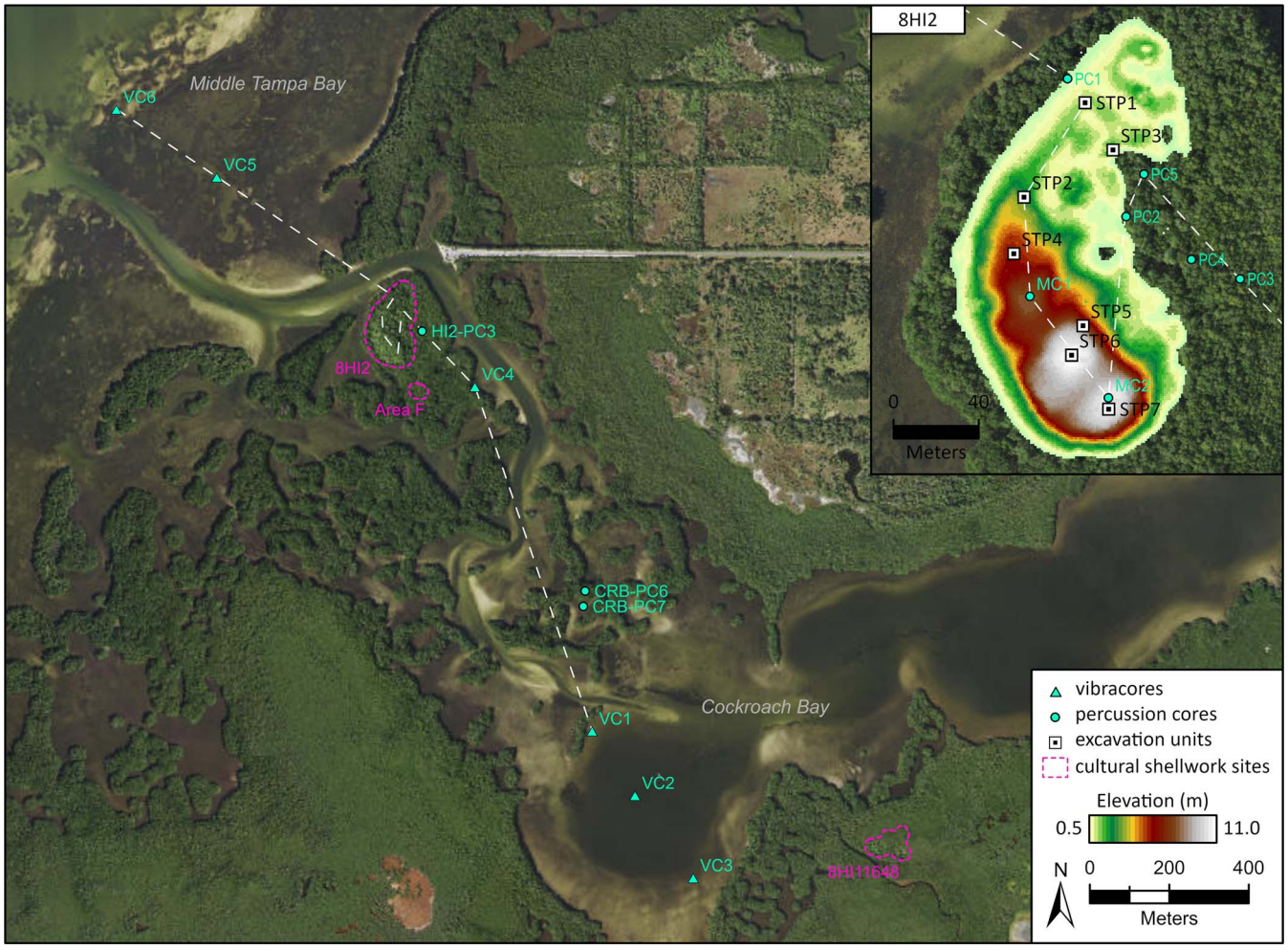

Figure 4. Left panel: Orthoimagery of Cockroach Bay (CRB) study area displaying vibracore and percussion core locations. Dashed white line indicates the stratigraphic cross-section depicted in Figure 9. Upper-right panel: Map of archaeological sampling at Cockroach Key (8HI2) with light detection and ranging (LIDAR)-derived digital elevation model (*ca*. 2019).

elevation. However, high points are common, rising to −0.7 m elevation beneath Cockroach Key (8HI2-PC5) and between −1 and −2 m elevation in open areas of Cockroach Bay (CRB-VC1, VC2, VC3). Maximum recovery was 1.1 m, but thickness is unknown. Sediments are white to grey lime-concreted sand with appreciable limestone and phosphate gravel (7–54%) and low organic content (<4%) (Figure 6b). Phosphatic vertebrate macrofossils are common.

Sedimentary Facies 2: Muddy Sand with Abundant Shell Debris

This facies was encountered at BH (BH-VC4, VC5, and VC6), where it overlies weathered Miocene limestone and underlies the Holocene estuarine sequence. Sediments are white to grey with whole and fragmentary mollusk-shell gravel (33–61%) in a matrix of carbonate mud (10–17%) and quartz sand (29–50%) (Figure 6c). The upper surface is situated between −2 and −2.5 m elevation, and thickness ranges from 1.5 to 2 m. Brooks *et al*. (2003) describe similar sediments below the inner shelf offshore of Tampa Bay, where they contain whole, articulated *Chione cancellata* shells, indicating a shallow marine or lagoonal environment dated by Sr isotopes to the mid-Pleistocene (*ca*. 1 mya). The shelly muddy sand subfacies encountered at BH also contains whole, articulated mollusk shells, but they belong to estuarine taxa (*Crassostrea virginica*, *Argopecten irradians*, and *Balanus* sp.).

Sedimentary Facies 3: Fine Sand

Fine-sand facies overlie weathered Miocene limestone and make up most of the Quaternary sequence at UTB and WI. Additionally, they compose much of the middle- to late-Holocene estuarine and terrestrial deposits across all study areas.

Organic Muddy-Sand (Pleistocene) Subfacies. Organic muddy-sand subfacies associated with terminal Pleistocene environments were encountered at UTB, WI, and CRB. These

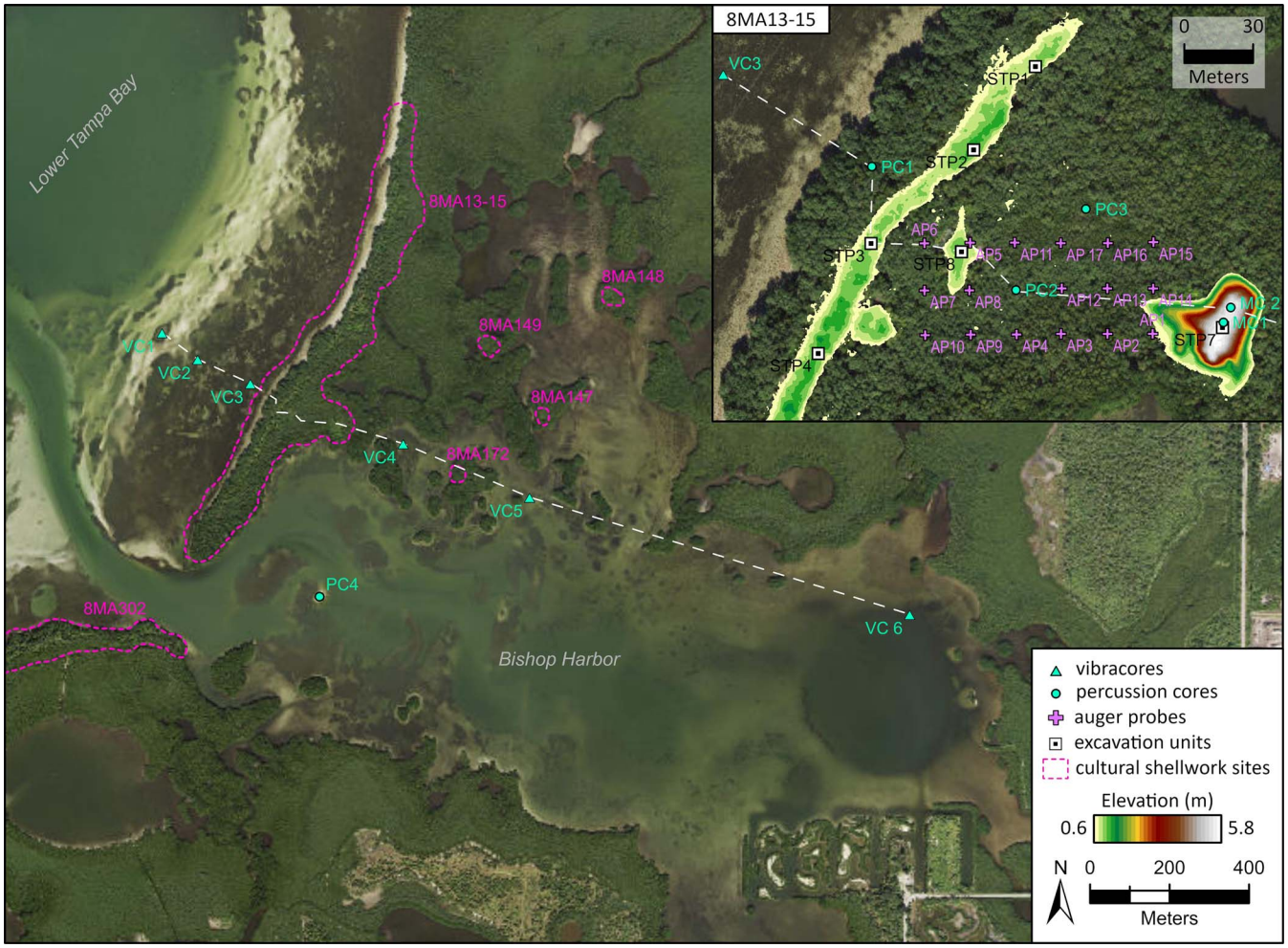

Figure 5. Left panel: Orthoimagery of Bishop Harbor (BH) study area displaying vibracore and percussion core locations. Dashed white line indicates the stratigraphic cross-section depicted in Figure 10. Upper-right panel: Map of archaeological sampling at Harbor Key (8MA13-15) with light detection and ranging (LIDAR)-derived digital elevation model (*ca*. 2019).

sediments are brown to black sand with variable organic mud content (6–53%) and with peatlike, woody, or herbaceous inclusions (Figure 6d). This subfacies typically overlies weathered Miocene limestone with a sharp contact and may be interbedded with clean aeolian sand deposits (brownish fine-sand subfacies). Deposits are less than 0.5-m thick, typically 0.2–0.3 m, but occasionally thinner where they are interbedded with clean sand lenses. Four AMS radiocarbon assays on deposits from UTB (UTB-VC3 and VC4) and CRB (CRB-VC4 and VC5) yielded late-Pleistocene ages. This subfacies represents freshwater wetland deposits coeval and ecologically linked to the lacustrine–freshwater wetland systems documented within Middle Tampa Bay during the LGM (Willard *et al*., 2007).

Brownish Fine-Sand Subfacies. This well-sorted subfacies was encountered throughout UTB and WI, and more limitedly at CRB. Its color is yellowish brown to white. White and brownish layers vary in thickness and are often interbedded (Figure 6e). This subfacies typically occurs in thick deposits (up to 6 m at WI) and upper surfaces occur from the modern supratidal zone to −5.5-m elevation. At UTB and WI this subfacies represents relic or reworked dune features. In basal deposits, the fine-sand packages are interbedded with Pleistocene-age wetland deposits, where they likely represent intervals of climatic aridity and aeolian transport. In terrestrial contexts at WI and UTB, this subfacies constitutes the parent material for modern coastal hammock soils. Middle- to late-Holocene Indigenous occupation of relic dune features at UTB and WI is evidenced by the recovery of flaked chert and silicified coral tools and tool-making debris from these deposits (Draskovich, 2021).

Muddy Fine-Sand Subfacies. This subfacies was encountered at UTB and WI, where it overlies Pleistocene wetland beds and underlies mid- to late-Holocene tidal wetland deposits. Sediments are massive or finely laminated; color is grey to gley-blue,

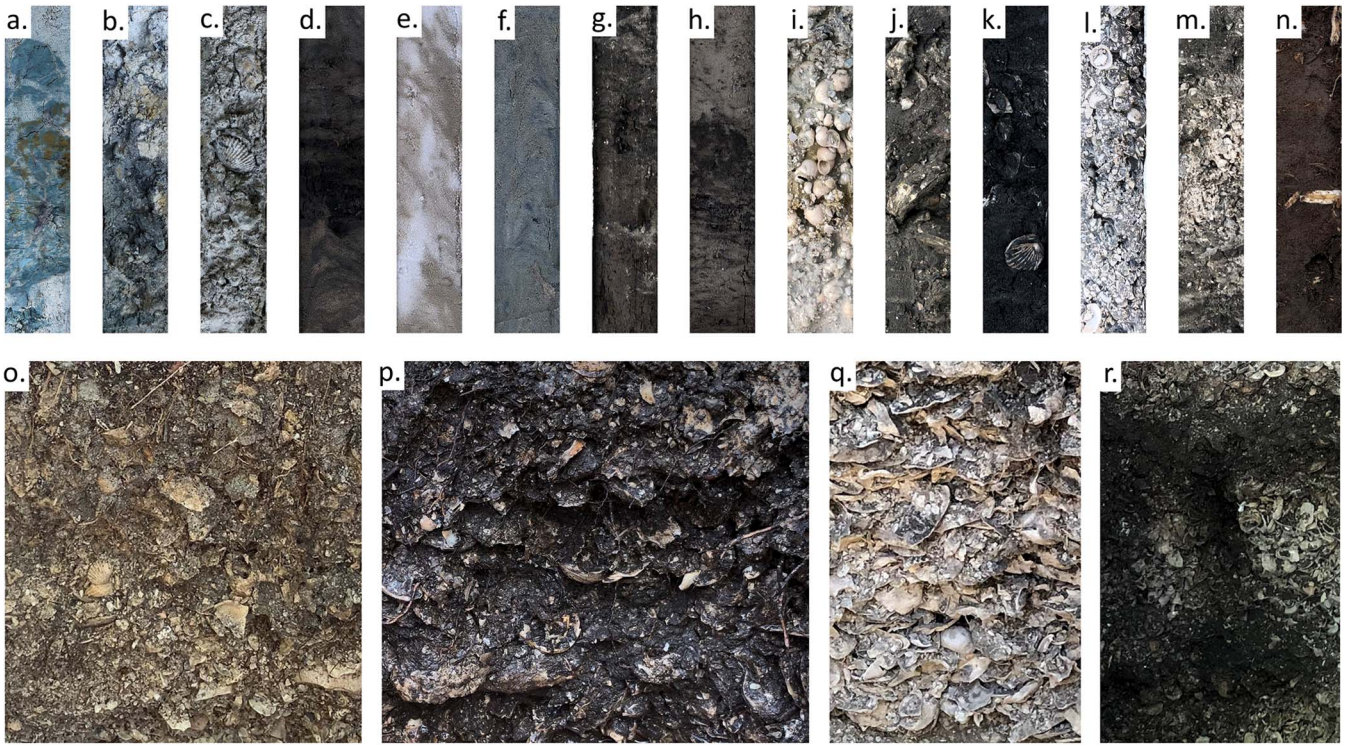

Figure 6. Photographs of exemplary sedimentary units representing each subfacies identified across inshore study areas in Tampa Bay: (a) blue-green clay residuum, (b) phosphatic limestone residuum, (c) muddy sand with abundant shell debris, (d) organic muddy sand (Pleistocene), (e) brownish fine sand, (f) muddy fine sand, (g) organic muddy sand (Holocene), (h) mud-laminated sand, (i) freshwater gastropod bed, (j) oyster reef, (k) cardite beds, (l) fossil-shell gravel, (m) crushed shell lenses, (n) mangrove peat, (o) reworked cultural shell, (p) shell midden, (q) unconsolidated clean shell, (r) fire/habitation features.

or sometimes brownish. Mud content is >10% and gravel content is <4% (Figure 6f). Bed thickness varies from 1 to 2 m, with elevations ranging from −2 to −5 m. The stratigraphic position of muddy fine-sand deposits at UTB suggests an association with the deglacial period and reworking of fine, well-sorted quartz sand within fluvial or lacustrine environments (Bertran *et al*., 2011; Sizov *et al*., 2020).

Organic Muddy-Sand (Holocene) Subfacies. Organic muddy-sand subfacies dating to the mid- and late Holocene were encountered in all subbasins, typically underlying bioturbated mud-laminated sand or mangrove peat. Sediments are sandy (70–96%) and brown to black in color, with peatlike herbaceous inclusions (Figure 6g). These units range from 0.5- to 1.5-m thick and are situated between 0 and −4 m elevation. Tidal lamina and estuarine mollusk-shell fragments are common, indicating tidal marsh or seagrass meadow habitats. Radiocarbon assays show that these beds began accumulating between *ca*. 5.3 and 3.5 kya. Many Holocene organic muddy-sand beds were truncated by mud-laminated sand, oyster reef, or cardite beds *ca*. 1.8 kya. Mean accumulation rates range from 0.2 to 0.4 mm/y, approximating the rate of late-Holocene sea-level rise and implying that these wetlands "kept pace" with rising sea levels for 2–3 millennia before they were transgressed. These deposits also characterize recent historical and extant tidal marsh environments at UTB, WI, and CRB. Recent/surficial tidal marsh units overlie aeolian sand beds at UTB and WI and overlie weathered limestone at CRB. In both cases, basal samples from these marsh units (*ca*. −0.5 to −0.7 m elevation) were radiocarbon dated to the late first millennium CE, *ca*. 1200–600 cal YBP.

Mud-Laminated Sand Subfacies. Bioturbated medium-fine sand beds with organic muddy lamina are ubiquitous across inshore subtidal zones of Tampa Bay. Sediment color is white to light grey with brownish grey-to-black muddy lamina (Figure 6h). Bioturbation by seagrasses and infauna is common, as are macrobotanical and mollusk-shell inclusions. Mollusk shell is found whole and fragmented, and mollusk assemblages exhibit high taxonomic richness relative to other facies. Analysis of mollusk-shell inclusions revealed a spatial trend of increasing taxonomic richness with proximity to the open Gulf (Appendix Table 2). Unit thickness typically measures <1 m, and deposits occur from *ca*. 0 to −2 m elevation. This subfacies commonly overlies marshy Holocene organic muddy sand deposits but may also directly overlie weathered Miocene limestone (CRB-VC1, VC2, and VC3), oyster reef (BH-VC4 and VC5), fossil-shell gravel (CRB-VC4), or reworked cultural shell (BH-VC3). Interbedding with shell hash is common, representing periodic high-energy events. Geochronology is constrained by dates on underlying units, indicating late-Holocene formation and continued accretion to the present.

Sedimentary Facies 4: *In Situ* Shell Gravels (Mollusk Beds)

In situ shell gravels were encountered within all subbasins. They are characterized by abundant whole to mostly whole mollusk shells. Where bivalves are dominant, articulated valves are present. Taxonomic richness is low relative to mud-laminated sand, *ex situ* shell gravels, and shell-bearing cultural deposits.

Freshwater Gastropod Bed Subfacies. Concentrations of freshwater gastropods were encountered at CRB (CRB-VC6), where a dense bed of *Viviparus georgianus* and *Planorbella scalaris* in calcareous muddy-sand matrix are situated, with a sharp contact, atop phosphatic limestone residuum along the seaward edge of the tidal flat (Figure 6i). The deposit is truncated by overlying estuarine sediments dated *ca*. 3 kya. Notably, *V. georgianus* and *P. scalaris* are not tolerant of salinity, and generally indicate low-energy riverine, slough, or lacustrine conditions with submerged aquatic vegetation. The observed unit is 0.7-m thick and sits between −2.6 and −3.3 m elevation. The geochronological sequence and elevation suggest a terminal-Pleistocene to mid-Holocene age.

Oyster Reef Subfacies. Living and buried oyster reefs were encountered within all subbasins. Sediments are light grey to dark grey in color, with dense clusters of whole and fragmented *C. virginica* shells (many articulated) in an organic muddy-sand matrix (Figure 6j). Commensal mollusk taxa (*Urosalpinx perrugata*, *Crepidula* sp., and *Geukensia* sp.) are typically present. Inshore oyster reef deposits are relatively thin, measuring between 0.2- and 1.5-m thick. They are found between *ca*. 0 and −2 m elevation. Oyster reefs typically overlie Holocene organic muddy sand beds and appear to establish directly atop thin (0.1- to 0.2-m thick) deposits of clean or shelly medium-fine sand (*i.e*. shoals, tempesites, *etc*.). Relic oyster reefs indicate estuarine conditions with tidal flow, freshwater input, and protection from high wind waves. Oyster reef deposits sampled here are late-Holocene in age, with basal AMS radiocarbon ages ranging from 2.2 kya to the mid-19th century CE. Buried oyster reefs are overlain by mud-laminated sand or recent mangrove peat deposits.

Cardite Beds Subfacies. Sandy beds with concentrations of whole, articulated *Cardites floridana* shells were encountered at CRB and BH. Sediment matrices are typically organic muddy sands, with variable shell-gravel content (4–31%) (Figure 6k). *Cardites floridana* is an indicator of seagrass meadow habitats, and other seagrass-associated mollusk taxa (*e.g*., *Cerithium* sp., *Prunum apicinum*, *A. irradians*) are represented. Deposits range in thickness from 0.2 to 0.5 m. At BH, they are situated between −3 and −4 m elevation and associated with mid-Holocene tidal wetland deposits. At CRB, cardite beds sit between −1.3 and −2 m elevation, dating *ca*. 1 kya and underlying oyster reef deposits. Notably, oyster valves found within reef deposits overlying cardite beds (CRB-PC6 and PC7) and within Native shell mound deposits at Cockroach Key site (8HI2) are sometimes found cemented to *Cardites floridana* shells, indicating that cardite beds provide(d) substrate for intertidal oyster reef establishment.

Sedimentary Facies 5: *Ex Situ* Shell Gravels

Deposits of poorly sorted shelly sand were encountered in all subbasins. Mollusk-shell assemblages are typically fragmentary and lack articulated bivalves but exhibit relatively high taxonomic richness. Clean fine sand matrix is most common. These deposits indicate high-energy conditions capable of transporting or winnowing shelly sediments.

Fossil-Shell Gravel Subfacies. Sandy gravels composed of whole and fragmentary fossil mollusk shell were encountered at WI and CRB. Sediments are white to light grey and composed of 14–39% shell gravel in fine sand matrix, with <5% organic matter (Figure 6l). Shells appear patinated or polished, and articulated bivalves are absent. The mollusk assemblage is dominated by the nearshore marine bivalve *Chione cancellata*, and includes other common nearshore marine taxa (*e.g*., *Macrocallista nimbosa, Noetia ponderosa*); evidence of drilling by predatory gastropods is common. Unit thickness ranges from 0.5 to 2 m, and beds are situated from −1.2 to −3.4 m elevation. These deposits are composed of reworked Pleistocene shell beds and were likely produced in association with the formation and migration of fluvial channels.

Crushed-Shell Lenses Subfacies. Thin (0.05- to 0.2-m thickness) deposits of highly fragmented shell debris occur within mud-laminated sand strata across all subbasins. Sediments are light to dark grey, poorly sorted and composed of fragmented mollusk shell in medium-coarse sand matrix (Figure 6m). Mollusk assemblages exhibit high taxonomic richness and include both marine and estuarine taxa. *Ammonia* sp. foraminifera are abundant. These deposits represent winnowing or transport of shell fragments during high-energy events (*i.e*. storms) affecting inshore tidal flats. The lenses occur between −1 and −3 m elevation. Radiocarbon assays on mud lamina directly overlying crushed-shell lenses at UTB and CRB yielded dates *ca*. 700 cal YBP.

Sedimentary Facies 6: Mangrove Peat

Mangrove forest peats were encountered across all subbasins where they occur as surficial beds throughout the intertidal zone. Recent work shows that mangrove forest was restricted to small islands and shoreline fringe before industrial-scale anthropogenic shoreline modification during the late 20th century (Jackson, Brooks, and Larson, 2021; Raabe, Roy, and McIvor, 2012). Unit thickness is variable (0.1–0.8 m) and deposit elevations ranged from 0.5 to −0.5 m. Sediments are sandy organic peats with variable mud (10–67%), sand (33–85%), and organic (10–68%) contents. Preserved wood, root, and leaf tissues from regional mangrove taxa (*i.e. Rhizophora mangle, Avicennia germinans, Laguncularia racemosa*) are abundant, and shells of commensal mollusks (*Littorina irrorata, Cerithium* sp., *Crassostrea virginica*) are common (Figure 6n). Mangrove peat beds encountered here are of relatively recent age, and overlie Holocene organic muddy sand, oyster reef, or shell-bearing cultural facies. Radiocarbon assays on basal mangrove peat deposits that accumulated atop cultural shell deposits at Harbor Key site (8MA15) (*ca*. −0.5 m elevation) yielded dates between *ca*. 300 and 500 cal YBP.

Sedimentary Facies 7: Shell-Bearing Cultural Deposits

Ancestral Native American peoples constructed durable coastal landforms from mollusk shell, quartz sand, organic sediments, and discarded artifacts that make up the seaward-most supratidal features of Tampa Bay's inshore subbasins. Terraformed shell-bearing sites in this region serve(d) as villages, civic-ceremonial centers, and mortuaries. Some sites, including 8HI2 (CRB) and 8MA13 (BH), support large shell pyramids or "platform mounds" with flat, rectangular summits raised up to 11 m above present mean sea level (MSL). At all subbasins, Native shell-bearing sites are associated with supratidal islands or peninsulas that partially enclose leeward bayous. At UTB and WI, relatively thin (0.5–1.5 m) shell midden deposits armor relic dune landforms. At CRB and BH, however, barrier landforms are composed entirely of thick (1.5–12+ m) anthropogenic deposits constructed atop weathered Miocene limestone or Pleistocene shelly facies, representing what Schwadron (2017:35) defines as Indigenous "shellworks." The earliest sampled shell-bearing cultural strata at CRB and BH are currently subtidal; charcoal inclusions from these contexts yielded radiocarbon dates *ca*. 4–2 kya, aligning with other middle- to late-Holocene (late-archaic/transitional-period) shell mounds on the peninsular Gulf Coast (Austin *et al*., 2018; Saunders and Russo, 2011; Schwadron, 2017). Much of the Indigenous shell terraforming within the study areas was accomplished between 2 and 1 kya, with later midden features at WI and UTB deposited *ca*. 700–500 cal YBP.

Shell Midden Subfacies. Shell midden deposits were encountered within all subbasins. These sediments develop(ed) as subaerial anthropogenic soils enriched by the concentrated discard of subsistence refuse at settlements (Figure 6p). They armor relic dunes at WI and UTB and were deposited atop phosphatic limestone residuum or shelly muddy sand at CRB and BH. Shell middens are composed of whole and fragmentary mollusk-shell gravel (16–85%), vertebrate faunal remains, and artifacts (ceramics, flaked stone, shell/bone tools, *etc*.) in a brownish grey-to-black organic muddy sand matrix (mud: 5–21%; sand: 11–70%). Shell concentrations vary considerably by subbasin (24–555 kg/m^3), with mean values less than adjacent unconsolidated clean shell subfacies but greater than fire/habitation features (Appendix Table 3). Mollusk assemblages are typically dominated by *C. virginica*, but *Sinistrofulgur sinistrum* and *Melongena corona* are common across all subbasins and are codominant with oyster in middens at WI (8PI56 and 8PI11491). Terrestrial snails (*Polygyra* sp.) that feed on and inhabit surficial organic detritus are ubiquitous, on average composing between 2 and 9% of MNI. Unit thickness varies, typically 0.2 to 2 m, and accumulation rates are relatively low, ranging from 0.16 to 1.14 cm/y. Shell midden deposits at all study sites typically represent *in situ* paleosols; however, they also occur within the construction sequences of platform mounds at 8HI2 and 8MA13, where they are interbedded with unconsolidated clean shell and fire/habitation features. In platform mound contexts, midden deposits commonly form inverted chronosequences, with older midden materials atop younger strata, indicating that Indigenous peoples mined antecedent midden deposits to produce material for mound building.

Unconsolidated Clean-Shell Subfacies. Clean shell deposits were documented within platform mounds at 8HI2 (CRB) and 8MA13 (BH). Sediments are composed predominantly of whole and fragmented shell gravel (50–91%), with <41% sand and <15% mud. Organic content is <10%, and void space typically makes up a substantial volume (Figure 6q). Clean shell strata exhibit the greatest shell concentrations among sampled shellwork deposits, with mean concentrations ranging from 553 to 630 kg/m^3. Mollusk assemblages exhibit greater taxonomic diversity and evenness than adjacent shell midden facies (Appendix Table 3). *Crassostrea virginica* is typically dominant, but less so than in middens; *M. corona* is codominant. At 8HI2, mollusk shells composing many clean-shell strata retain their original pigmentation, suggesting that these shell packages were deposited and buried quickly after harvesting and processing (protecting them from ultraviolet and other subaerial weathering). Soil-associated *Polygyra* sp. snails are scarce or absent, making up <2% of MNI on average. The thickness of discrete clean shell layers varies considerably (*ca*. 0.3–2 m) because of interbedding with shell midden and fire/habitation features, but thicknesses >1 m are common. Average accumulation rates vary by context. In some cases, rates approximate those observed in shell middens (*e.g*., 0.22 cm/y at 8HI2-ST2); however, deposition of clean shell strata during platform mound construction involved more rapid accumulation, commonly ranging 2–4 cm/y and periodically reaching 32–40 cm/y.

Fire/Habitation Features Subfacies. Cultural deposits associated directly with fires (*e.g*., hearths, roasting pits, smudge pits, ash dumps, *etc*.) and habitation surfaces (*i.e*. floors) were encountered at Cockroach Key (CRB) and Harbor Key (BH) as thin (0.03–0.2 m) and discrete lenses preserved within thicker packages of clean shell or shell midden. Coloration varies considerably, from light grey to black, with burned shell fragments often exhibiting an oxidized reddish-brown coating. Sediments are relatively fine (10–67% mud) and organic (2–30%), with highly variable sand (24–78%) and shell gravel (1–47%) content. Mollusk shell is typically highly fragmented and burned; shell content (281–362 kg/m^3) is typically less than in adjacent shell midden and clean shell deposits (Figure 6r). Mollusk assemblages are dominated by *C. virginica* and *M. corona*; taxonomic richness is relatively low, but diversity and evenness are greater than adjacent shell midden and clean shell deposits. Accumulation rates are low, ranging from 0.07 to 0.39 cm/y.

Reworked Cultural Shell Subfacies. The seawardmost features of Indigenous shell-terraformed settlements at UTB and BH subbasins are low ridges (0.5–2 m height) oriented parallel to the estuary shoreline. Although previously interpreted as *in situ* linear accumulations of shell midden (Bullen, 1952; Burger, 1979; Luer and Almy, 1982), recent analyses reveal that these structures are coastal berms formed by the reworking of seaward cultural shell deposits by sea-level rise and storms (Rogers and Jackson, 2022). Sediments are white to light grey and composed of whole and fragmentary shell gravel

(1–79%) in sand (20–98%) matrix, with low mud (<11%) and organic (<10%) content (Figure 6o). Medium sand is conspicuously abundant (mean = 17%) in comparison with shell midden and clean shell facies ($\bar{x} = 5\%$). These deposits exhibit characteristic bedding with alternating coarser and finer layers. Artifacts are present in low concentrations, and ceramic sherds are weathered/waterworn by wave-induced abrasion. Woody and herbaceous inclusions are common and appear intrusive. Mollusk assemblages are generally like adjacent shell middens but are readily distinguished from *in situ* cultural deposits by high percentages of small tidal-zone gastropods (*e.g.*, *P. apicinum*, *L. irrorata*, and *Cerithium* sp.) that have been entrained from seaward tidal wetlands and incorporated into coastal berm sediments during storm conditions. These taphonomic mollusk inclusions compose up to 60% of MNI in reworked deposits at UTB ($\bar{x} = 21\%$ MNI) and up to 80% of MNI in reworked deposits at BH ($\bar{x} = 30\%$ MNI). These taxa are rare within *in situ* shell midden samples, making up <7% of MNI at BH ($\bar{x} = 1.6\%$) and <1.3% of MNI at UTB ($\bar{x} = 0.13\%$). Radiocarbon assays on charcoal inclusions from basal portions of the coastal berm at 8MA15 (65–75 cm below surface) yielded recent-historic and modern dates, further indicating that these features were formed recently by storms. Of importance, older reworked cultural shell deposits were found underlying the *in situ* shellwork complex at 8MA15 (BH), extending from −0.6 to −1.6 m elevation. Radiocarbon assays on charcoal inclusions from these beds suggest that reworking transpired at or before *ca*. 2 kya.

Subbasin Stratigraphic Sequences

Cross-sectional stratigraphy for each of the four subbasins was charted by correlating records from vibracores, percussion cores, and excavation units (Figures 7–10). These stratigraphic sections enable the interpretation of paleoenvironmental histories and the understanding of terraformed Native settlements as durable infrastructure affecting the developmental trajectory and modern morphodynamics of inshore estuarine basins.

Upper Tampa Bay

The unconsolidated Quaternary sediments of the UTB subbasin unconformably overlie weathered Miocene limestone (Figure 7; Appendix Figure 1). The weathered limestone surface slopes generally seaward (to the south) but is uneven. Core UTB-VC1 encountered a karst depression measuring at least 3 m in depth from the surrounding limestone surface. Terrestrial wetland deposits are preserved atop the weathered limestone surface in UTB-VC1, 3, and 4; radiocarbon dates place their formation between 37 and 33 kya. In UTB-VC1 and VC4 late-Pleistocene wetland deposits are interbedded with fine sand lenses, likely representing episodic influxes of aeolian sand from contemporaneous dune fields located on upland terraces to the north and west (White, 1970).

The interval between *ca*. 33 kya and the mid-Holocene is represented by fluvioaeolian or lacustrine–aeolian muddy fine-sand deposits. The sharp contacts bounding this stratum and the considerable chronological span it occupies suggest the influence of erosional processes brought on by hydrologic and climatic fluctuations of the LGM and the deglacial period (Willard *et al*., 2007).

After *ca*. 4850 cal YBP paralic marshes became established across UTB. Consistent with regional sea-level reconstructions (*e.g.*, Hawkes *et al*., 2016; Stathakopoulos, Riegl, and Toth, 2020), these deposits bare evidence of marine influence, such as tidal lamination and estuarine mollusk shell. Accumulation rates range from 2.4 cm/century (UTB-VC2) to 4.4 cm/century (UTB-VC3), approximating the rate of sea-level rise during this period (Wanless, 1982) and therefore implying that wetland accretion kept pace with rising seas for approximately 3 millennia. Human occupation of relic upland environments contemporaneous with these coastal marshes is evidenced by concentrations of flaked stone (chert, silicified coral) artifacts documented within the brownish fine-sand bed underlying basal shell midden deposits at 8HI6698, 8HI6699, 8HI996, and 8HI981 (Appendix Figures 2 and 3; Supplementary Figures 1–3).

After *ca*. 1885 cal YBP, tidal marshes were transgressed and converted to the sand-flat–seagrass meadow environments that currently dominate the Bay's lower intertidal zone. Stratigraphic evidence for corresponding transgressive events has been documented at various peninsular Gulf Coast locales (Goodbred, Wright, and Hine, 1998; McFadden, 2016; Parkinson, 1989; Wright *et al*., 2005), suggesting a broad-scale driver, such as a small sea-level excursion. The wetland conversions *ca*. 1885 BP were closely followed by the onset of shell midden deposition atop relic dune features at UTB. Basal *in situ* shell midden deposits at 8HI6698 and 8HI6699 date to 1680 ± 57 cal YBP and 1620 ± 76 cal YBP, respectively. Mollusk assemblages from UTB shell middens indicate a focus on oyster harvesting ($\bar{x} = 82\%$ MNI), with minor harvesting of estuarine gastropods (Appendix Table 3).

Shell-bearing cultural features at UTB are composed of *in situ* and reworked midden and are found from *ca*. 2 m elevation to MSL. Thus, although these cultural features have always been within the range of severe storm surge, their history of direct interaction with wind waves and spring tides most likely began *ca*. 1000 cal YBP—after the main interval of occupation at 8HI6698 and 8HI6699, but contemporaneous with the later phase of occupation at 8HI996 (910–722 cal YBP). Nonetheless, these cultural deposits armor the seawardmost landforms of the subbasin along the open bay and have been substantially altered by storms. Upper strata at 8HI6698 are deflated and lack the "greasy" texture of well-preserved *in situ* midden soils (*i.e.* fine organic sediments have been oxidized or extracted during storm-surge events). These deflated shell midden deposits appear to retain stratigraphic integrity, artifact (ceramic and shell-tool) concentrations, and unaltered mollusk compositions. Upper strata at 8HI6699 and 8HI996 are composed of cultural shell deposits that once lay seaward but have been reworked during storms into coastal berms with appreciable medium-sand content, superimposed fining-upward sequences, and high concentrations ($\bar{x} = 21\%$ MNI) of intrusive mollusk shells (*i.e. P. apicinum*, *L. irrorata*, *Cerithium* sp.) (Supplementary Figures 1–3; Appendix Table 3). Today, *in situ* and reworked cultural shell deposits at UTB comprise the seawardmost landforms of the subbasin, constraining tidal flow and protecting expansive areas of oyster reef and salt marsh from higher-energy conditions.

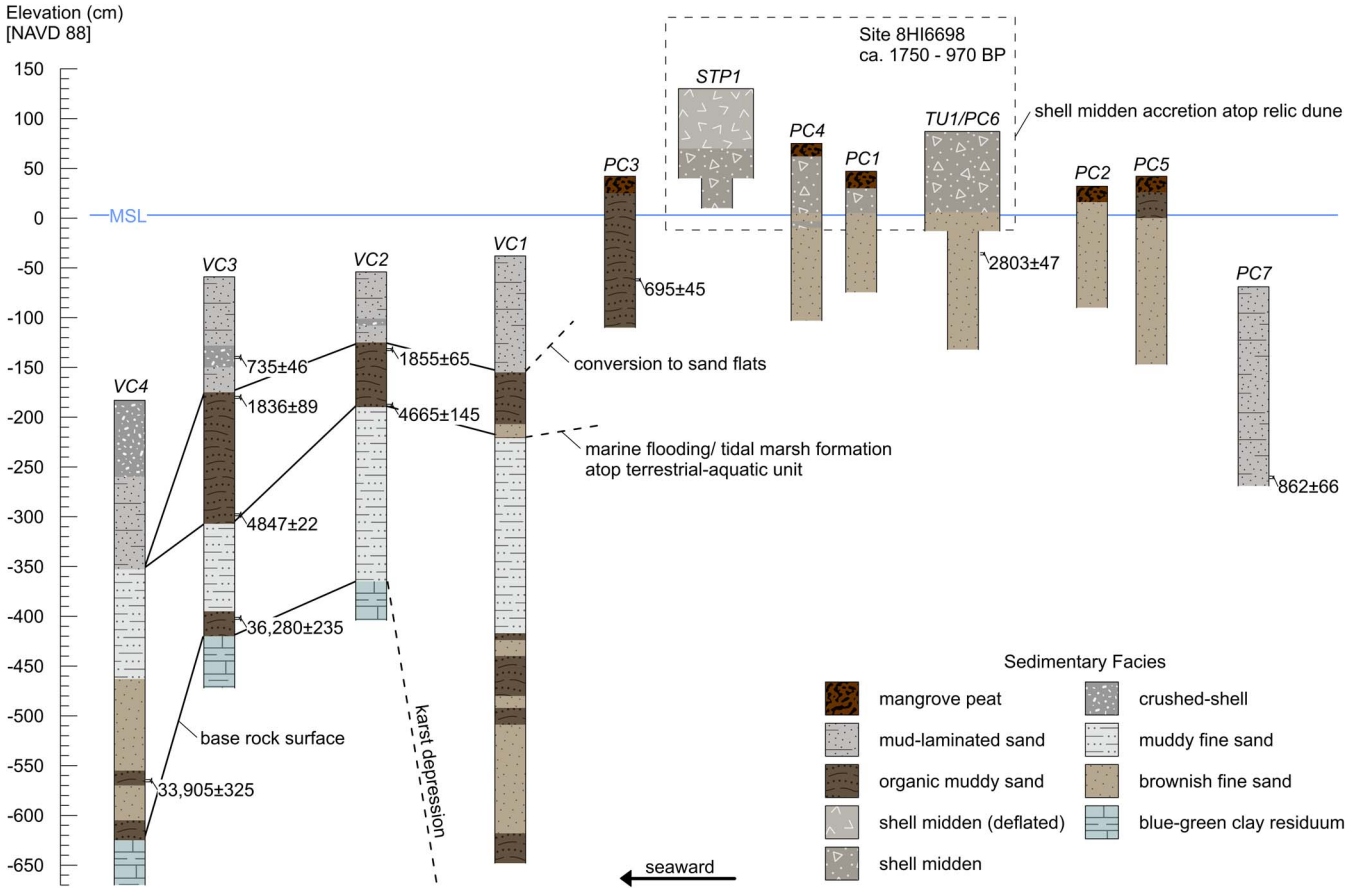

Figure 7. Cross-sectional stratigraphy and interpretation of cores and excavation units from UTB and 8HI6698 depicting pre-estuarine and estuarine sequences as well as the stratigraphic situation of seaward archaeological features. Radiocarbon dates are reported in calibrated years BP with 2-sigma error. Core locations are shown in Figure 2.

Weedon Island

The WI subbasin is characterized by thick aeolian sand beds that extend from the apex of supratidal dune ridges (*ca*. 4 m elevation) to below the maximum sampling depth (*ca*. −8 m elevation) (Figure 8). Beneath the modern seabed, fluvioaeolian and lacustrine–aeolian deposits are predominant, with seaward-dipping upper surfaces (Appendix Figures 4 and 5; Supplementary Figure 4). Deeply buried organic wetland beds such as those observed at UTB are present at WI (*e.g*., WI-VC4 and VC6). Poorly sorted beds of fragmented fossil shell in WI-VC3 situated between −4.7 and −3.6 m elevation likely represent higher-energy conditions during the onset of estuarine flooding at mid-Holocene. The fossil-shell bed is truncated by gleyed muddy fine sand, consistent with lower-energy, reducing conditions, and continued aeolian transport. Peat-rich tidal wetlands began accumulating on the margins of Ross and Googe islands *ca*. 4850 cal YBP and continued until *ca*. 1770 cal YBP, when they were converted to sand flats. As at UTB, an accumulation rate of 3.8 cm/century for the coastal marsh bed in WI-VC4 is consistent with the reconstructed pace of regional sea-level rise.

Indigenous occupation of parabolic dune uplands at WI during the mid-Holocene is evidenced by ubiquitous concentrations of flaked stone artifacts within buried aeolian deposits at Ross Island (8PI56, 8PI11491) and Weedon Island site (8PI1) (Draskovich, 2021). The occurrence of flaked stone tools and tool-making debris at substantial depth (>1 m below surface) within dune ridges suggests that aeolian accretion continued through the mid-Holocene.

Shell-bearing cultural deposits at WI are shell midden soils formed in fine sands; they are relatively thin (<1 m), and shell density is low ($\bar{x} = 24$ kg/m^3) relative to other Tampa Bay study areas. This pattern is likely influenced by the higher initial elevation of the dunes. Early shell midden deposits at Ross Island South (8PI56) date to 2510 ± 156 cal YBP, indicating Native harvesting of fishes and mollusks from estuarine habitats contemporaneous with the tidal marshes documented in WI-VC2 and 4. Indigenous occupation of 8PI56 continued across the conversion of marshes to sand flats (*ca*. 1770 cal YBP), with later midden deposits dating to 1470 ± 70 cal YBP. Well-preserved mollusk assemblages at 8PI56 (*e.g*., 8PI56-ST5) are dominated by oyster ($\bar{x}$ = 65% MNI), with lesser

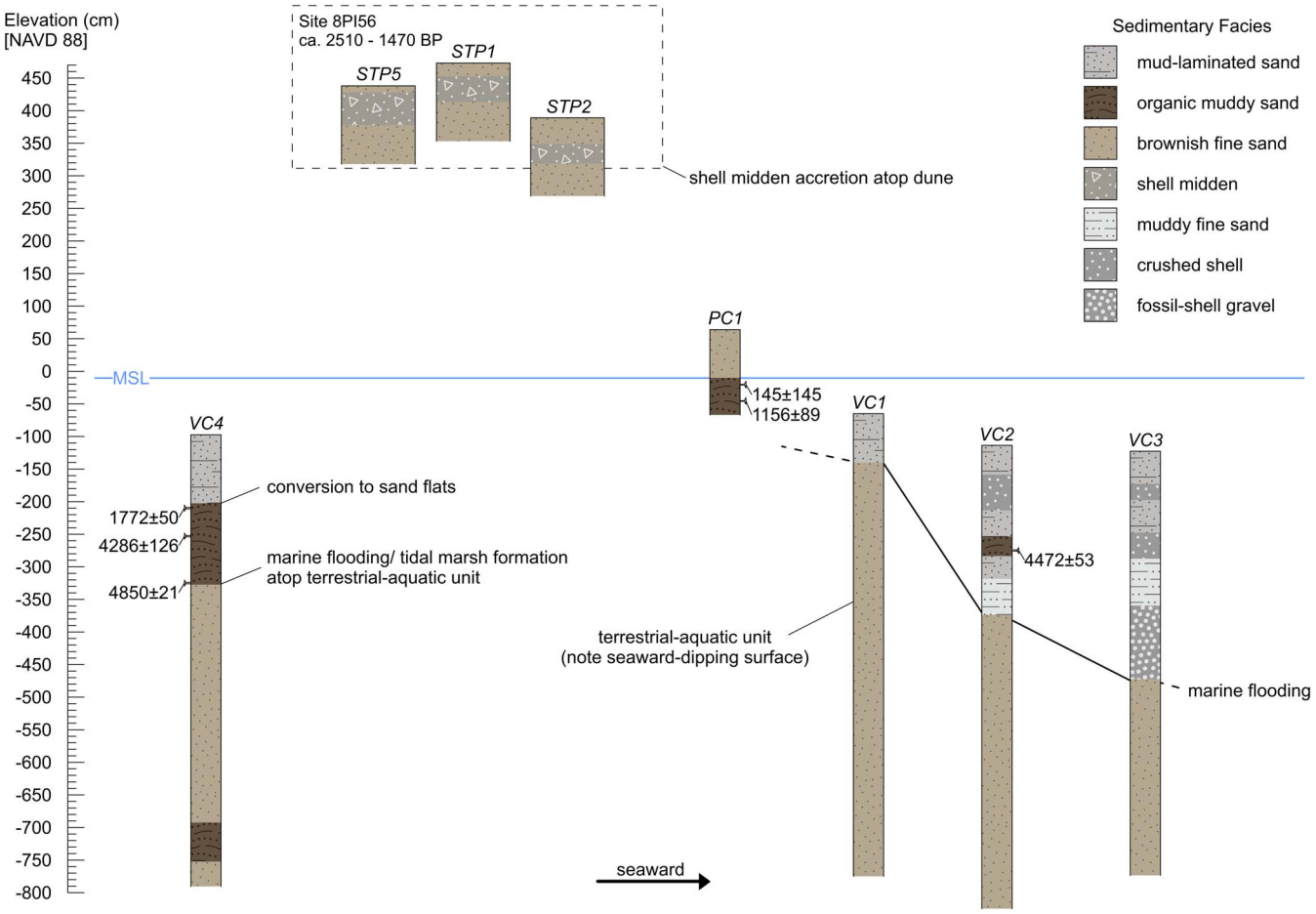

Figure 8. Cross-sectional stratigraphy and interpretation of cores and excavation units from WI and 8PI56 depicting pre-estuarine and estuarine sequences, as well as the situation of shell midden deposits atop dune features at Ross Island. Radiocarbon dates are reported in calibrated years BP with 2-sigma error. Core locations are shown in Figure 3.

representation of estuarine gastropods (Appendix Table 3). Shell middens at Ross Island North (8PI11491-ST2, ST3, ST4) were deposited centuries later, between 772 and 544 cal YBP, and are dominated by estuarine gastropods ($\bar{x} = 90\%$ MNI) with relatively scant representation of oyster ($\bar{x} = 5\%$ MNI).

Cockroach Bay (CRB)

The Quaternary stratigraphy of Cockroach Bay uncomformably overlies Miocene phosphatic limestone residuum (Figure 9). The upper limestone residuum surface is uneven and was found from −0.7 m (8HI2-PC5) to −5.5 m elevation (CRB-VC5), indicating significant karst morphology. Compared to UTB and WI subbasins, terrestrial facies at CRB are considerably thinner because of the higher base rock limiting accommodation space. Freshwater wetland beds are preserved overlying the limestone residuum in CRB-VC4 and VC5 and yielded radiocarbon dates preceding the LGM, *ca*. 32 and 24 kya respectively (Appendix Figure 6). Shelly quartz sand and fossil-shell gravels make up the LGM-to-early-Holocene sedimentary sequence at CRB, likely representing channel fill and shoal features within a fluvial environment. A freshwater gastropod bed (*V. georgianus* and *P. scalaris*) directly overlies a limestone high in CRB-VC6 (*ca*. −2.6 to −3.3 m elevation), indicating low-energy riverine, slough, or marginal lacustrine conditions with submerged aquatic vegetation before the onset of marine influence (Appendix Figure 7). Coastal marshes were established at CRB by 3595 cal YBP and accreted until at least *ca*. 2800 cal YBP (3.1 cm/century, CRB-VC5), after which they were truncated by crushed shell lenses and mud-laminated sand deposits produced within sand-flat/seagrass meadow environments.

Early phases of Native occupation and shell midden deposition at Cockroach Key (8HI2) are preserved between −0.2 to −1.2 m elevation beneath the standing shellworks (8HI2-PC1 and PC2) and beneath *ca*. 0.5 m of mangrove peat in a broad tidally inundated area landward (east) of the shell mounds (8HI2-PC4 and PC5) (Supplementary Figure 5). Where encountered, these basal cultural features overlie a thin bed of fine quartz sand; 8HI2-PC5 suggests that the 8HI2 shellworks are situated atop a limestone high. Radiocarbon

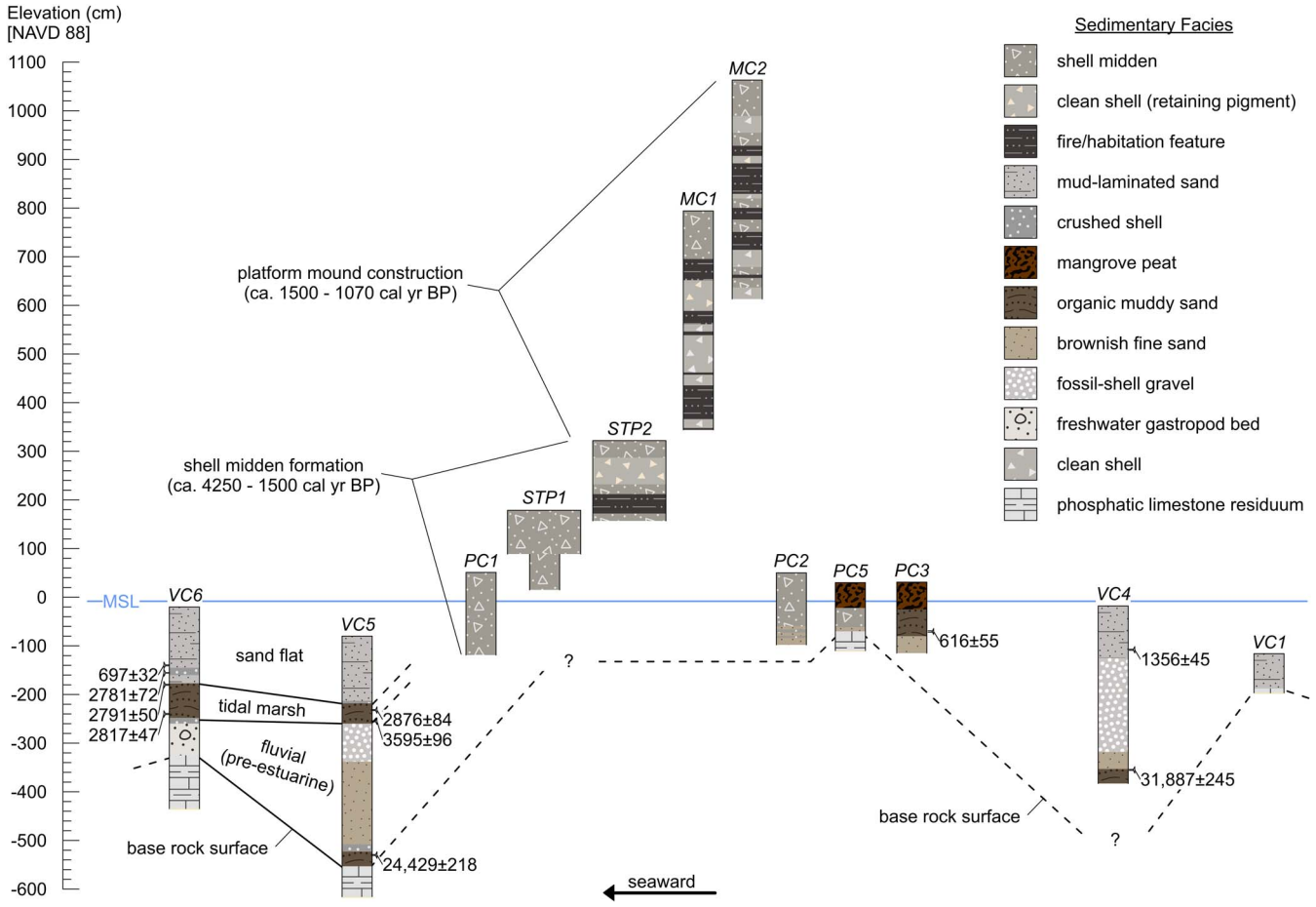

Figure 9. Cross-sectional stratigraphy and interpretation of cores and excavation units from CRB and 8HI2 depicting pre-estuarine and estuarine sequences, as well as the stratigraphic situation and character of seaward cultural shellwork features. Radiocarbon dates are reported in calibrated years BP with 2-sigma error. Core locations are shown in Figure 4.

dates on midden charcoal from subtidal deposits place early occupation between 4250 ± 126 cal YBP (8HI2-PC5) and 2574 ± 148 cal YBP (8HI2-PC2), spanning the interval of coastal marsh establishment and conversion to sand flats. These early shell midden features at 8HI2 are composed of *C. virginica* ($\bar{x}$ = 67% MNI), *M. corona* ($\bar{x}$ = 12% MNI), and *Geukensia* sp. ($\bar{x}$ = 5.6% MNI), along with charcoal, fish bone, and ceramic sherds (Appendix Table 3; Supplementary Data). Intensified Native settlement and the accretion of dense ($\bar{x}$ = 555 kg/m^3) oyster-rich ($\bar{x}$ = 71% MNI) shell midden at 8HI2 is apparent from *ca*. 1800 to 1500 cal YBP (8HI2-ST1 and ST4).

Native construction of the large shell platform mound features at 8HI2 likely began *ca*. 1500 cal YBP (8HI2-MC1 and MC2) and had waned by 1070 ± 107 cal YBP (8HI2-ST7). Thick (>1 m) packages of unconsolidated clean shell compose much of the mound fill and are separated by thinner deposits of *in situ* shell midden and fire/habitation features (Supplementary Figure 6). Antecedent shell midden soils were mined and utilized as mound fill, producing characteristic inverted radiocarbon sequences. The rapid accumulation and burial of clean shell packages at 8HI2 suggest that mound-building activities were episodic and closely associated with intensive mollusk harvests that provisioned civic–ceremonial aggregations (Pluckhahn, Thompson, and Rink, 2016).

The onset of mound construction at 8HI2 *ca*. 1500 cal YBP was followed by changing energetic and ecological conditions leeward of the shellworks (CRB-VC4) where coarse, shelly channel-fill deposits are truncated at *ca*. −1.25 m elevation by organic mud-laminated sand, yielding a basal date of 1356 ± 45 cal YBP. Further landward (CRB-PC6 and PC7) cardite beds were replaced by oyster reefs *ca*. 1 kya. Following the major interval of Native settlement and mound building at 8HI2 (*ca*. 4250 – 1070 cal YBP), the shellworks have continued to influence ecological dynamics in leeward areas. Percussion cores 8HI2-PC3, PC4, and PC5 document the encroachment of tidal marsh and mangrove atop lower-lying areas of the ancient settlement that are protected from wind waves and tidal current by the supratidal shellworks. Radiocarbon analysis of basal marsh peat (−0.7 m elevation) places tidal wetland encroachment at 616 ± 55 cal YBP.

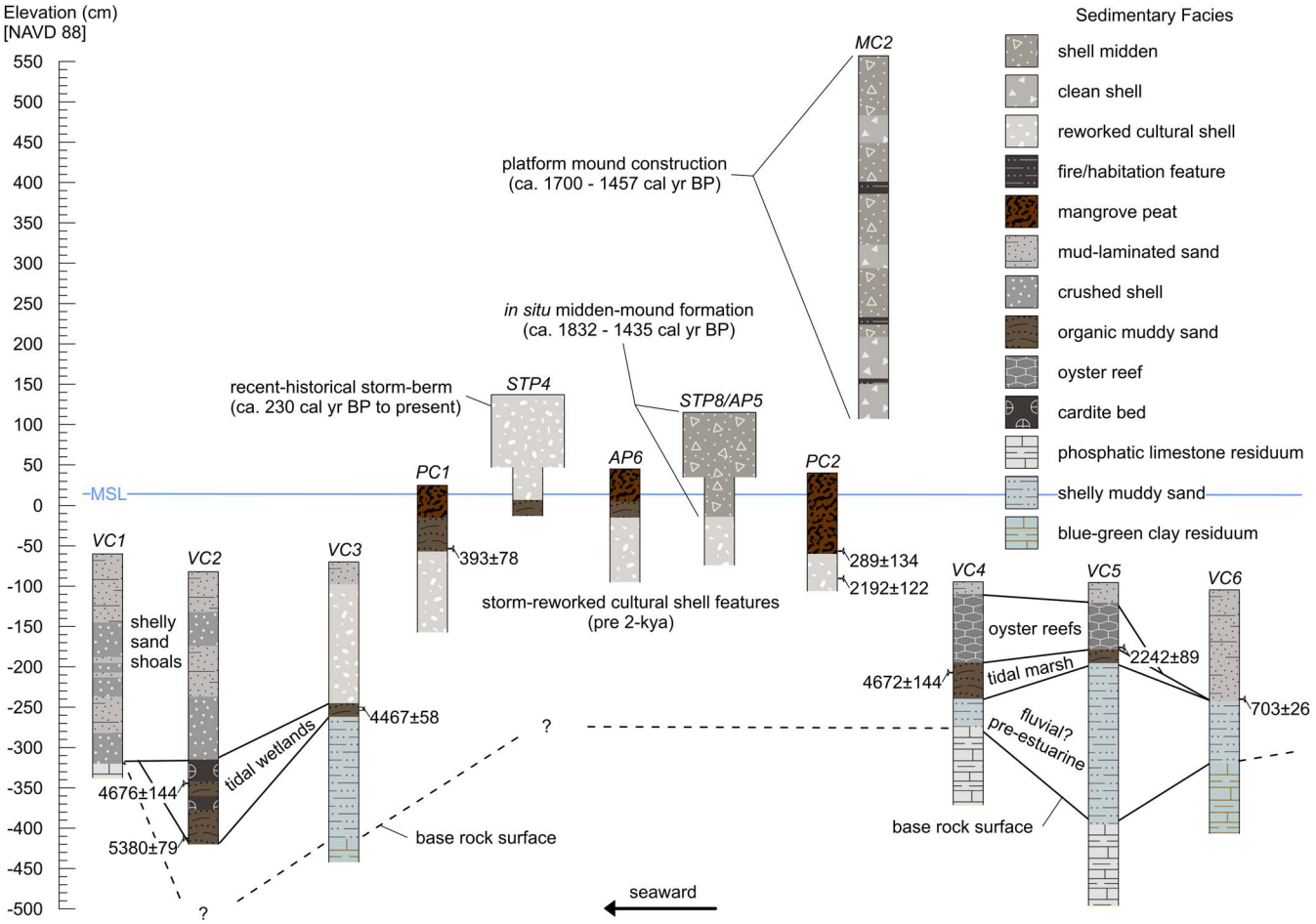

Figure 10. Cross-sectional stratigraphy and interpretation of cores and excavation units from BH and 8MA13-15 depicting pre-estuarine and estuarine sequences, as well as the stratigraphic situation of seaward cultural shellwork features. Radiocarbon dates are reported in calibrated years BP with 2-sigma error. Core locations are shown in Figure 5.

Bishop Harbor (BH)

The Bishop Harbor study area exhibits a higher degree of marine influence than the other three subbasins (Figure 10), likely owing to its position facing the main Tampa Bay entrance (Figure 1). Weathered Miocene-age phosphatic limestone residuum makes up the basal unit; its uneven upper surface occurs between *ca*. −2.7 and −4 m elevation. Like CRB, shallower base rock resulted in thinner terrestrial facies, as compared to UTB and WI. Muddy sand deposits rich in estuarine mollusk shell overlie the limestone, likely representing the reworking of Pleistocene shell beds within terrestrial–aquatic (*i.e*. fluvial–palustrine) environments during the deglacial Pleistocene and early Holocene.

Unlike UTB, WI, and CRB, terminal Pleistocene wetland beds were not encountered at BH. In contrast, organic mid- to late-Holocene wetland sediments accumulated above sharp contacts with limestone or reworked shelly deposits. Organic muddy sands and cardite beds accumulated in a depression feature (*ca*. −3.2 to −4.2 m elevation) at BH-VC2 between 5380 ± 79 cal YBP and 4676 ± 144 cal YBP (Appendix Figure 8). Thin organic muddy sand strata in BH-VC3 and VC4 also date to the mid-Holocene (4467 ± 58 cal YBP and 4672 ± 144 cal YBP, respectively), representing paralic wetland environments.

The recovery of fiber-tempered ceramics from eroding shell midden deposits seaward of Harbor Key (8MA13) and Mariposa Key (8MA302) by Burger (1979, 1986) indicates that Indigenous occupation and shell midden deposition were underway by *ca*. 4 kya. Percussion cores reveal that basal cultural shell deposits at 8MA15 are located from *ca*. MSL to −2.4 m elevation beneath *in situ* supratidal midden mounds (8MA15-AP5 and PC3), beneath 0.5–1 m of mangrove peat in low-lying areas of the site (8MA13-PC1 and 2), and beneath the tidal flat at BH-VC3 (Supplementary Figure 7). These cultural deposits are substantially reworked, likely recording the impacts of ancient storms. Charcoal inclusions recovered from the reworked cultural strata in 8MA15-PC2 and PC3 yielded radiocarbon dates of 2192 ± 122 cal YBP and 2038 ± 87 cal

YBP, respectively. Given that the extant coastal berm at 8MA15 (also composed of reworked cultural shell) contained predominantly modern and recent-historical charcoal inclusions, the dates from buried reworked deposits may best indicate the time frame of disturbance and redeposition. High-energy conditions are also preserved in seaward vibracores BH-VC1 and VC2, where the mud-laminated sand unit is interbedded with numerous shell debris lenses from the modern seabed to −3 m elevation.

In situ organic shell midden deposits were encountered at 8MA13-ST8/AP5 and 8MA13-PC3, where they overlie reworked cultural shell deposits. Basal *in situ* midden strata yielded a radiocarbon date of 1832 ± 89 cal YBP, providing a *terminus ante quem* for the deposition of underlying reworked cultural shell beds. Midden accretion continued here until at least 1435 ± 79 cal YBP, recording a subsistence adaptation focused on oystering ($\bar{x}$ = 74% MNI), with lesser extraction of gastropods (Appendix Table 3). Construction of the Harbor Key platform mound likely began *ca*. 1700 cal YBP (8MA13-MC1 and MC2). The mound contains a limited volume of unconsolidated clean shell and was built predominately from *in situ* and repurposed shell midden, separated by thin fire/habitation features. As at Cockroach Key and other Gulf Coast shell mounds (Austin and Mitchem, 2014; Pluckhahn and Thompson, 2017; Randall and Sassaman, 2017; Schwadron, 2017; Thompson *et al*., 2016), inverted radiocarbon sequences suggest that mound building involved the mining of antecedent cultural deposits for use as mound fill. Nevertheless, internal consistency among dates within the stratigraphic sequence suggests that mound building was relatively rapid (spanning a *ca*. 250-y interval), with the most recent mound fills dating to 1457 ± 53 cal YBP (8MA13-ST7).

The modern sand flats landward of the Harbor Key shellworks (BH-VC4 and VC5) are underlain by transgressed oyster reefs, situated between −2 and −1.1 m elevation (Appendix Figure 9). A radiocarbon assay on plant macrofossils from the base of the reef in BH-VC5 places reef establishment at 2242 ± 89 cal YBP. As at 8HI2, lower-lying areas of the Harbor Key complex that are sheltered from wind waves have been encroached by mangrove forest, and the site's once-terrestrial ground surface currently underlies 0.4 to 1.0 m of tidal wetland peat. Basal radiocarbon dates on these peat beds (*ca*. −0.5 m elevation) fall at 393 ± 78 cal YBP (8MA15-PC1) and 289 ± 134 cal YBP (8MA15-PC2).

DISCUSSION

This program of subsurface investigation yielded well-resolved sedimentary and geoarchaeological records that demonstrate the close intertwining of Tampa Bay's geological, ecological, and cultural histories. In the discussion below, these records are integrated to refine the understanding of Holocene estuary development, resolve elements of mid- and late-Holocene sea-level history, and recognize the morphodynamic effect of Indigenous shell terraforming within inshore ecosystems.

Inshore Estuarine Development in Tampa Bay

The stratigraphic frameworks assembled here generally support the four-stage model of Tampa Bay's Holocene estuary evolution by Brooks and Doyle (1998), involving (1) exposure of the karst-controlled drainage network during the LGM, (2) fluvial deposition within the karst drainage system, (3) infilling by brackish wetlands attending sea-level rise, and (4) continued estuarine infilling through the present. However, new analyses from Tampa Bay's inshore subbasins refine chronostratigraphic understanding and highlight linkages between sedimentary sequences and broader paleoclimatic patterns. Furthermore, these new data reveal considerable spatial variation in antecedent substrates, marine influence, and energy regimes.

Late-Pleistocene freshwater wetland sediments are preserved atop uneven weathered Miocene surfaces at UTB, WI, and CRB. However, similar deposits were not encountered at BH, where exposure to open Gulf waves, particularly during storms, might have led to the erosion of late-Pleistocene and Holocene strata during marine flooding. At the more protected northern end of Tampa Bay (UTB), late-Pleistocene deposits were better preserved and dated *ca*. 36 and 34 cal kya, aligning with a cool, arid interval associated with the advance of expansive ambrosia–oak savannas and reduced forest cover (Grimm *et al*., 2006). Dates on similar contexts at CRB (32 and 24 kya) correspond with pine-forest advances that Grimm *et al*. (2006) attribute to increased atmospheric convection and precipitation brought on by thermohaline conveyor disruption and warmer Gulf waters (van Beynen *et al*., 2017). The character of late-Pleistocene wetlands described here may be analogous to the LGM- and deglacial-age groundwater-fed wetland environments reconstructed by Willard *et al*. (2007) from late-Pleistocene sediments preserved in the deep Middle Tampa Bay basin, which persisted as wetlands across significant hydrologic fluctuations. Fine-sand lenses within late-Pleistocene wetland units likely record arid climatic intervals with increased aeolian transport. Given the relative accessibility of these deposits, future research might resolve these signals at a finer temporal scale with trapped-charge dating (*e.g*., optically stimulated luminescence) or AMS ^{14}C dating on fossil pollen.

Increased precipitation across the deglacial period (Willard *et al*., 2007) and enhanced groundwater discharge during the early Holocene (*e.g*., Kenney *et al*., 2016) acted on the topographic gradients between the karst depressions of proto-Tampa Bay and encompassing uplands to generate fluvial and palustrine–lacustrine environments. At UTB and WI, deeper base rock provided greater accommodation space, and protection from open Gulf waves provided by the Pinellas peninsula improved the preservation potential of pre-estuarine terrestrial deposits. Continued aeolian transport and interactions between streams and antecedent dune fields facilitated the accumulation of reworked fine sand and muddy fine-sand beds. At CRB and BH, contemporaneous fluvial processes reworked antecedent fossil-shell beds of Plio-Pleistocene age. At CRB, freshwater gastropod (*V. georgianus* and *P. scalaris*) deposits of deglacial or early-Holocene age indicate oligotrophic conditions and abundant aquatic vegetation.

During the mid-Holocene, interactions between marine flooding and enhanced precipitation produced paralic wetland systems throughout inshore Tampa Bay. The initial marine flooding of Middle Tampa Bay and lower Hillsborough Bay *ca*. 7.5 kya (Cronin *et al*., 2007) was followed by the onset of warm,

wet climate and major expansions of pine forests across the Florida peninsula (van Beynen *et al*., 2017; van Soelen *et al*., 2010; Watts, 1969, 1971, 1975, 1980; Watts and Hansen, 1994). The mid-Holocene expansion of southeastern coniferous forests, and particularly Florida's fire-dependent pinelands, has been associated with increased sedimentation rates in depositional basins (Delcourt, 1985; Wright, 1981). Drawing on biomarker and elemental analyses of sediment cores from Charlotte Harbor, van Soelen *et al*. (2012) identified an interval of enhanced terrestrial runoff *ca*. 5.5–4.5 kya—showing that mid-Holocene hydrological and vegetational shifts affected conditions within Gulf Coast estuaries. The stratigraphy presented here suggests that increased runoff and sediment supply to the Tampa Bay depression at mid-Holocene contributed to the development and proliferation of tidal wetlands.

The concurrent formation of tidal wetlands between 5.5 and 4.5 kya within widely distributed marginal subbasins of Tampa Bay indicates that initial marine flooding, documented in the Middle Tampa Bay *ca*. 6–7 kya, reached quite far inland. The spatial extent of marine flooding was largely controlled by irregular karst morphology and associated stream systems. This finding motivates a reconsideration of the spatial and temporal pattern of marine flooding and estuarine development in Tampa Bay, which previously has been understood as a gradual landward progression of marine influence like that observed in flooded river valley estuaries (Donahue *et al*., 2003). The karst-controlled pattern evidenced here would justify future geophysical survey in Tampa Bay focused on Old Tampa Bay, Hillsborough Bay, and their inshore subbasins in search of buried karst drainage networks connecting Middle Tampa Bay to inshore bay heads.

Continued sea-level rise throughout the late Holocene resulted in the flooding of Tampa Bay's present spatial extent. The formation of a more open estuary likely produced increased wave forcing during both normal and storm conditions. The increased wave energy, along with a slowed rate of sea-level rise, converted paralic wetlands to sand flats *ca*. 2 kya at UTB and WI. The timing of paralic wetland conversion at the southern study sites (CRB and BH) is less distinctive because of the greater influence of wave-induced erosion. However, stratigraphic sequences at more protected locales at CRB (*e.g*., LCRB-PC8) and BH (*e.g*., BH-VC5) indicate that marshy wetlands were flooded *ca*. 2 kya and converted to oyster reefs.

Stratigraphic studies along the open, low-energy Gulf Coast north of Tampa Bay by Goodbred, Wright, and Hine (1998), Hutton (1986), McFadden (2016), and Wright *et al*. (2005) documented similar conversions from restricted wetlands to more open sand shoals (also see Evans *et al*., 1985; Fletcher *et al*., 1993; Parkinson, 1989; van de Plassche, 1991). Many of these studies, particularly Goodbred, Wright, and Hine (1998) and Wright *et al*. (2005), attribute this environmental change to a punctuated sea-level excursion attended by sedimentary reworking during storms. In core records from Charlotte Harbor, van Soelen *et al*. (2012) observed a stark decrease in terrestrial organic matter during the late Holocene (after *ca*. 3.5 kya). This pattern may be attributed to the expansion of lakes, sloughs, marshes, and swamps throughout the peninsular interior (Arnold *et al*., 2018; Donders, 2014; Lammertsma *et al*., 2015; Pollock *et al*., 2017), resulting in decreased hydrologic gradients and reduced sediment export to the coast. Paleotempest studies along the Florida Gulf Coast, from the Shark River slough (Yao *et al*., 2020) to the Panhandle (Liu and Fearn, 2000), suggest that the interval *ca*. 3 to 1 kya was a particularly active period for tropical cyclones (also see Goorbred, Wright, and Hine, 1998; Lane *et al*., 2011; van Soelen *et al*., 2012). Heightened storm activity, along with attendant tidal and wave forcing, presents a compounding mechanism for the conversion of paralic wetlands in Tampa Bay during the late Holocene.

Extant tidal marsh and mangrove environments have developed atop formerly terrestrial quartz sand beds, oyster reefs, and shell-bearing archaeological features. Basal dates from these peat deposits range from *ca*. 1100 to 300 cal YBP. As discussed by Hesterberg, Jackson, and Bell (2022), many of Tampa Bay's inshore mangrove islands are very recent habitats that formed during the late 20th century after regional warming and enhanced propagule supplies enabled mangroves to encroach and bury intertidal oyster reefs.

Implications for Understanding Holocene Sea-Level Changes

The peninsular Gulf Coast of Florida is regarded as an ideal physiographic region for documenting sea-level histories because of its tectonic stability, significant distance from ice sheets (and isostatic effects), generally low energy, and favorable preservation potential (Balsillie and Donoghue 2004, 2011; Joy, 2019). However, mid- to late-Holocene sea-level history in the Gulf of Mexico has remained somewhat enigmatic, with the most significant discord concerning several potential highstands purportedly exceeding present sea level, *ca*. 6–5 kya, 4.5–4 kya, 3.7–3.1 kya, 1.9–1.7 kya, and 1.1–0.8 kya (Balsillie and Donoghue, 2004, 2011; Walker, 2013). Most typically, Holocene sea-level research based on sampling seaward of the present shoreline has produced more "gradualistic" reconstructions (lacking evidence for highstands above present sea level), whereas "Fairbridgian" sea-level curves (proposing major highstands) have relied on interpretations of supratidal landforms such as beach ridges (*e.g*., Stapor, Mathews, and Lindfors-Kearns, 1991; Walker, Stapor, and Marquardt, 1995). Beach ridges form under high-energy conditions related to storm wave run-up, and therefore may not be reliable indicators of sea level. Recently, research on salt-marsh sediment cores from Florida's Gulf and Atlantic coasts produced well-resolved sea-level curves for the mid- to late Holocene that support a gradualistic pattern (Gerlach *et al*., 2017; Hawkes *et al*., 2016). However, as Balsillie and Donoghue (2011), among others, have argued, sedimentary studies restricted to present tidal and subtidal zones may not yield evidence for past highstands simply because of the elevation of the samples. Sampling during the present study spanned subtidal, intertidal, and supratidal zones across four subbasins of Tampa Bay, producing a variety of indicators that can be used to evaluate whether this region experienced the major sea-level oscillations proposed for the Gulf Coast by beach ridge studies (*e.g*., Stapor, Mathews, and Lindfors-Kearns, 1991; Tanner, 1992; Walker, 2013).

Organic muddy sand beds at UTB and WI, representing tidal marshes that accreted from *ca*. 4.8 to 1.8 kya, were encountered

below the modern tidal zone, between −3 and −1 m elevation. Similar beds at CRB dating between *ca*. 3.5 and 2.7 kya were also encountered in the present subtidal zone, *ca*. −2.5 to −1.8 m elevation. The formation, accretion, and truncation of these tidal zone indicator beds align well with the local sea-level reconstruction by Hawkes *et al*. (2016) and with regional coastal evolution studies by Goodbred, Wright, and Hine (1998) and Wright *et al*. (2005). Barring a mechanism for marsh peat production several meters below sea level, these sediment records do not support a higher-than-present sea level *ca*. 4.5–4 kya and 3.7–3.1 kya. The recovery of *in situ* subaerial shell midden deposits dated *ca*. 4250 cal YBP from subtidal contexts (*ca*. −0.55 m elevation) at 8HI2-PC5 (CRB) further rules out a contemporaneous higher-than-present sea level.

The conversion of paralic wetlands to more open sandy shoals after *ca*. 1800 cal YBP at UTB, WI, and BH is interpreted here as the result of prolonged wave action during slow sea-level rise. This interpretation agrees with that of a small, punctuated sea-level excursion within an overall context of decelerating rates of rise (Goodbred, Wright, and Hine, 1998; McFadden, 2016; Parkinson, 1989; Wright *et al*., 2005). Chronostratigraphic evidence from *in situ* subaerial shell middens throughout Tampa Bay's coastal strand are inconsistent with the hypothesis of (a) sea-level highstand(s) during the early centuries of the common era. *In situ* shell midden soils accreted at 8HI6698-TU1 (UTB) from *ca*. 1680 to 1595 cal YBP and presently reside between 0.05 and 0.55 m elevation. *In situ* shell midden soils accreted at 8HI2-STP1 and STP4 (CRB) from *ca*. 1836 to 1615 cal YBP and presently sit between 0.55 and 1.25 m elevation. *In situ* shell midden soils at 8MA15-ST8 were dated *ca*. 1832 to 1451 cal YBP and reside between 0.4 and 1.0 m elevation. The elevations and chronostratigraphy of these widely distributed midden soils preclude a contemporaneous higher-than-present sea-level stand.

Archaeological data from *in situ* shell midden deposits also fail to support the hypothesis of a sea-level highstand *ca*. 1.1 to 0.8 kya. Excavations at 8HI996-STP4 and TU1 documented the subaerial accumulation of shell midden from *ca*. 1620 to 1011 cal YBP and *ca*. 831 to 757 cal YBP, respectively. These midden strata are situated between 0.15 and 0.45 m elevation, inconsistent with deposition during higher-than-present sea level.

Indigenous Settlement and Shell Terraforming

The geologic and paleoenvironmental histories of Holocene estuary evolution in Tampa Bay are interwoven with the cultural history of Indigenous land use and settlement, which extends back at least to the deglacial period of the late Pleistocene, *ca*. 14.5 kya (Halligan, 2022). This study shows that freshwater wetland systems were widely distributed throughout the Tampa Bay basin during the late Pleistocene, and not restricted to the previously studied Middle Tampa Bay depression (Cronin *et al*., 2007; Willard *et al*., 2007). AMS radiocarbon assays and sedimentary data suggest that, as in Middle Tampa Bay, these wetlands persisted across arid intervals, including pre-LGM cooling phases (*e.g*., 37–34 kya), the LGM (*ca*. 22–18 kya), and punctuated climatic reversals of the deglacial period (*i.e*. 14.3–14.1 kya, 13.7–13.5 kya, 13.2–13 kya, and 12.9–11.4 kya). These conditions may help explain the conspicuous spatial concentration of terminal Pleistocene-age projectile points in the region (Anderson *et al*., 2010, 2019). Such persistent wetland systems support Thulman's (2009) "oasis" settlement model and may explain the uncharacteristic permanence of terminal-Pleistocene and early-Holocene sites in the region (*e.g*., Daniel and Wisenbaker, 1987).

As archaeologists working on Florida's Gulf Coast have amply discussed (*e.g*., Cook-Hale, Hale, and Garrison, 2019; Faught, 2004; Halligan, 2021), Holocene sea-level rise has likely inundated most coastal Native settlements predating the common era. Further, the widely observed transgressive pulse *ca*. 1.8 kya likely exacerbated scouring, reworking, and burial of mid-Holocene sites (*e.g*., Austin *et al*., 2018; McFadden, 2014). Whereas mid-Holocene shell-bearing cultural deposits are indeed rare in Tampa Bay's modern tidal and supratidal zones, the expansion and persistence of estuarine wetlands (*ca*. 4.8–1.8 kya) observed in sediment cores are duly reflected by currently subtidal shell midden strata from 8HI2 dated between *ca*. 4.2 and 2.5 kya, as well as reworked cultural shell strata from 8MA15 underlying the common-era mound center.

Intensified occupation and shell terraforming after *ca*. 1.8 kya at sites throughout inshore Tampa Bay conforms with a broader archaeological pattern of shifting settlement along the peninsular Gulf Coast (*e.g*., Kolianos, 2020; McFadden, 2016; Pluckhahn and Thompson, 2018; Sassaman *et al*., 2017). As elsewhere in the region, Native peoples of Tampa Bay estuary developed early common-era settlements atop landforms that were occupied centuries to millennia earlier by ancestral peoples. Stratigraphic sequences composing platform mounds at Cockroach Key and Harbor Key contain much older shell midden sediments, recording the mining of ancestral cultural shellwork deposits for use as mound fill, an Indigenous terraforming practice observed at several Gulf Coast shell mound sites (Austin, Mitchem, and Weisman, 2014; Luer, 2007:40; Pluckhahn and Thompson, 2017:79; Randall and Sassaman, 2017; Schwadron, 2017:50; Thompson *et al*., 2016).

Correlations between cultural shellwork chronostratigraphy and late-Holocene estuarine sediment sequences at CRB and BH suggest that shell terraforming influenced physical conditions in leeward bayous by limiting fetch and protecting tidal habitats from wind waves, as well as detaining terrestrial freshwater input, perhaps in a similar manner to large reef chains (*e.g*., Alonso *et al*., 2022; Lunt, Reustle, and Smee, 2017). Further, the proliferation of high-intertidal wetlands atop formerly terrestrial cultural shell features at UTB, CRB, and BH (*ca*. 650 cal YBP to present) further attests to the role of ancient, terraformed features in structuring the distribution of historical and modern estuarine habitats.

CONCLUSIONS

This stratigraphic and archaeological research in Tampa Bay's inshore subbasins produced the following conclusions. First, karst-controlled pre-Holocene freshwater wetlands in the Tampa Bay depression were not restricted to the previously described palustrine–lacustrine Paleolake Edgar system in Middle Tampa Bay, but instead were widely distributed. Marine flooding and enhanced precipitation during the mid-Holocene acted on this karst network to produce tidally

influenced paralic wetland systems throughout much of the bay between *ca*. 5.5 and 4.5 kya. Marine transgression *ca*. 1.8 kya due to slow sea-level rise, coupled with increased wave and storm forcing, converted vast paralic wetlands to sandy tidal flats. Where inshore conditions were favorable (hard substrate, tidal flow, and protection from large waves), oyster reefs proliferated.

Second, terraformed shell-bearing cultural features compose the seawardmost supratidal landforms of the Tampa Bay inshore. Basal strata of extant cultural shellworks at the southern study areas—now occupying subtidal elevations—were deposited during the mid- to late Holocene, *ca*. 4.6 to 2.3 kya, contemporaneous with paralic wetland formation. After a punctuated marine transgression *ca*. 1.8 kya, maritime Native societies intensified settlement and began constructing large shell-mound complexes at the mouths of major tidal bayous. Contemporaneous shifts in energy regime and estuary conditions (including proliferation of oyster reefs) in areas leeward of shell-bearing sites suggest that Indigenous terraforming influenced early common-era estuarine development by attenuating energy. With subsequent sea-level rise, since *ca*. 650 cal YBP, low-lying portions of ancient Native settlements have provided landforms ideally situated for encroachment by high-intertidal wetland habitats.

Last, the elevations and ages of buried tidal beds across the Tampa Bay inshore are consistent with recent gradualistic sea-level curves developed by Hawkes *et al*. (2016) and Gerlach *et al*. (2017). Furthermore, elevation and radiocarbon data from numerous *in situ* shell midden deposits at UTB, CRB, and BH directly conflict with proposed higher-than-present sea-level stands (*ca*. 6–5 kya, 4.5–4 kya, 3.7–3.1 kya, 1.9–1.7 kya, and 1.1–0.8 kya).

ACKNOWLEDGMENTS

Funding was provided by the National Science Foundation (award #2024397), the Alliance for Weedon Island Archaeological Research and Education, and the PaleoWest Foundation. We thank Jeff Moates, Elizabeth Royer, Jacob Adam, and the University of South Florida 2021 archaeological field school students for their invaluable assistance in the field. We thank Florida Department of Environmental Protection, the Florida Park Service, Tampa Bay Aquatic Preserves, and Florida Division of Historical Resources for permitting access to research sites. We also thank two anonymous reviewers for insightful comments that improved the quality of this manuscript.

LITERATURE CITED

Alonso, A.; Nelson, A.G.; Yurek, S.; Kaplan, D.; Olabarrieta, M., and Frederick, P., 2022. Estimating the influence of oyster reef chains on freshwater detention at the estuary scale using Landsat-8 imagery. *Estuaries and Coasts*, 45, 1–16.

Anderson, D.G.; Echeverry, D.; Miller, D.S.; White, A.A.; Yerka, S.J.; Kansa, E.; Kansa, S.W.; Moore, C.R.; Myers, K.N.; Wells, J.J.; Bissett, T.G., and Smallwood, A.M., 2019. Paleoindian settlement in the southeastern United States: The role of large databases. *In*: Thulman, D.K. and Ervan, G.G. (eds.), *New Directions in the Search of the First Floridians*. Gainesville, Florida: University Press of Florida, pp. 241–275.

Anderson, D.G.; Miller, D.G.; Yerka, S.J.; Gillam, J.C.; Johanson, E.N.; Anderson, D.T.; Goodyear, A.C., and Smallwood, A.M., 2010. PIDBA (Paleoindian Database of the Americas) 2010: Current status and findings. *Archaeology of Eastern North America*, 38, 63–89.

Arnold, T.E.; Kenney, W.F.; Curtis, J.H.; Bianchi, T.S., and Brenner, M., 2018. Sediment biomarkers elucidate the Holocene ontogeny of a shallow lake. *PLoS ONE*, 13(1), e0191073.

Austin, R.J.; DuChemin, G.R.; Lanning, B.; Altes, K.; Newsom, L.A., and Cannarozzi, N.R., 2018. Phase III data recovery and archaeological monitoring, 8MA6A, Perico Island North Midden, Harbour Isles Marina Project, Manatee County, Florida. Tampa, Florida: Compliance report prepared for Minto Marina, LLC. 731p.

Austin, R.J. and Mitchem, J.M., 2014. Chronology, site formation, and the Woodland–Mississippian transition at Bayshore Homes, Florida. *Southeastern Archaeology*, 33(1), 68–86.

Austin, R.J.; Mitchem, J.M., and Weisman, B.R., 2014. Radiocarbon dates and the late prehistory of Tampa Bay. *In:* Wallis, N.J. and Randal, A.R. (eds.), *New Histories of Pre-Columbian Florida*. Gainesville, Florida: University Press of Florida, pp. 94–120.

Bailey, G. and Milner, N., 2003. Coastal hunter-gatherers and social evolution: Marginal or central? *Before Farming*, 3/4, 1–15.

Baird, D. and Ulanowicz, R.E., 1993. Comparative study on the trophic structure, cycling and ecosystem properties of four tidal estuaries. *Marine Ecology Progress Series*, 99, 221–237.

Balsillie, J.H., 1995. William F. Tanner on environmental clastic granulometry. Tallahassee, Florida: Florida Geological Survey Special Publication No. 40, 142p.

Balsillie, J.H. and Donoghue, J.F., 2004. High resolution sea-level history for the Gulf of Mexico since the Last Glacial Maximum. Tallahassee, Florida: Florida Geological Survey Report of Investigations No. 103, 65p.

Balsillie, J.H. and Donoghue, J.F., 2011. Northern Gulf of Mexico sea-level history for the past 20,000 years. *In:* Buster, N.A. and Holmes, C.W. (eds.), *Gulf of Mexico Origin, Waters, and Biota: Volume 3, Geology*. College Station, Texas: Texas A&M University Press, pp. 53–69.

Bertran, P.; Bateman, M.D.; Hernandez, M.; Mercier, N.; Millet, D.; Sitzia, L., and Tastet, J.P., 2011. Inland aeolian deposits of southwest France: Facies, stratigraphy and chronology. *Journal of Quaternary Science*, 26(4), 374–388.

Bronk Ramsey, C., 2009. Bayesian analysis of radiocarbon dates. *Radiocarbon*, 51, 337–360.

Brooks, G.R., 2011. Florida Gulf Coast estuaries: Tampa Bay and Charlotte Harbor. *In:* Buster, N.A. and Holmes, C.W. (eds.), *Gulf of Mexico Origin, Waters, and Biota: Volume 3, Geology*. College Station, Texas: Texas A&M University Press, pp. 73–87.

Brooks, G.R. and Doyle, L.J., 1998. Recent sedimentary development of Tampa Bay, Florida: A microtidal estuary incised into Tertiary platform carbonates. *Estuaries*, 21(3), 391–406.

Brooks, G.R.; Doyle, L.J.; Johansson, R.; Squires, A.; Zsoldos, H.D., and Byrne, R.H., 1991. Distribution patterns and accumulation rates of fine-grained sediments in upper Tampa Bay, Florida. *Gulf Coast Association of Geological Societies Transactions*, 41, 60–71.

Brooks, G.R.; Doyle, L.J.; Suthard, B.C.; Locker, S.D., and Hine, A.C., 2003. Facies architecture of the mixed carbonate/siliciclastic inner continental shelf of west-central Florida: Implications for Holocene barrier development. *Marine Geology*, 200, 325–349.

Brooks, G.R.; Larson, R.A.; Edgar, N.T.; Pierce, R.H.; Wetzel, D.; Holmes, C.W., and Henry, M., 2004. Holocene depositional history in two Florida Gulf Coast estuaries: Tampa Bay and Charlotte Harbor. *Geological Society of America Abstracts with Programs*, 36(5), 301.

Brush, G.C., 2009. Historical land use, nitrogen, and coastal eutrophication: A paleoecological perspective. *Estuaries and Coasts*, 32, 18–28.

Bullen, R.P., 1952. The Harbor Key site, Manatee County, Florida. *Florida Anthropologist*, 5(1–2), 21–23.

Burger, B.W., 1979. *Man in the Coastal Zone: Bishop Harbor/Terra Ceia Island, Manatee County, Florida*. Sarasota, Florida: New College of the University of South Florida, 180p.

Burger, B.W., 1986. Salvage Excavations of the Bishop Harbor archaeological site located in section 31, township 35 east, range

18 east, Manatee County, Florida. Tallahassee, Florida: Florida Division of Historical Resources.
Cáceres, L.M.; Gómez, P.; González-Regalado, M.L.; Clemente, M.J.; Rodríguez-Vidal, J.; Toscano, A.; Monge, G.; Abad, M.; Izquierdo, T.; Monge-Soares, A.M.; Ruiz, F.; Campos, J.M.; Bermejo, J.; Martínez-Aguirre, A., and López, G.I., 2018. Modelling the mid-late Holocene evolution of the Huelva Estuary and its human colonization, South-Western Spain. *Marine Geology*, 406, 12–26.
Cook-Hale, J.W.; Hale, N.L., and Garrison, E.G., 2019. What is past is prologue: Excavations at the Ecofina Channel site, Apalachee Bay, Florida, USA. *Southeastern Archaeology*, 38(1), 1–22.
Cronin, T.; Edgar, N.T.; Brooks, G.R.; Hastings, D.; Larson, R.A.; Hine, A.C.; Locker, S.; Suthard, B.; Flower, B.; Hollander, D.; Wehmiller, J.; Willard, D., and Smith, S., 2007. Sea level rise in Tampa Bay. *Eos*, 88(10), 117–118.
Dalrymple, R.W.; Zaitlin, B.A., and Boyd, R., 1992. Estuarine facies models: Conceptual basis and stratigraphic implications. *Journal of Sedimentary Petrology*, 62(6), 1130–1146.
Daniel, I.R. and Wisenbaker, M., 1987. *Harney Flats: A Florida Palei-Indian Site*. Farmingdale, New York: Baywood Publishing Co., 288p.
Davis R.A., 1994. Barriers of the Florida Gulf Peninsula. *In:* R.A. Davis (ed.), *Geology of Holocene Barrier Island Systems*. Heidelberg, Germany: Springer-Verlag, pp. 167–206.
Davis, R.A., 2011. Beaches, barrier islands, and inlets of the Florida Gulf Coast. *In:* Buster, N.A. and Holmes, C.W. (eds.), *Gulf of Mexico Origin, Waters, and Biota: Volume 3, Geology.* College Station, Texas: Texas A&M University Press, pp. 89–99.
Davis, R.A.; Yale, K.E.; Pekala, J.M., and Hamilton, M.V., 2003. Barrier island stratigraphy and Holocene history of west-central Florida. *Marine Geology*, 200, 103–123.
Dean, W.E., 1974. Determination of carbonate and organic matter in calcareous sediments and sedimentary rocks by loss on ignition: Comparison with other methods. *Journal of Sedimentary Petrology*, 44, 242–248.
Delcourt, P.A., 1985. The influence of late-Quaternary climatic and vegetational change on paleohydrology in unglaciated eastern North America. *Ecologia Mediterranea*, 11(1), 17–26.
Delcourt, P.A. and Delcourt, H.R., 2004. *Prehistoric Native Americans and Ecological Change: Human Ecosystems in Eastern North America since the Pleistocene*. Cambridge: Cambridge University Press, 203p.
Donahue, B.T.; Hine, A.C.; Tebbens, S.; Locker, S.D., and Twichell, D.C., 2003. Late Holocene estuarine–inner shelf interactions; is there evidence of an estuarine retreat path for Tampa Bay, Florida? *Marine Geology*, 200, 219–241.
Donders, T.H., 2014. Middle Holocene humidity increase in Florida: Climate or sea-level? *Quaternary Science Reviews*, 103, 170–174.
Doyle, L.J.; Brooks, G.R.; Fanning, K.A.; Van Vleet, E.S.; Byrne, R.H., and Blake, N.J., 1989. *A Characterization of Tampa Bay Sediments*. Tampa, Florida: Center for Nearshore Marine Science, 100p.
Draskovich, H.E., 2021. Rethinking Settlement Patterns at the Weedon Island Site (8PI1) on Florida's Central Gulf Coast. Tampa, Florida: University of South Florida Master's thesis, 183p.
Duncan, D.S.; Locker, S.D.; Brooks, G.R.; Hine, A.C., and Doyle, L.J., 2003. Mixed carbonate–siliciclastic infilling of a Neogene carbonate shelf-valley system: Tampa Bay, west-central Florida. *Marine Geology*, 200, 125–156.
Elliott, M. and Whitfield, A.K., 2011. Challenging paradigms in estuarine ecology and management. *Estuarine, Coastal and Shelf Science*, 94, 306–314.
Evans, M.W.; Hine, A.C.; Belknap, D.F., and Davis, R.A., 1985. Bedrock controls on barrier island development: West-central Florida coast. *Marine Geology*, 63, 263–283.
Faught, M.K., 2004. Submerged paleoindian and archaic sites of the Big Bend, Florida. *Journal of Field Archaeology*, 29(3–4), 273–290.
Faught, M.K. and Pevny, C.D., 2019. Pre-Clovis to the early archaic: Human presence, expansion, and settlement in Florida over four millennia. *PaleoAmerica*, 5(1), 73–87.
Fletcher, C.H.; Van Pelt, J.E.; Brush, G.C., and Sherman, J., 1993. Tidal wetland record of Holocene sea-level movements and climate history. *Palaeogeography, Palaeoclimatology, Palaeoecology*, 102, 177–213.
Gamble, L.H., 2017. Feasting, ritual practices, social memory, and persistent places: New interpretations of shell mounds in southern California. *American Antiquity*, 83(3), 427–451.
Gerlach, M.J.; Engelhart, S.E.; Kemp, A.C.; Moyer, R.P.; Smoak, J.M.; Bernhardt, C.E., and Cahill, N., 2017. Reconstructing common era relative sea-level change on the Gulf Coast of Florida. *Marine Geology*, 390, 254–269.
Giaime, M.; Artzy, M.; Jol, H.M.; Salmon, Y.; López, G.I., and Hamid, A.A., 2022. Refining late-Holocene environmental change of the Akko coastal plain and its impacts on the settlement and anchorage patterns of Tel Akko (Israel). *Marine Geology*, 447, 106778.
Goodbred, S.L.; Wright, E.E., and Hine, A.C., 1998. Sea-level change and storm-surge deposition in a late Holocene Florida salt marsh. *Journal of Sedimentary Research*, 68(2), 240–252.
Goodyear, A.C.; Upchurch, S.B.; Brooks, M.J., and Goodyear, N.N., 1983. Paleo-Indian manifestations in the Tampa Bay region, Florida. *Florida Anthropologist*, 36(1–2), 40–66.
Grier, C., 2014. Landscape construction, ownership and social change in the southern Gulf Islands of British Columbia. *Canadian Journal of Archaeology*, 38(1), 211–249.
Grier, C.; Angelbeck, B., and McLay, E., 2017. Terraforming and monumentality as long-term social practice in the Salish Sea region of the Northwest Coast of North America. *Hunter Gatherer Research*, 3.1, 107–132.
Grimm, E.C.; Watts, W.A.; Jacobson, G.L.; Hansen, B.C.S.; Almquist, H.R., and Dieffenbacher-Krall, A.C., 2006. Evidence for warm wet Heinrich events in Florida. *Quaternary Science Reviews*, 25, 2197–2211.
Halligan, J.J., 2021. Crossing the water line: Integrating terrestrial and submerged site investigations in the Aucilla River, Florida. *Journal of Island and Coastal Archaeology*, 16(1), 46–63.
Halligan, J.J., 2022. Submerged inland landscapes of the Aucilla basin, Northwest Florida, USA: Populating the late Pleistocene and early-Holocene landscape. *World Archaeology*, 54(1), 122–141.
Halligan, J.J.; Waters, M.R.; Perrotti, A.; Owens, I.J.; Feinberg, J.M.; Bourne, M.D.; Fenerty, B.; Winsborough, B.; Carlson, D.; Fisher, D.C.; Stafford, T.W., and Dunbar, J.S., 2016. Pre-Clovis occupation 14,550 years ago at the Page-Ladson site, Florida, and the peopling of the Americas. *Science Advances*, 2, e1600375.
Hawkes, A.D.; Kemp, A.C.; Donnelly, J.P.; Horton, B.P.; Peltier, W.R.; Cahill, N.; Hill, D.F.; Ashe, E., and Alexander, C.R., 2016. Relative sea-level change in northeastern Florida (USA) during the last ~8.0 ka. *Quaternary Science Reviews*, 142, 90–101.
Hesterberg, S.G.; Jackson, K., and Bell, S.S., 2022. Climate drives coupled regime shifts across subtropical estuarine ecosystems. *Proceedings of the National Academy of Sciences of the United States of America*, 119(33), e2121654119.
Hine, A.C.; Brooks, G.R.; Davis, R.A.; Duncan, D.S.; Locker, S.D.; Twichell, D.C., and Gelfenbaum, G., 2003. The west-central Florida inner shelf and coastal system: A geologic conceptual overview and introduction to the special issue. *Marine Geology*, 200, 1–17.
Hine, A.C.; Suthard, B.C.; Locker, S.D.; Cunninghan, K.J.; Duncan, D.S.; Evans, M., and Morton, R.A., 2009. Karst sub-basins and their relationship to the transport of Tertiary siliciclastic sediments on the Florida Platform. *International Association of Sedimentology Special Publication*, 41, 179–197.
Hutton, J., 1986. Bedrock Control, Sedimentation and Holocene Evolution of the Marsh Archipelago Coast, West-Central Florida. Tampa, Florida: University of South Florida, Master's thesis, 121p.
Jackson, J.B.C.; Kirby, M.X.; Berger, W.H.; Bjorndal, K.A.; Botsford, L.W.; Bourque, B.J.; Bradbury, R.H.; Cooke, R.; Erlandson, J.; Estes, J.A.; Hughes, T.P.; Kidwell, S.; Lange, C.B.; Lenihan, H.S.; Pandolfi, J.M.; Peterson, C.H.; Steneck, R.S.; Tegner, M.J., and Warner, R.R., 2001. Historical overfishing and the recent collapse of coastal ecosystems. *Science*, 293, 629–637.
Jackson, K.; Brooks, G.R., and Larson, R.A., 2021. Of marsh and mangrove: Coupled biophysical and anthropogenic drivers of 20th century wetland conversion in Tampa Bay Estuary, Florida (USA). *Anthropocene*, 34, 100295.

Joy, S., 2019. The trouble with the curve: Reevaluating the Gulf of Mexico sea-level curve. *Quaternary International*, 525, 103–113.
Kennett, D.J. and Kennett, J.P., 2006. Early state formation in southern Mesopotamia: Sea levels, shorelines, and climate change. *Journal of Island and Coastal Archaeology*, 1(1), 67–99.
Kenney, W.F.; Brenner, M.; Curtis, C.H.; Arnold, E., and Schelske, C.L., 2016. A Holocene sediment record of phosphorous accumulation in shallow Lake Harris, Florida (USA) offers new perspectives on recent cultural eutrophication. *PLoS ONE*, 11(1), e0147331.
Kirby, M.X., 2004. Fishing down the coast: Historical expansion and collapse of oyster fisheries along continental margins. *Proceedings of the National Academy of Sciences of the United States of America*, 101(35), 13096–13099.
Kolianos, P.E., 2020. The archaeology of the Anclote River region, Florida. *Florida Anthropologist*, 73, 273–307.
Lammertsma, E.I.; Donders, T.H.; Pearce, C.; Cremer, H.; Gaiser, E.E., and Wagner-Cremer, F., 2015. Sensitivity of wetland hydrology to external climate forcing in central Florida. *Quaternary Research*, 84, 287–300.
Lane, P.; Donnelly, J.P.; Woodruff, J.D., and Hawkes, A.D., 2011. A decadally-resolved paleohurricane record archived in the late Holocene sediments of a Florida sinkhole. *Marine Geology*, 287, 14–30.
Lanesky, D.E.; Logan, B.W.; Brown, B.W., and Hine, A.C., 1979. A new approach to portable vibracoring underwater and on land. *Journal of Sedimentary Petrology*, 49, 54–57.
Larson, R.A.; Brooks, G.R., and Edgar, N.T., 2004. Sedimentary architecture of Tampa Bay, Florida: A complex infilling history. *Geological Society of America Abstracts with Programs*, 36(50), 301.
Larson, R.A.; Brooks, G.R.; Edgar, N.T.; Swarzinski, P., and Cronin, T., 2006. *Sedimentary Record in Tampa Bay, Florida: Anthropogenic Implications*. Paper presented at: American Geophysical Union ASLO Ocean Sciences Convention, Honolulu, Hawaii.
LaViolette, A. and Fleisher, J., 2009. The urban history of a rural place: Swahili archaeology on Pemba Island, Tanania, 700–1500 AD. *International Journal of African Historical Studies*, 42(3), 433–455.
Li, C.; Wang, P.; Sun, H.; Zhang, J.; Fan, D., and Deng, B., 2002. Late Quaternary incised-valley fill of the Yangtze delta (China): Its stratigraphic framework and evolution. *Sedimentary Geology*, 152, 133–158.
Liu, K.B. and Fearn, M.L., 2000. Reconstruction of prehistoric landfall frequencies of catastrophic hurricanes in northwestern Florida from lake sediment records. *Quaternary Research*, 54, 238–245.
Lotze, H.K.; Lenihan, H.S.; Bourque, B.J.; Bradbury, R.H.; Cooke, R.G.; Kay, M.C.; Kidwell, S.M.; Kirby, M.X.; Peterson, C.H., and Jackson, J.B.C., 2006. Depletion, degradation, and recovery potential of estuaries and coastal seas. *Science*, 312, 1806–1809.
Luer, G.M., 2007. Mound Building and Subsistence during the Late Weedon Island Period (ca. AD 700-1000) at Big Mound Key (8CH10), Florida. Gainesville, Florida: University of Florida, Ph.D. dissertation, 947p.
Luer, G.M. and Almy, M.M., 1982. A definition of the Manasota culture. *Florida Anthropologist*, 35(1), 34–58.
Lunt, J.; Reustle, J., and Smee, D.L., 2017. Wave energy and flow reduce the abundance and size of benthic species on oyster reefs. *Marine Ecology Progress Series*, 569, 25–36.
Mason, R.D.; Peterson, M.L., and Tiffany, J.A., 1998. Weighing vs. counting: Measurement reliability and the California school of midden analysis. *American Antiquity*, 63, 303–324.
McFadden, P.S., 2014. Archaeological investigations of threatened stratified sites in Horseshoe Cove, northern Gulf Coast, Florida. *Florida Anthropologist*, 67(4), 179–195.
McFadden, P.S., 2016. Coastal dynamics and Pre-Columbian human occupation in Horseshoe Cove on the northern Gulf Coast of Florida, USA. *Geoarchaeology*, 31(5), 355–375.
McLusky, D.S. and Elliot, M., 2007. Transitional waters: A new approach, semantics, or just muddying the waters? *Estuarine, Coastal and Shelf Science*, 71, 359–363.
Parkinson, R.W., 1989. Decelerating Holocene sea-level rise and its influence on southwest Florida coastal evolution: A transgressive/regressive stratigraphy. *Journal of Sedimentary Petrology*, 59(6), 960–972.
Pinto, R.; Patrício, J.; Magalhães-Neto, J.; Salas, F., and Marques, J.C., 2010. Assessing estuarine quality under the ecosystem services scope: Ecological and socioeconomic aspects. *Ecological Complexity*, 7, 389–402.
Pluckhahn, T.J.; Jackson, K., and Rogers, J.A., 2021. Hidden in plain sight: Digital documentation of Cockroach Key (8HI2), a first millennium Native American mound complex on the western coast of Florida, USA. *Studies in Digital Heritage*, 5(2), 107–130.
Pluckhahn, T.J.; Jackson, K., and Rogers, J.A., 2022. "Let us all enjoy the fish": AlterNative pathways and contingent histories of collective action and governance among maritime societies of the western peninsular coast of Florida, USA, 100–1600 CE. *Frontiers in Political Science*, 4, 804084.
Pluckhahn, T.J. and Thompson, V.D., 2017. Woodland-period mound building as historical tradition: Dating the mounds and monuments at Crystal River. *Journal of Archaeological Science: Reports*, 15, 73–94.
Pluckhahn, T.J. and Thompson, V.D., 2018. New Histories of Village Life at Crystal River. Gainesville, Florida: University Press of Florida, 298p.
Pluckhahn, T.J.; Thompson, V.D., and Rink, J.W., 2016. Evidence for stepped pyramids of shell in the woodland period of eastern North America. *American Antiquity*, 81(2), 345–363.
Pollock, A.L.; van Beynen, P.E.; DeLong, K.L.; Polyak, V., and Asmerom, Y., 2017. A speleothem-based mid-Holocene precipitation reconstruction for west-central Florida. *Holocene*, 27(7), 987–996.
Pritchard, D.W., 1967. What is an estuary? Physical viewpoint. *In:* Lauff, G.H. (ed.), *Estuaries*. Washington, D.C.: American Association for the Advancement of Science, Publication 83, pp 3–5.
Punwong, P.; Selby, K., and Marchant, R., 2018. Holocene mangrove dynamics and relative sea-level changes along the Tanzanian coast, East Africa. *Estuarine, Coastal and Shelf Science*, 212, 105–117.
Purdy, B.A. and Hine, A.C., 2021. Paleo-Americans and the potential for Florida offshore paleohabitation sites in the Gulf of Mexico. *Florida Anthropologist*, 73(4), 262–272.
Raabe, E.A.; Roy, L.C., and McIvor, C.C., 2012. Tampa Bay coastal wetlands: Nineteenth to twentieth century tidal marsh-to-mangrove conversion. *Estuaries and Coasts*, 35, 1145–1162.
Radabaugh, K.R.; Dontis, E.E.; Chappel, A.R.; Russo, C.E., and Moyer, R.P., 2021. Early indicators of stress in mangrove forests with altered hydrology in Tampa Bay, Florida, USA. *Estuarine, Coastal, and Shelf Science*, 254, 107324.
Radabaugh, K.R.; Moyer, R.P.; Chappel, A.R.; Powell, C.E.; Bociu, I.; Clark, B.C., and Smoak, J.M., 2018. Coastal blue carbon assessment of mangroves, salt marshes, and salt barrens in Tampa Bay, Florida, USA. *Estuaries and Coasts*, 41, 1496–1510.
Randall, A.R. and Sassaman, K.E., 2017. Terraforming the middle ground in ancient Florida. *Hunter Gatherer Research*, 3.1, 9–29.
Reimer, P.J.; Austin, W.E.N.; Bard, E.; Bayliss, A.; Blackwell, P.G.; Bronk-Ramsey, C.; Butzin, M.; Cheng, H.; Lawrence-Edwards, R.; Friedrich, M.; Grootes, P.M.; Guilderson, T.P.; Hajdas, I.; Heaton, T.J.; Hogg, A.G.; Highen, K.A.; Kromer, B.; Manning, S.W.; Muscheler, R.; Palmer, J.G.; Pearson, C.; van der Plicht, J.; Reimer, R.W.; Richards, D.A.; Marian-Scott, E.; Southon, J.R.; Turney, C. S.M.; Wacker, L.; Adolphi, F.; Büntgen, U.; Capano, M.; Fahrni, S.M.; Fogtmann-Schultz, A.; Friedrich, R.; Köhler, P.; Kudsk, S.; Miyake, F.; Olsen, J.; Reinig, F.; Sakamoto, M.; Sookdeo, A., and Talamo, S., 2020. The IntCal20 northern hemisphere radiocarbon age calibration curve (0–55 cal kBP). *Radiocarbon*, 62(4), 725–757.
Reitz, E.J. and Wing, E.S., 2008. *Zooarchaeology*. New York: Cambridge University Press, 558p.
Riddick, N.L.; Boyce, J.I.; Şahoğlu, V.; Erkanal, H.; Tuğcu, I.; Alkan, Y.; Reinhardt, E.G., and Goodman-Tchernov, B.N., 2022. Coastal palaeoenvironmental record of late Bronze Age to Iron Age harbour development at Liman Tepe-Clazomenae, western Anatolia, Turkey. *Marine Geology*, 450, 106842.

Rogers, J.A. and Jackson, K., 2022. Sea-level rise, storm surge, and the transformation of coastal shellworks in the upper reaches of the Tampa Bay Estuary. Paper presented at: Florida Anthropological Society Conference, Miami, Florida.

Russo, M. and Quitmyer, I.R., 2008. Developing models of settlement for the Florida Gulf Coast. *In:* Reitz, E.J.; Scarry, C.M., and Scudder, S.J. (eds.), *Case Studies in Environmental Archaeology*. New York: Springer Science, pp. 235–254.

Sassaman, K.E.; Wallis, N.J.; McFadden, P.S.; Mahar, G.J.; Jenkins, J.A.; Donop, M.C.; Monés, M.P.; Palmiotto, A.; Boucher, A.; Goodwin, J.M., and Oliveira, C.I., 2017. Keeping pace with rising sea: the first 6 years of the Lower Suwannee Archaeological Survey, gulf coastal Florida. *Journal of Island and Coastal Archaeology*, 12(2), 173–199.

Saunders, R. and Russo, M., 2011. Coastal shell middens in Florida: A view from the Archaic period. *Quaternary International*, 239, 38–50.

Schwadron, M. 2017. Shellworks: Prehistoric terraformed communities of the Ten Thousand Islands, Florida. *Hunter Gatherer Research*, 3.1, 31–63.

Scott, T.M., 2011. Geology of the Florida platform: Pre-Mesozoic to recent. *In:* Buster, N.A. and Holmes, C.W. (eds.), *Gulf of Mexico Origin, Waters, and Biota: Volume 3, Geology*. College Station: Texas A&M University Press, pp. 17–31.

Shannon, C.E. and Weaver, W., 1949. *The Mathematical Theory of Communication*. Urbana, Illinois: University of Illinois Press, 144p.

Sheldon, A.L., 1969. Equitability indices: Dependence on the species count. *Ecology*, 50, 466–467.

Sizov, O.; Konstantinov, A.; Volvakh, A., and Molodkov, A., 2020. Timing and sedimentary record of late-Quaternary fluvio-aeolian successions of the Tura-Pyshma Interfluve (SW western Siberia, Russia). *Geosciences*, 10, 396.

Stahl, L.E., 1970. The Marine Geology of Tampa Bay. Tallahassee, Florida: Florida State University, Master's thesis, 70p.

Stapor, F.W.; Mathews, T.D., and Lindfors-Kearns, F.E., 1991. Barrier-island progradation and Holocene sea-level history in southwest Florida. *Journal of Coastal Research*, 7(3), 815–838.

Stathakopoulos, A.; Riegl, B.M., and Toth, L.T., 2020. A revised Holocene coral sea-level database from the Florida reef tract, USA. *PeerJ*, 8, e8350.

Suthard, B.C., 2005. A siliciclastic-infilled sedimentary basin within a large carbonate platform, Tampa Bay, Florida. St. Petersburg, Florida: University of South Florida, Master's thesis, 79p.

Tanabe, S.; Nakashima, R., and Mizuno, K., 2022. Holocene filling of a narrow estuary in a regressive coast: the Paleo-Kinu Bay region, central Japan. *Marine Geology*, 447, 106795.

Tanner, W.F., 1992. Late-Holocene sea-level changes from grain-size data: Evidence from the Gulf of Mexico. *Holocene*, 2, 249–254.

Thompson, V.D.; Marquardt, W.H.; Cherkinsky, A.; Roberts-Thompson, A.D.; Walker, K.J.; Newsom, L.A., and Savarese, M., 2016. From shell midden to midden-mound: the geoarchaeology of Mound Key, an anthropogenic island in southwest Florida, USA. *PLoS ONE*, 11(4), e0154611.

Thompson, V.D.; Marquardt, W.H.; Walker, K.J.; Thompson, A.R., and Newsom, L.A., 2018. Collective action, state building, and the rise of the Calusa, Southwest Florida. *Journal of Anthropological Archaeology*, 51, 28–44.

Thompson V.D.; Rick, T.; Garland, C.J.; Smith, K.Y.; Thomas, D.H.; Sanger, M.; Tucker, B.; Lulewicz, I.; Semon, A.M.; Schalles, J.; Hladik, C.; Alexander, C., and Ritchison, B.T., 2020. Ecosystem stability and Native American oyster harvesting along the Atlantic Coast of the United States. *Science Advances*, 6, eaba9652.

Thulman, D.K., 2009. Freshwater availability as the constraining factor in the middle Paleoindian occupation of north-central Florida. *Geoarchaeology*, 24(3), 243–276.

van Beynen, P.; Polk, J.S.; Asmerom, Y., and Polyak, V., 2017. Late Pleistocene and mid-Holocene climate change derived from a Florida speleothem. *Quaternary International*, 449, 75–82.

van de Plassche, O., 1991. Late Holocene sea-level fluctuations on the shore of Connecticut inferred from transgressive and regressive overlap boundaries in salt-marsh deposits. *In:* Gayes, P.T.; Lewis, R.S., and Bokuniewicz, H.J. (eds.), *Quaternary Geology of Long Island Sound and Adjacent Coastal Areas: Walter S. Newman Memorial Volume*. *Journal of Coastal Research*, Special Issue No. 11, pp. 159–179.

van Soelen, E.E.; Brooks, G.R.; Larson, R.A.; Sinninghe-Damsté, J.S., and Reichart, G.J., 2012. Mid- to late-Holocene coastal environmental changes in southwest Florida, USA. *Holocene*, 22(8), 929–938.

van Soelen, E.E.; Lammertsma, E.I.; Cremer, H.; Donders, T.H.; Sangiorgi, F.; Brooks, G.R.; Larson, R.A.; Sinninghe-Damsté, J.S.; Wagner-Cremer, F., and Reichart, G.J., 2010. Late Holocene sea-level rise in Tampa Bay: Integrated reconstruction using biomarkers, pollen, organic-walled dinoflagellate cysts, and diatoms. *Estuarine, Coastal and Shelf Science*, 86, 216–224.

Walker, K.J., 2013. Excavations and chronostratigraphy at the Pineland site complex:1988–1995. *In:* Marquardt, W.H. and Walker, K.J. (eds.), *The Archaeology of Pineland: A Coastal Southwest Florida Site Complex, A.D. 50–1710*. Institute of Archaeology and Paleoenvironmental Studies, Monograph 4. Gainesville, Florida: University Press of Florida, pp. 23–52.

Walker, K.J.; Stapor, F.W., and Marquardt, W.H., 1995. Archaeological evidence for a 1750–1450 BP higher-than-present sea level along Florida's Gulf Coast. *In:* Finkl, C.W., Jr. (ed.), *Holocene Cycles: Climate, Sea Level, and Sedimentation*. *Journal of Coastal Research*, Special Issue No. 17, pp. 205–218.

Wang, P. and Beck, T.M., 2022. *Beach–Inlet Interaction and Sediment Management*. Cambridge: Cambridge University Press, 363pp.

Wanless, H.R., 1982. Sea level is rising—So what? *Journal of Sedimentary Petrology*, 52, 1051–1054.

Watts, W.A., 1969. A pollen diagram from Mud Lake, Marion County, north-central Florida. *Geological Society of America Bulletin*, 80, 631–642.

Watts, W.A., 1971. Postglacial and interglacial vegetation history of southern Georgia and central Florida. *Ecology*, 52(4), 676–690.

Watts, W.A., 1975. A late Quaternary record of vegetation from Lake Annie, south-central Florida. *Geology*, 3, 344–346.

Watts, W.A., 1980. The late Quaternary vegetation history of the southeastern United States. *Annual Review of Ecology and Systematics*, 11, 287–409.

Watts, W.A. and Hansen, B.C.S., 1994. Pre-Holocene and Holocene pollen records of vegetation history from the Florida peninsula and their climatic implications. *Palaeogeography, Palaeoclimatology, Palaeoecology*, 109, 163–176.

White, W.A., 1970. *TheGgeomorphology of the Florida Peninsula*. Tallahassee, Florida: State of Florida Department of Natural Resources, Bureau of Geology, Geological Bulletin No. 51, 164p.

Whitfield, A. and Elliott, M., 2011. Ecosystem and biotic classifications of estuaries and coasts. *In:* Wolanski, E. and McLusky, D.S. (eds.), *Treatise on Estuarine and Coastal Science, Volume 1*. Waltham, Massachusetts: Academic Press, pp. 99–124.

Willard, D.A.; Bernhardt, C.E.; Brooks, G.R.; Cronin, T.M.; Edgar, T., and Larson, R.A., 2007. Deglacial climate variability in central Florida, USA. *Palaeogeography, Palaeoclimatology, Paleoecology*, 251, 366–382.

Willis, J.W., 1984. The Shallow Structure of Tampa Bay. St. Petersburg, Florida: University of South Florida, Master's thesis, 85p.

Wright, E.E.; Hine, A.C.; Goodbred, S.L., and Locker, S.D., 2005. The effect of sea-level and climate on the development of a mixed siliciclastic–carbonate, deltaic coastline: Suwannee River, Florida, U.S.A. *Journal of Sedimentary Research*, 75, 621–635.

Wright, H.E., 1981. The role of fire in land/water interactions. *In:* Mooney, H.A.; Bonnickson, T.M.; Christensen, N.L.; Lotan, J.E., and Reiners, W.A. (eds.), *Fire Regimes and Ecosystem Properties*. Washington D.C.: U.S. Forest Service General Technical Report WO-26, pp. 421–444.

Yao, Q.; Liu, K.B.; Rodrigues, E.; Bianchette, T.; Aragón-Moreno, A.A., and Zhang, Z., 2020. A geochemical record of late-Holocene hurricane events from the Florida Everglades. *Water Resources Research*, 56, e2019WR026857.

Zedler, J.B. and Kercher, S., 2005. Wetland resources: Status, trends, ecosystem services, and restorability. *Annual Review of Environmental Resources*, 30, 39–74.

APPENDIX

Table 1A. *Summaries of physical sedimentological and qualitative data by subfacies (*N = *363 samples). Granulometric data for all analyzed samples are available in Supplementary Data.*

Facies/ Subfacies	Mean Size (phi)	Sorting (phi)	Mud (%)	Sand (%)	Gravel (%)	Total Organic Matter (%)	$CaCO_3$ (%)	Color/Inclusions/Age	Notes on Thickness, *etc.*
Blue-Green Clay Residuum								Gley-blue to white, veins of yellowish red oxidation; dense mud, sandier near upper contacts; Miocene	Basal, thickest recovery ~0.5 m
Mean	3.23	0.88	44	55.6	0.4	13.9	1.4		
Range	2.75–4.69	0.77–1.09	16–73	27–84	0–1	8–26	0–3		
Phosphatic Limestone Residuum								Greyscale; phosphate gravel common; Miocene	Basal, thickest recovery ~0.8 m
Mean	0.76	2.94	13	56	31	3	14		
Range	−0.74–2.25	1.63–2.94	4–23	42–70	7–54	1–5	11–18		
Muddy Shelly Sand								Light grey to gley-blue; whole to fragmentary estuarine mollusk shell; Plio/ Pleistocene?	1.5 to 2-m thick
Mean	0.54	2.45	14	38	49	2	24		
Range	0.20–0.85	1.69–3.05	10–17	29–50	33–61	2–3	21–27		
Organic Muddy Sand (Pleistocene)								Brown to black; woody or herbaceous macrobotanicals; terminal Pleistocene/LGM	Unconformably overlying Miocene facies, thickness <50 cm, typically 20–30 cm
Mean	3.14	0.89	30	70	1	3	15		
Range	2.71–3.48	0.79–0.97	6–53	47–92	0–2	1–7	1–34		
Brownish Fine Sand								Reddish-brown to white; macro/microfossils uncommon; late-Pleistocene/ Holocene	To ~6 m in thickness in assoc. with parabolic dune fields at WI
Mean	2.61	0.74	6	93	1	4	8		
Range	0.66–3.24	0.36–2.41	1–33	67–99	0–26	0–31	0–29		
Muddy Fine Sand								Grey to gley-blue; macro/ microfossils uncommon; deglacial Pleistocene/early Holocene	1–2-m thickness
Mean	2.90	0.70	16	84	1	14	1		
Range	2.55–3.01	0.14–1.17	10–22	78–90	0–4	1–33	0–4		
Organic Muddy Sand (Holocene)								Brown to black; herbaceous macrobotanicals and tidal–estuarine shell fragments common; Holocene	0.5- to 1.5-m thickness; accumulation rates range from 0.02 to 0.04 cm/y
Mean	2.66	0.87	12	87	1	5	8		
Range	2.34–3.02	0.53–1.73	4–30	70–96	0–8	0–53	0–29		
Mud-Laminated Sand								Grey to white; bioturbation and estuarine/marine mollusk shell fragments common (high species richness); late Holocene	0.1- to 0.5-m thick; typically, gradual contact with underlying Holocene organic muddy sand facies
Mean	2.51	0.85	6	93	1	5	7		
Range	1.84–2.84	0.56–1.86	2–13	76–98	0–13	0–24	0–36		
Freshwater Gastropod Bed								Light grey; *Viviparus georgianus* and *Planorbella* sp. shells; late Pleistocene/ early Holocene?	0.7-m thick
Mean	0.66	2.84	8	60	33	5	12		
Range	0.11–1.21	2.60–3.08	5–10	54–65	25–41	2– 9	10–14		
Oyster Reef								Light to dark grey; dense *Crassostrea virginica*, mostly whole, articulated, or culched valves; commensal mollusks common; matrix muddy, late Holocene	Thickness 0.2–1.5 m, shell and mud near surface, increasingly sandy with depth; commonly overlying coarse shelly lenses
Mean	0.50	2.88	10	51	38	3	7		
Range	−1.12–1.90	2.19–3.48	4–21	28–72	19–67	1–18	0–36		
Cardite Bed								Grey to black; *Cardites floridana,* mostly whole and articulated; seagrass-associated mollusks common; Holocene	0.2–0.5-m thick; underlying oyster reef facies in CRB. Oyster valves cemented to cardites
Mean	1.47	2.03	8	76	16	7	16		
Range	0.43–2.30	1.37–2.67	4–13	65–88	4–31	2–29	3–30		
Fossil-Shell Gravel/Shelly Sand								White to grey; *Chione cancellata* dominant (many drilled); reworked Pleistocene-age deposits (early/mid-Holocene)	0.7–1.9-m thick; uncomformably overlying LGM-age organic muddy sand, sharp contact with overlying mud-laminated sand
Mean	1.07	2.27	6	69	26	2	3		
Range	−0.02–1.79	1.71–2.86	3–12	58–83	14–39	0–5	0–9		

Table 1A. *(continued)*.

Facies/ Subfacies	Mean Size (phi)	Sorting (phi)	Mud (%)	Sand (%)	Gravel (%)	Total Organic Matter (%)	$CaCO_3$ (%)	Color/Inclusions/Age	Notes on Thickness, *etc*.
Crushed Shell Lenses								White to grey; dense fragmentary shell; high taxonomic richness; late Holocene (*ca*. 1 kya).	0.1–0.2-m thick in UTB, WI, CRB; to 0.7-m thick at BH; interbedded with mud-laminated sand facies
Mean	0.85	2.41	5	69	26	3	2		
Range	0.11–1.69	1.82–2.99	3–10	50–85	12–40	1–9	0–4		
Mangrove Peat								Grey to dark brown; mollusks uncommon, commensal taxa present; late Holocene	0.1–0.6-m thick; typically overlies Holocene OMS facies, oyster reef, or shellworks
Mean	2.68	1.34	33	63	4	28	10		
Range	0.75–3.55	0.87–2.45	10–67	33–85	0–24	10–68	0–68		
Shell Midden								Brownish grey to black; cultural artifacts abundant; *Polygyra* sp. ubiquitous; Holocene	0.2–2-m thick; accumulation rates <1.2 cm/y ($\bar{x}$ = 0.45 cm/y)
Mean	−0.48	2.75	11	35	54	5	22		
Range	−2.64–1.88	1.81–3.34	5–21	11–70	16–85	2–22	5–40		
Unconsolidated Clean Shell								White to light grey; shells often retaining natural pigments; Holocene	0.3–2+-m thick; accumulation rates highly variable, 0.2–40.0 cm/y ($\bar{x}$ = 18.8 cm/y)
Mean	−1.01	2.56	9	27	64	4	22		
Range	−3.01–0.30	2.09–2.84	4–15	4–41	50–91	1–10	1–36		
Fire/Habitation Features								Greyscale; charcoal/ash abundant; shell oxidized, burned, and fragmentary; Holocene	0.02–0.2-m thick, interbedded variably within other shellwork deposits
Mean	1.25	2.36	33	48	30	6	21		
Range	0.28–3.01	1.06–2.83	10–67	28–78	1–47	2–30	2–40		
Reworked Cultural Shell								White to light grey; small tidal-zone gastropods abundant; Holocene	0.2–1.5-m thick, typically overlying *in situ* shellwork deposits or transgressed terrestrial landforms
Mean	0.35	2.23	4	61	35	2	17		
Range	−2.59–2.63	0.77–3.16	1–11	20–98	1–79	1–10	1–37		

Table 2A. *Summaries of presence–absence faunal–macrofossil data by subfacies and study area.*

Facies/Subfacies	Upper Tampa Bay	Weedon Island	Cockroach Bay	Bishop Harbor
Blue-Green Clay Residuum	None	n/a	n/a	n/a
Phosphatic Limestone Residuum	n/a	n/a	Unidentified vertebrate fossils	Unidentified vertebrate fossils
Muddy Shelly Sand	n/a	n/a	n/a	*Ammonia* sp., *Crassostrea virginica*, *Argopecten irradians*, *Balanus* sp.
Organic Muddy Sand (Pleistocene)	None	None	None	n/a
Brownish Fine Sand	None	None	None	n/a
Muddy Fine Sand	None	None	None	n/a
Organic Muddy Sand (Holocene)	*Balanus* sp., *Geukensia* sp., *Crassostrea virginica*	*Cerithium muscarum*	*Cerithium muscarum*	*Cardites floridana*, *Balanus* sp., *Cerithium muscarum*
Mud-Laminated Sand	*Crassostrea virginica*, *Balanus* sp., *Geukensia* sp., *Urosalpinx perrugata*	*Cerithium muscarum*, *Nassarius vibex,* *Balanus* sp., *Sinistrofulgur sinistrum*, *Prunum apicinum*, *A. auberiana*	*Ammonia* sp., *Chione cancellata, Prunum apicinum*, *Mercenaria* sp., *Macrocallista nimbosa*, *Trachycardium egmontianum*, *Cerithium muscarum*, *Neverita* sp., *Balanus* sp., *C. floridana*, *N. vibex*	*Ammonia* sp., *Crassostrea virginica*, *Cerithium muscarum*, *Balanus* sp., *Neverita* sp., *Macrocallista nimbosa*, *Anomalocardia auberiana*, *Prunum apicinum*, *Persicula multilineata*, *Modulus modulus*, *Crepidula* sp., *Melongena corona*
Freshwater Gastropod Bed	n/a	n/a	*Viviparus georgianus*, *Palnorbella scalaris*	n/a
Oyster Reef	*Crassostrea virginica*, *Urosalpinx perrugata*, *Melongena corona*	*Crassostrea virginica*, *Geukensia* sp.	*Crassostrea virginica*; *Cardites floridana*	*Ammonia* sp., *Crassostrea virginica*, *Cardites floridana*, *Anomalocardia auberiana*, *Cerithium muscarum*, *Balanus* sp., *Crepidula* sp., *Urosalpinx perrugata*, *Chione cancellata*, *Modulus modulus*, *Geukensia* sp., *Persicula multilineata*, *Nassarius vibex*, *Cinctura hunteria*, *Melongena corona*
Cardite Bed	n/a	n/a	*Cardites floridana*, *Cerithium muscarum*, *Crepidula* sp., *Chione cancellata*, *Prunum apicinum*, *Anomalocardia auberiana*	*Cardites floridana*, *Persicula multilineata*, *Argopecten irradians*, Scaphandridae
Fossil-Shell Gravel	n/a	n/a	*Chione cancellata*, *Balanus* sp., *Geukensia* sp., *Cerithium muscarum*, *Macrocallista nimbosa*, *Noetia ponderosa*, *Prunum apicinum*	n/a
Crushed Shell Lenses	*Ammonia* sp., *Crassostrea virginica*, *Anomalocardia auberiana*, *Nassarius vibex*, *Cerithium muscarum*, *Balanus* sp., *Crepidula* sp., *Geukensia* sp.	*Anomalocardia auberiana*, *Macrocallista nimbosa*, *Prunum apicinum*, *Nassarius vibex*, *Balanus* sp.	*Ammonia* sp., *Mercenaria* sp., *Cardites floridana*, *Prunum apicinum*, *Balanus* sp., *Geukensia* sp., *Cerithium muscarum*, *Anomalocardia auberiana*, *Crassostrea virginica*, *Pisania tincta*, *Crepidula* sp., *Noetia ponderosa*, *Urosalpinx perrugata*, *Abra alba*, *Melampus* sp., *Sinistrofulgur sinistrum*, *Macrocallista nimbosa*, *Argopecten Irradians*	*Ammonia* sp., *Crassostrea virginica*, *Cerithium muscarum*, *Prunum apicinum*, *Balanus* sp., *Pisania tincta*, *Cardites floridanus*, *Chione cancellata,* Columbellidae, *Modulus modulus*
Mangrove Peat	*Littorina irrorata*, *Cerithium* sp.	*Littorina irrorata*, *Cerithium* sp.	*Littorina irrorata*, *Cerithium* sp.	*Littorina irrorata*, *Cerithium* sp.

Table 3A. *Summaries of quantitative mollusk–zooarchaeological data (*N = *378 samples) by cultural shell deposit subfacies and study area. Summary values are derived from the MNI data set; raw data for all analyzed samples are available in Supplementary Data.*

Cultural Shell Subfacies	Upper Tampa Bay (8HI996; 8HI6698; 8HI6699)	Weedon Island (8PI56; 8PI11491)	Cockroach Bay (8HI2)	Bishop Harbor (8MA13-15)
Shell Midden	*Crassostrea virginica* ($\bar{x}$ = 82%), *Polygyra* sp. ($\bar{x}$ = 9%), *Melongena corona* ($\bar{x}$ = 2%); richness = 23, Shannon's H = 0.49, evenness = 0.07; shell content mean = 182 kg/m^3	*Sinistrofulgur sinistrum* ($\bar{x}$ = 31%), *Crassostrea virginica* ($\bar{x}$ = 24%), *Melongena corona* ($\bar{x}$ = 24%), *Mercenaria* sp. ($\bar{x}$ = 5%), *Neverita* sp. ($\bar{x}$ = 4%), *Fulguropsis spirata* ($\bar{x}$ = 3%), *Cinctura hunteria* ($\bar{x}$ = 3%), *Polygyra* sp. ($\bar{x}$ = 3%); richness = 27, Shannon's H = 1.64, Evenness = 0.19; shell content $\bar{x}$ = 24 kg/m^3	*Crassostrea virginica* ($\bar{x}$ = 71%), *Melongena corona* ($\bar{x}$ = 14%), *Geukensia* sp. ($\bar{x}$ = 6%), *Polygyra* sp. ($\bar{x}$ = 2%), *Cinctura hunteria* ($\bar{x}$ = 2%); richness = 28, Shannon's H = 1.07, evenness = 0.10; shell content $\bar{x}$ = 555 kg/m^3	*Crassostrea virginica* ($\bar{x}$ = 74%), *Cerithium muscarum* ($\bar{x}$ = 5%), *Melongena corona* ($\bar{x}$ = 4%), *Polygyra* sp. ($\bar{x}$ = 3%), *Sinistrofulgur sinistrum* ($\bar{x}$ = 3%), *Macrocallista nimbosa* ($\bar{x}$ = 2%), *Strombus alatus* ($\bar{x}$ = 2%); richness = 30, Shannon's H = 1.08, evenness = 0.09; shell content $\bar{x}$ = 419 kg/m^3
Unconsolidated Clean Shell	n/a	n/a	*Crassostrea virginica* ($\bar{x}$ = 59%), *Melongena corona* ($\bar{x}$ = 20%), *Geukensia* sp. ($\bar{x}$ = 9%), *Fulguropsis spirata* ($\bar{x}$ = 3%), *Sinistrofulgur sinistrum* ($\bar{x}$ = 3%), *Cinctura hunteria* ($\bar{x}$ = 3%); richness = 34, Shannon's H = 1.39, evenness = 0.1176; shell content $\bar{x}$ = 630 kg/m^3	*Crassostrea virginica* ($\bar{x}$ = 65%), *Melongena corona* ($\bar{x}$ = 15%), *Balanus* sp. ($\bar{x}$ = 7%), *Sinistrofulgur sinistrum* ($\bar{x}$ = 2%); richness = 29, Shannon's H = 1.37, evenness = 0.14; shell content $\bar{x}$ = 553 kg/m^3
Fire/Habitation Feature	n/a	n/a	*Melongena corona* ($\bar{x}$ = 37%), *Crassostrea virginica* (= 21%), *Geukensia* sp. ($\bar{x}$ = 11%), *Cerithium* sp. ($\bar{x}$ = 6%), *Nassarius vibex* ($\bar{x}$ = 4%), *Neverita* sp. ($\bar{x}$ = 3%), *Cardites floridana* ($\bar{x}$ = 3%), *Cinctura hunteria* ($\bar{x}$ = 3%); richness = 21, Shannon's H = 2.06, evenness = 0.68; shell content $\bar{x}$ = 362 kg/m^3	*Crassostrea virginica* ($\bar{x}$ = 52%), *Melongena corona* ($\bar{x}$ = 14%), *Polygyra* sp. (11%), *Balanus* sp. ($\bar{x}$ = 6%), *Cinctura hunteria* ($\bar{x}$ = 4%), *Crepidula* sp. ($\bar{x}$ = 3%), *Sinistrofulgur sinistrum* ($\bar{x}$ = 2%); richness = 21, Shannon's H = 1.78, evenness = 0.28; shell content $\bar{x}$ = 281 kg/m^3
Reworked Cultural Shell	*Crassostrea virginica* ($\bar{x}$ = 65%), *Prunum apicinum* ($\bar{x}$ = 18%), *Littorina irrorata* ($\bar{x}$ = 7%), *Polygyra* sp. ($\bar{x}$ = 3%); *Melongena corona* ($\bar{x}$ = 2%); richness = 20, Shannon's H = 1.301, evenness = 0.18; shell content $\bar{x}$ = 52 kg/m^3	n/a	n/a	*Crassostrea virginica* ($\bar{x}$ = 50%), *Cerithium muscarum* ($\bar{x}$ = 23%), *Prunum apicinum* ($\bar{x}$ = 7%), *Polygyra* sp. ($\bar{x}$ = 5%), *Cardites floridana* ($\bar{x}$ = 3%), *Melongena corona* ($\bar{x}$ = 2%); richness = 38, Shannon's H = 1.78, evenness = 0.49; shell content $\bar{x}$ = 268 kg/m^3

Table 4A. *Radiocarbon results from all study areas.*

Study Area	Lab Identification (UGAMS#)	Provenience	Material	^{13}C, 0/00	^{14}C BP	±	Percent Modern Carbon	±	68.2% Probability	95.4% Probability	Cal. YBP (2-sigma)
UTB	51111	UTB-VC2, 78 cm below surface (bs)	Macrobotanical	−25.9	1960	20	78.31	0.19	30–110 CE	0–130 CE	1950–1820
UTB	51112	UTB-VC2, 134 cmbs	Organic sediment	−23.9	4100	20	60	0.16	2840–2580 BCE	2860–2570 BCE	4810–4520
UTB	56578	UTB-VC3, 81 cmbs	Wood charcoal	−26.9	840	20	90.11	0.24	1177–1255 CE	1170–1261 CE	780–689
UTB	51440	UTB-VC3, 121 cmbs	Macrobotanical	−26.8	1930	20	78.59	0.22	67–125 CE	25–203 CE	1925–1747
UTB	51441	UTB-VC3, 239 cmbs	Organic sediment	−22.87	4270	25	58.77	0.17	2904–2886 BCE	2918–2875 BCE	4868–4825
UTB	51110	UTB-VC3, 333 cmbs	Organic sediment	−21.9	31,940	100	1.88	0.02	34,420–34,210 BCE	34,570–34,100 BCE	36,520–36,040
UTB	51109	UTB-VC4, 382 cmbs	Organic sediment	−25.9	29,280	80	2.61	0.02	32,110–31,800 BCE	32,280–31,630 BCE	34,240–33,570
UTB	51114	HI6698-PC2, 50 cmbs	Macrobotanical	−25.1	310	20	96.18	0.23	1520–1640 CE	1500–1650 CE	450–300
UTB	51113	HI6698-PC3, 104 cmbs	Macrobotanical	−26	750	20	91.09	0.22	1265–1280 CE	1220–1290 CE	730–660
UTB	51439	HI6698-PC4, 75 cmbs	Charcoal	−25.7	1700	20	80.88	0.22	265–404 CE	259–413 CE	1691–1537
UTB	51115	HI6698-PC5, 96 cmbs	Macrobotanical	−25.2	1510	20	82.88	0.2	560–590 CE	540–610 CE	1410–1340
UTB	51578	HI6698-PC6, 25 cmbs	Organic sediment	−23.49	2690	20	71.54	0.19	892–809 BCE	899–806 BCE	2849–2756
UTB	55330	HI6698-PC7, 192 cmbs	Macrobotanical	−25.5	980	20	88.47	0.24	1025–1145 CE	1022–1154 CE	796–928
UTB	48208	HI6698-STP1, 40–50 cmbs	Wood charcoal	−25.8	1170	25	86.39	0.23	776–941 CE	772–972 CE	990–1180
UTB	48209	HI6698-STP1, 105–120 cmbs	Wood charcoal	−25.9	1540	25	82.5	0.22	441–580 CE	435–595 CE	1370–1530
UTB	48210	HI6698-STP2, 20–30 cmbs	Wood charcoal	−25.1	1660	25	81.33	0.21	365–427 CE	261–531 CE	1520–1690
UTB	48211	HI6698-STP2, 60–70 cmbs	Wood charcoal	−24.9	1760	25	80.3	0.22	247–337 CE	236–375 CE	1570–1740
UTB	54625	HI6698-STP3, 40–50 cmbs	Wood charcoal	−24.45	1250	20	85.59	0.24	688–820 CE	677–873 CE	1077–1273
UTB	51581	HI6698-TU1, 30–40 cmbs	Wood charcoal	−25.58	1700	20	80.87	0.21	265–404 CE	258–413 CE	1655–1535
UTB	51580	HI6698-TU1, 50–60 cmbs	Wood chacoal	−24.96	1690	20	81.02	0.21	268–410 CE	261–416 CE	1689–1535
UTB	51579	HI6698-TU1, 70–80 cmbs	Wood charcoal	−26.25	1800	20	79.92	0.21	231–318 CE	215–326 CE	1736–1623
UTB	53234	HI6698-PC2, 46 cmbs	Charcoal	−26.18	1490	20	83.04	0.23	569–601 CE	549–638 CE	1312–1401
UTB	53235	HI6698-PC2, 73 cmbs	Charcoal	−22.3	3100	30	67.96	0.24	1417–1306 BCE	1434–1278 BCE	3228–3384
UTB	56570	HI6698-PC1, 35 cmbs	Charcoal	−25.99	1380	20	84.24	0.23	646–662 CE	608–670 CE	1342–1280
UTB	56573	HI996-TU1, 44–54 cmbs	Charcoal	−24.13	860	20	89.89	0.24	1175–1219 CE	1158–1228 CE	792–722
UTB	56574	HI996-TU1, 54–64 cmbs	Charcoal	−26.23	880	20	89.59	0.25	1164–1211 CE	1053–1220 CE	897–730
UTB	56575	HI996-TU1, 64–72 cmbs	Charcoal	−23.2	920	20	89.18	0.24	1047–1164 CE	1040–1198 CE	910–752
UTB	56571	HI996-STP4, 20–30 cmbs	Charcoal	−24.37	1120	20	87	0.23	893–977 CE	889–989 CE	1061–961
UTB	56572	HI996-STP4, 50–60 cmbs	Charcoal	−25.99	1720	20	80.72	0.21	259–380 CE	254–406 CE	1696–1544
UTB	56576	HI996-STP2, 50–60 cmbs	Charcoal	−25.51	1400	20	84.03	0.23	610–658 CE	605–662 CE	1345–1288
UTB	56577	HI996-PC6, 29 cmbs	Charcoal	−26.67	890	20	89.52	0.23	1158–1212 CE	1048–1220 CE	902–730
CRB	51104	CRB-VC4, 90 cmbs	Macrobotanical	−26.1	1500	20	82.97	0.2	564–597 CE	545–634 CE	1405–1316
CRB	51105	CRB-VC4, 337 cmbs	Organic sediment	−23.4	27,960	80	3.08	0.03	30,000–29,783 BCE	30,161–29,672 BCE	32,111–31,622
CRB	55327	CRB-VC5, 152 cmbs	Macrobotanical	−24.88	2790	25	70.68	0.21	983–904 BCE	1010–842 BCE	2960–2792
CRB	51106	CRB-VC5, 175 cmbs	Macrobotanical	−25.5	3370	20	65.73	0.17	1687–1621 BCE	1741–1549 BCE	3691–3499
CRB	51107	CRB-VC5, 450 cmbs	Organic sediment	−25	20,350	60	7.94	0.06	22,606–22,354 BCE	22,697–22,261 BCE	24,647–24,211
CRB	57207	CRB-VC6, 120 cmbs	Macrobotanical	−12.56	760	30	90.92	0.3	1231–1281 CE	1222–1285 CE	728–665
CRB	57208	CRB-VC6, 135 cmbs	Charcoal	−26.33	2630	30	72.08	0.29	813–790 BCE	888–774 BCE	2838–2724
CRB	55328	CRB-VC6, 160 cmbs	Macrobotanical	−26.86	2650	20	71.85	0.2	817–799 BCE	891–791 BCE	2841–2741
CRB	51108	CRB-VC6, 220 cmbs	Macrobotanical	−25.9	2730	20	71.14	0.18	898–833 BCE	914–820 BCE	2864–2770
CRB	57209	CRB-PC6, 96 cmbs	Macrobotanical	−26.67	220	25	97.3	0.3	1648–1799 CE	1642–1930 CE	308–146
CRB	55329	CRB-PC7, 124 cmbs	Macrobotanical	−26.14	1180	20	86.34	0.24	775–887 CE	774–944 CE	1176–1006
CRB	57206	HI2-PC5, 87 cmbs	Charcoal	−25.24	3830	25	62.09	0.19	2339–2205 BCE	2450–2151 BCE	4400–4100
CRB	53222	HI2-PC2, 111 cmbs	Charcoal	−18.74	2480	30	73.42	0.24	756–543 BCE	772–476 BCE	2722–2426
CRB	53223	HI2-PC3, 102 cmbs	Macrobotanical	−25.86	670	20	92.05	0.25	1286–1381 CE	1280–1389 CE	670–561
CRB	52446	HI2-STP1, 30–40 cmbs	Wood charcoal	−24.99	1560	20	82.38	0.22	438–556 CE	433–566 CE	1517–1384
CRB	52447	HI2-STP1, 50–60 cmbs	Deer tooth	−14.14	1410	25	83.89	0.25	607–655 CE	601–660 CE	1349–1290
CRB	52448	HI2-STP1, 60–70 cmbs	Wood charcoal	−26.8	1660	20	81.29	0.22	382–423 CE	262–528 CE	1688–1422
CRB	52449	HI2-STP1, 80–90 cmbs	Wood charcoal	−25.44	1730	20	80.66	0.22	256–375 CE	250–404 CE	1700–1546
CRB	52450	HI2-STP1, 130–140 cmbs	Wood charcoal	−24.76	1800	20	79.93	0.22	231–318 CE	215–326 CE	1735–1624
CRB	48216	HI2-STP2, 60–68 cmbs	Deer humerus	−21.7	1250	25	85.61	0.22	687–821 CE	675–876 CE	1275–1074
CRB	55463	HI2-STP2, 80–90 cmbs	Wood charcoal	−26.05	1500	20	82.93	0.23	564–597 CE	545–634 CE	1405–1317
CRB	48217	HI2-STP2, 115–125 cmbs	Carya nutshell	−24.7	1590	25	82.08	0.22	433–536 CE	420–545 CE	1530–1311
CRB	48218	HI2-STP2, 155–165 cmbs	Wood charcoal	−26.4	1510	25	82.81	0.22	552–594 CE	481–639 CE	1469–1311
CRB	52451	HI2-STP3, 40–50 cmbs	Wood charcoal	−25.43	1440	20	83.57	0.23	605–642 CE	594–650 CE	1356–1300
CRB	52452	HI2-STP3, 80–90 cmbs	Wood charcoal	−25.81	1440	20	83.57	0.23	605–642 CE	594–650 CE	1356–1300
CRB	53435	HI2-STP4, 20–30 cmbs	Wood charcoal	−25.74	1640	20	81.56	0.23	405–530 CE	381–535 CE	1692–1415
CRB	53436	HI2-STP4, 60–70 cmbs	Wood charcoal	−26.39	1700	20	80.87	0.23	265–404 CE	258–413 CE	1692–1545
CRB	53437	HI2-STP4, 100–110 cmbs	Wood charcoal	−24.83	1730	25	80.66	0.24	255–378 CE	250–405 CE	1700–1545
CRB	53438	HI2-STP4, 130–140 cmbs	Wood charcoal	−25.95	1930	20	78.66	0.22	66–125 CE	25–203 CE	1925–1747
CRB	52453	HI2-STP5, 67–78 cmbs	Wood charcoal	−25.7	1410	20	83.95	0.23	609–654 CE	605–657 CE	1345–1293
CRB	52454	HI2-STP5, 98–108 cmbs	Wood charcoal	−25.33	1500	20	82.97	0.23	564–597 CE	545–634 CE	1405–1316
CRB	52455	HI2-STP5, 138–148 cmbs	Wood charcoal	−18.08	2030	20	77.67	0.22	46–8 BCE	93 BCE–58 CE	2043–1892

Table 4A. *(continued)*.

Study Area	Lab Identification (UGAMS#)	Provenience	Material	^{13}C, 0/00	^{14}C BP	±	Percent Modern Carbon	±	68.2% Probability	95.4% Probability	Cal. YBP (2-sigma)
CRB	53439	HI2-STP6, 20–30 cmbs	Wood charcoal	−25.95	1490	20	83.11	0.23	569–601 CE	549–638 CE	1401–1312
CRB	53440	HI2-STP6, 40–50 cmbs	Wood charcoal	−25.03	1270	20	85.39	0.24	685–743 CE	670–789 CE	1280–1152
CRB	53442	HI2-STP6, 90–100 cmbs	Wood charcoal	−25.81	1470	20	83.31	0.23	580–638 CE	569–643 CE	1381–1307
CRB	52456	HI2-STP7, 0–10 cmbs	Wood charcoal	−27.69	220	20	97.24	0.26	1650–1798 CE	1644–1940 CE	306–10
CRB	52458	HI2-STP7, 50–60 cmbs	Wood charcoal	−25.36	1380	20	84.24	0.23	646–662 CE	608–670 CE	1342–1280
CRB	52460	HI2-STP7, 80–90 cmbs	Wood charcoal	−24.75	1930	20	78.61	0.22	66–125 CE	25–203 CE	1925–1747
CRB	53431	HI2-MC1, str. 4	Wood charcoal	−25.45	1340	20	84.58	0.24	655–675 CE	650–773 CE	1300–1177
CRB	53448	HI2-MC1, str. 11	Wood charcoal	−25.42	3060	30	68.29	0.27	1389–1274 BCE	1412–1227 BCE	3362–3177
CRB	53432	HI2-MC1, str. 13	Wood charcoal	−26.11	1530	20	82.66	0.23	541–580 CE	440–599 CE	1510–1351
CRB	53433	HI2-MC1, str. 16b	Wood charcoal	−26.08	1450	20	83.46	0.23	602–641 CE	583–649 CE	1367–1301
CRB	53434	HI2-MC1, str. 20	Wood charcoal	−26.43	1690	20	81	0.23	268–410 CE	261–416 CE	1689–1534
CRB	53424	HI2-MC2, str. 6	Wood charcoal	−27.13	1320	20	84.79	0.24	661–772 CE	656–775 CE	1294–1175
CRB	53425	HI2-MC2, str. 10	Wood charcoal	−26.33	1400	20	83.96	0.23	610–658 CE	605–662 CE	1345–1288
CRB	53426	HI2-MC2, str. 12	Wood charcoal	−25.33	1350	30	84.48	0.28	648–758 CE	641–775 CE	1309–1175
CRB	53427	HI2-MC2, str. 17	Wood charcoal	−26.18	1510	20	82.81	0.21	556–591 CE	541–604 CE	1409–1346
CRB	53428	HI2-MC2, str. 19	Wood charcoal	−26.81	1580	20	82.09	0.23	435–541 CE	429–546 CE	1521–1404
CRB	53429	HI2-MC2, str. 22	Wood charcoal	−24.32	1380	25	84.22	0.24	646–662 CE	608–670 CE	1342–1280
CRB	53430	HI2-MC2, str. 24	Wood charcoal	−24.06	2930	30	69.46	0.24	1201–1056 BCE	1222–1016 BCE	3172–2966
WI	51438	WI-VC2, 161 cmbs	Macrobotanical	−26.09	4010	25	60.67	0.18	2569–2475 BCE	2575–2469 BCE	4525–4419
WI	55331	WI-VC4, 112 cmbs	Organic sediment	−18.96	1820	20	79.75	0.22	211–246 CE	133–323 CE	1627–1817
WI	51436	WI-VC4, 155 cmbs	Macrobotanical	−25.65	3870	25	61.77	0.18	2451–2291 BCE	2461–2210 BCE	4411–4160
WI	51437	WI-VC4, 227 cmbs	Macrobotanical	−26.87	4280	25	58.71	0.17	2907–2889 BCE	2920–2879 BCE	4870–4829
WI	51434	WI-PC1, 85 cmbs	Macrobotanical	−24.71	190	20	97.65	0.26	1664–1950 CE	1660–1950 CE	290–0
WI	51435	WI-PC1, 110 cmbs	Macrobotanical	−25.71	1220	20	85.87	0.23	774–874 CE	706–883 CE	1244–1067
WI	48206	PI56-STP1, 40–50 cmbs	UID long bone	−20.3	2290	25	75.24	0.2	399–266 BCE	403–230 BCE	2360–1720
WI	51433	PI56-STP1, 40–50 cmbs	Wood charcoal	−24.11	2410	20	74.07	0.2	513–410 BCE	717–404 BCE	2667–2354
WI	48207	PI56-STP5, 30–40 cmbs	Mammal long bone	−19.3	1580	25	82.11	0.22	435–541 CE	423–550 CE	1540–1400
WI	51432	PI56-STP7, 60–70 cmbs	Wood charcoal	−25.68	2110	20	76.92	0.22	165–59 BCE	193–50 BCE	2144–2000
WI	51428	PI11491-STP2, 10–20 cmbs	Wood charcoal	−23.73	590	20	92.93	0.25	1323–1399 CE	1307–1407 CE	643–544
WI	51429	PI11491-STP2, 30–40 cmbs	Wood charcoal	−26.46	650	20	92.2	0.24	1296–1387 CE	1287–1392 CE	663–559
WI	51430	PI11491-STP3, 20–30 cmbs	Wood charcoal	−25.77	750	20	91.12	0.25	1265–1281 CE	1229–1287 CE	722–664
WI	51431	PI11491-STP3, 30–40 cmbs	Carya sp. hull	−18.57	610	20	92.66	0.25	1307–1396 CE	1302–1400 CE	648–552
BH	53228	BH-VC2, 262 cmbs	Organic sediment	−18.8	4130	25	59.79	0.18	2856–2630 BCE	2869–2582 BCE	4819–4532
BH	53229	BH-VC2, 330 cmbs	Organic sediment	−19.61	4620	25	56.27	0.17	3493–3362 BCE	3508–3351 BCE	5458–5301
BH	53230	BH-VC3, 182 cmbs	Organic sediment	−20.56	3980	25	60.92	0.18	2563–2468 BEC	2574–2459 BCE	4524–4409
BH	53231	BH-VC4, 112 cmbs	Macrobotanical	−27	4120	25	59.9	0.18	2850–2626 BCE	2866–2578 BCE	4816–4528
BH	53232	BH-VC5, 80 cmbs	Macrobotanical	−25.59	2230	20	75.77	0.21	365–209 BCE	381–203 BCE	2331–2153
BH	53233	BH-VC6, 135 cmbs	Organic sediment	−21.45	790	20	90.62	0.24	1228–1268 CE	1222–1273 CE	728–677
BH	53224	MA15-PC1, 78 cmbs	Macrobotanical	−26	340	20	95.79	0.25	1497–1631 CE	1479–1635 CE	471–315
BH	53225	MA15-PC2, 96 cmbs	Macrobotanical	−26.9	260	20	96.85	0.26	1638–1660 CE	1527–1795 CE	423–155
BH	53226	MA15-PC2, 130 cmbs	Charcoal	−26.37	2180	30	76.19	0.25	352–174 BCE	364–120 BCE	2314–2070
BH	53227	MA15-PC3, 120 cmbs	Charcoal	−23.58	2090	25	77.11	0.23	149–51 BCE	174–1 BCE	2124–1951
BH	52467	MA15-STP1, 10–20 cmbs	Wood charcoal	−25.24	2110	20	76.91	0.21	165–59 BCE	193–50 BCE	2143–2000
BH	53973	MA15-STP1, 70–80 cmbs	Wood charcoal	−26.1	2010	25	77.84	0.24	43 BCE–25 CE	51 BCE–77 CE	2001–1873
BH	53974	MA15-STP2, 60–70 cmbs	Wood charcoal	−23.06	230	20	97.2	0.27	1650–1795 CE	1640–1800 CE	310–140
BH	53975	MA15-STP3, 70–80 cmbs	Wood charcoal	−24.6	190	20	97.7	0.27	1665–1940 CE	1659–1925 CE	291–25
BH	52468	MA13-STP7, 0–10 cmbs	Wood charcoal	−26.01	1570	20	82.29	0.23	436–547 CE	431–556 CE	1519–1394
BH	52469	MA13-STP7, 20–30 cmbs	Deer bone collagen	−20.42	1680	20	81.12	0.22	365–415 CE	262–420 CE	1688–1530
BH	52470	MA13-STP7, 30–40 cmbs	*Carya* nutshell	−26.75	1660	20	81.3	0.23	382–423 CE	262–528 CE	1688–1432
BH	53977	MA13-STP7, 50–60 cmbs	Wood charcoal	−26.94	1750	20	80.41	0.23	250–345 CE	242–375 CE	1708–1575
BH	53978	MA13-STP7, 70–80 cmbs	Wood charcoal	−25.24	2010	20	77.89	0.22	41 BCE–23 CE	BCE 47–62 CE	1997–1888
BH	53979	MA13-STP7, 80–90 cmbs	Wood charcoal	−23.02	1850	20	79.41	0.22	134–236 CE	129–238 CE	1821–1712
BH	54624	MA15-STP8, 10–20 cmbs	Wood charcoal	−24.76	1560	20	82.36	0.23	438–556 CE	433–566 CE	1517–1384
BH	52466	MA15-STP8, 20–30 cmbs	Deer bone collagen	−20.61	1540	20	82.51	0.22	481–575 CE	436–595 CE	1514–1355
BH	53976	MA15-STP8, 70–80 cmbs	Wood charcoal	−24.1	1920	25	78.75	0.23	67–201 CE	29–207 CE	1921–1743
BH	53962	MA13-MC1, str. 5	Wood charcoal	−23.49	1980	25	78.1	0.24	28 BCE–76 CE	41 BCE–118 CE	1991–1832
BH	53963	MA13-MC1, str. 7	Wood charcoal	−25.86	1910	25	78.84	0.23	81–203 CE	61–213 CE	1889–1737
BH	53964	MA13-MC1, str. 21	Wood charcoal	−23.01	1810	25	79.87	0.23	215–311 CE	164–332 CE	1786–1618
BH	53965	MA13-MC2, str. 4	Wood charcoal	−25.47	1720	25	80.76	0.23	258–383 CE	251–410 CE	1699–1540
BH	53966	MA13-MC2, str. 5	Wood charcoal	−24.64	1770	25	80.18	0.24	244–329 CE	231–361 CE	1719–1589
BH	53967	MA13-MC2, str. 14	Wood charcoal	−17.64	1900	25	78.98	0.23	89–204 CE	70–215 CE	1880–1735
BH	53968	MA13-MC2, str. 17	Wood charcoal	−23.51	1760	20	80.28	0.23	247–337 CE	236–375 CE	1714–1575
BH	53969	MA13-MC2, str. 25	Wood charcoal	−23.24	13,310	100	19.08	0.24	14,210–13,896 BCE	14,352–13,763 BCE	16,302–15,713
BH	53970	MA13-MC2, str. 36	Wood charcoal	−26.37	2270	25	75.34	0.22	392–234 BCE	397–209 BCE	2347–2159
BH	53971	MA13-MC2, str. 41	Wood charcoal	−25.24	1980	25	78.13	0.23	125–203 CE	80–225 CE	1870–1725
BH	53972	MA13-MC2, str. 44	Wood charcoal	−26.31	2090	25	77.12	0.22	149–51 BCE	175–1 BCE	2125–1951

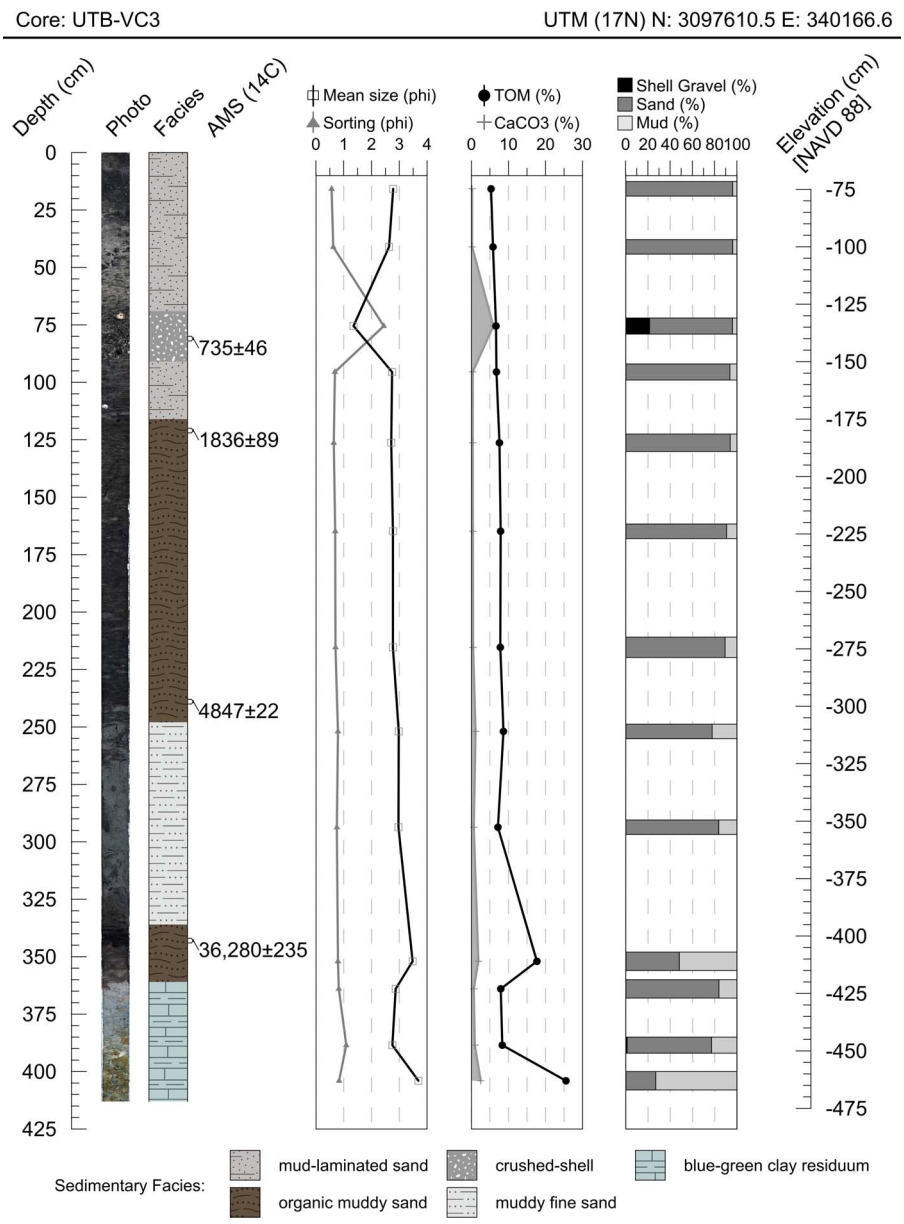

Figure 1A. Core log for UTB-VC3.

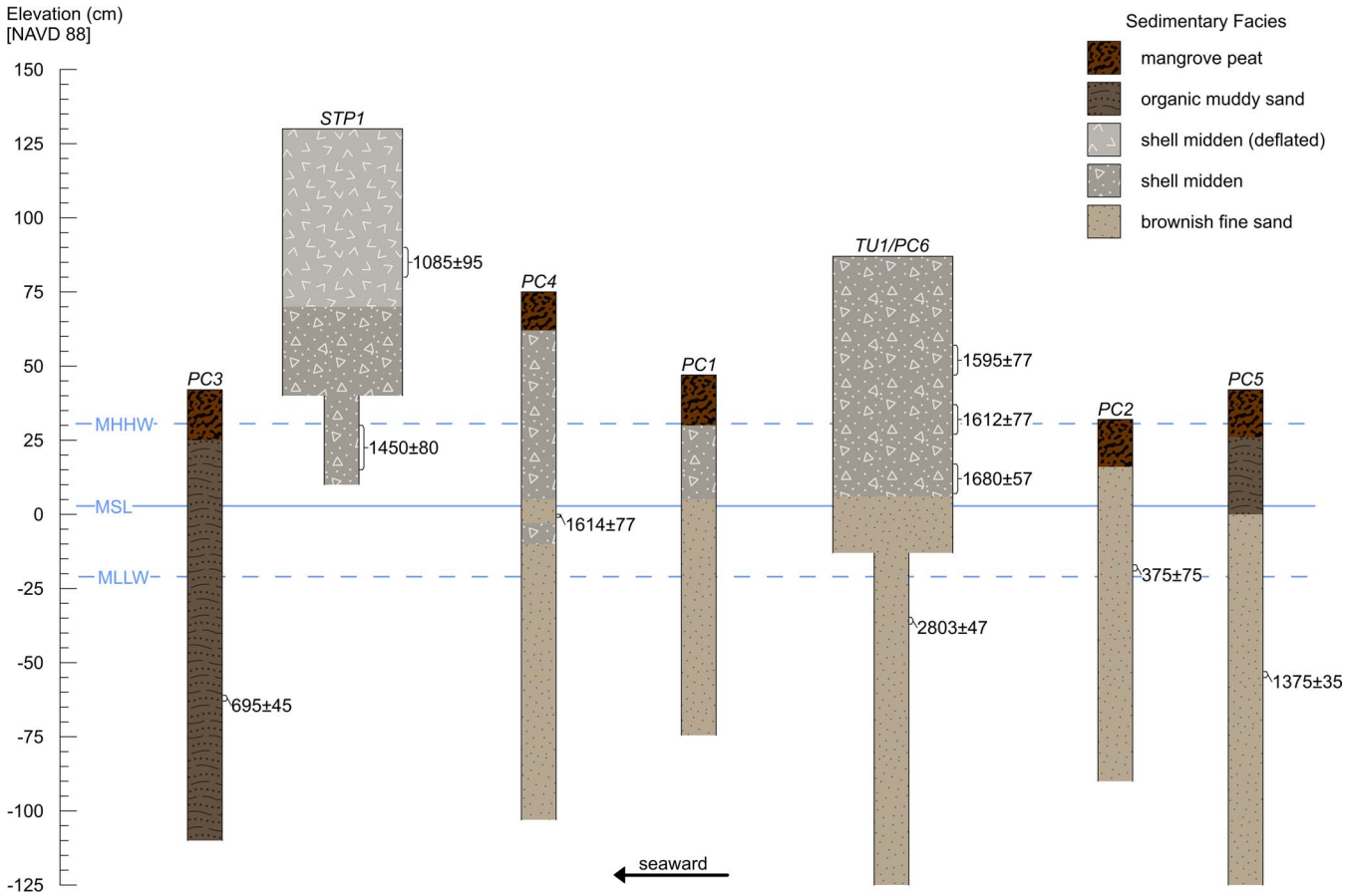

Figure 2A. Cross-sectional stratigraphic diagram of Cabbagehead Bayou site (8HI6698), Upper Tampa Bay. Radiocarbon dates are reported in calibrated years BP (cal YPB) with 2-sigma error ranges. Tidal elevation data are from Mobbly Bayou tide gauge (station identification 8726769).

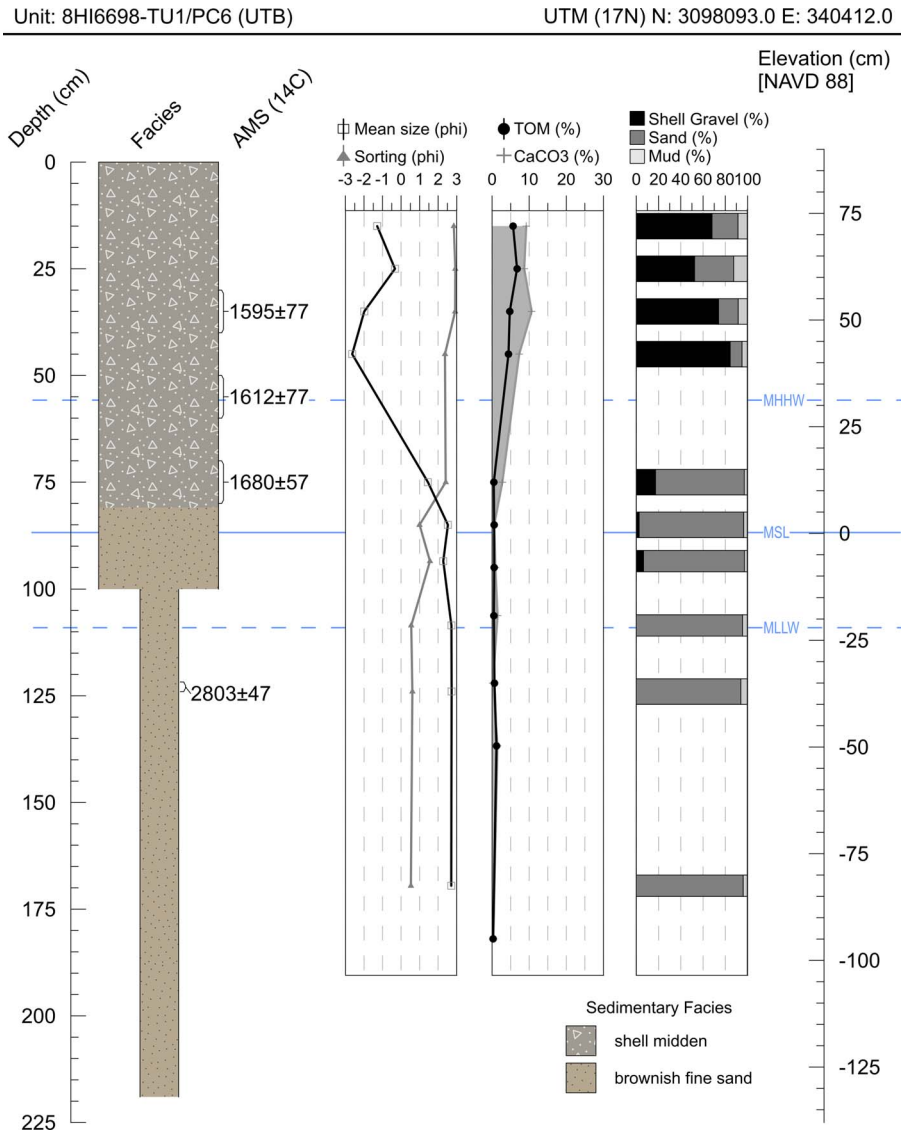

Figure 3A. Unit-log and physical sedimentary data for 8HI6698-TU1/PC6 (UTB) demonstrating the strong contrast between antecedent dune landforms and overlying late-Holocene shell middens at Upper Tampa Bay.

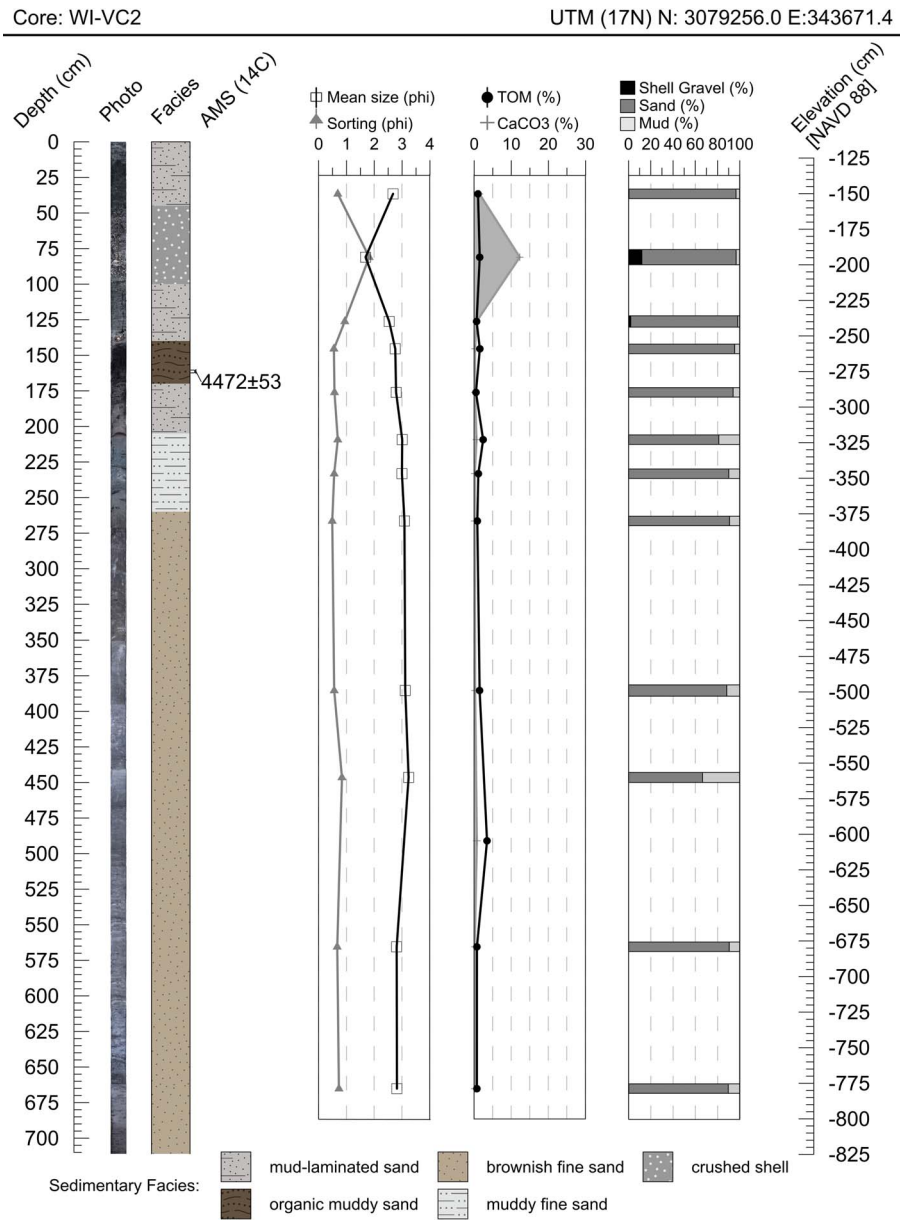

Figure 4A. Core log for WI-VC2.

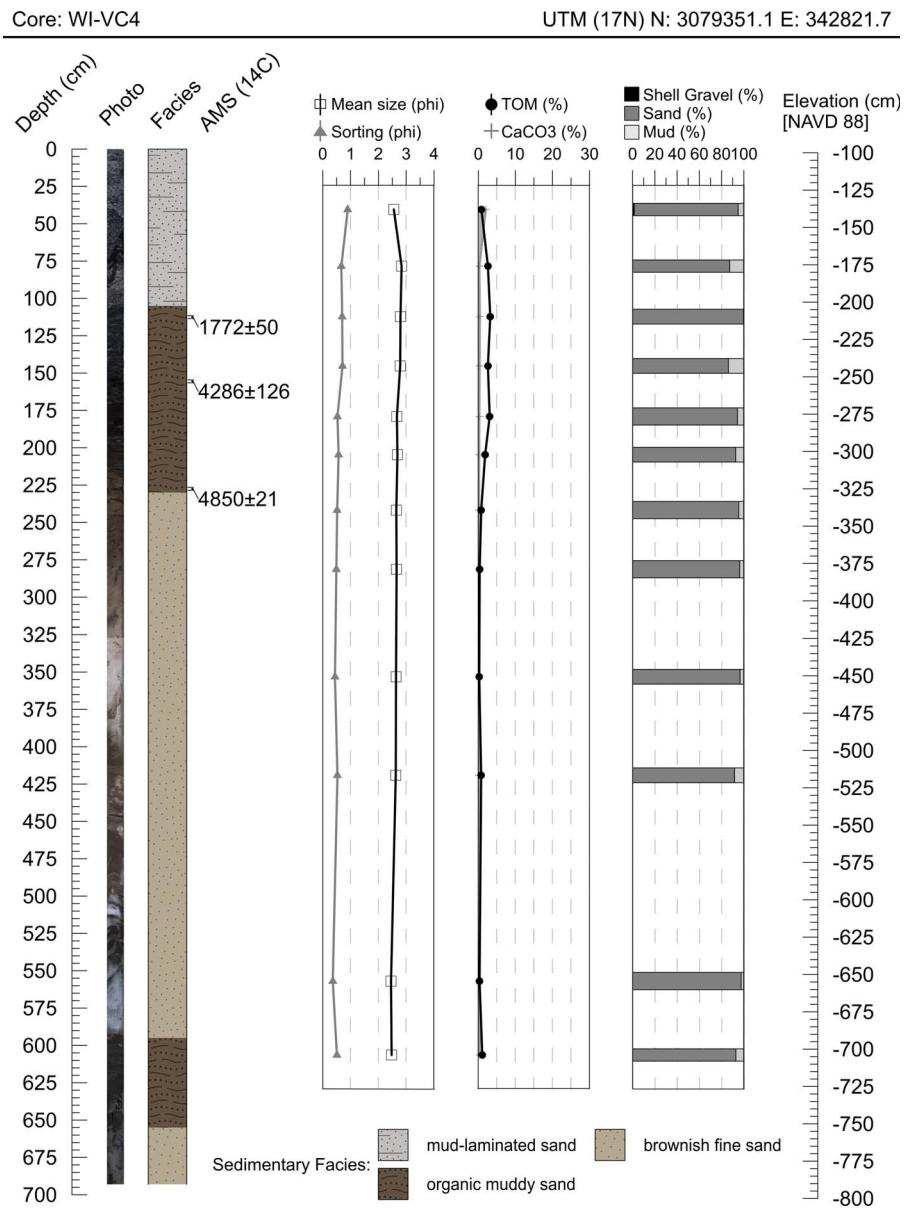

Figure 5A. Core log for WI-VC4.

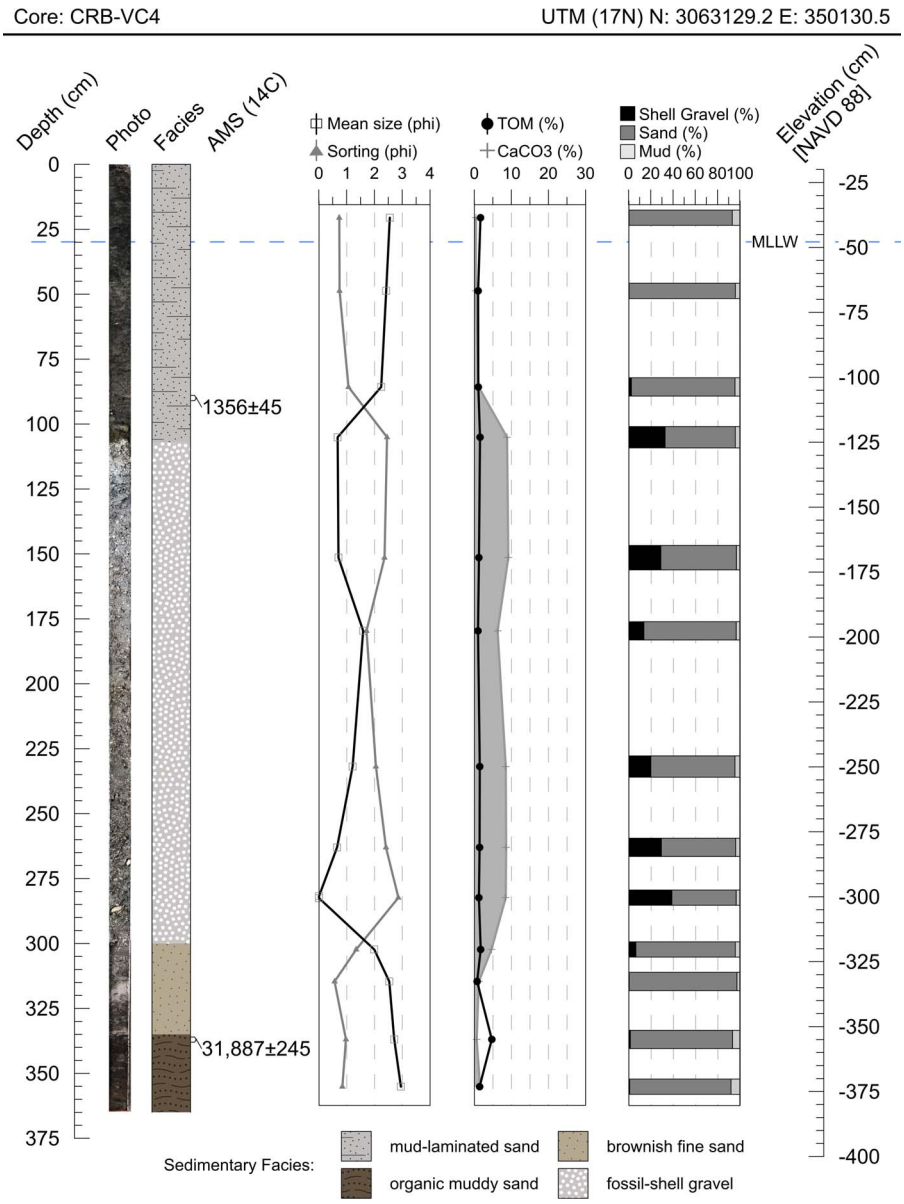

Figure 6A. Core log for CRB-VC4.

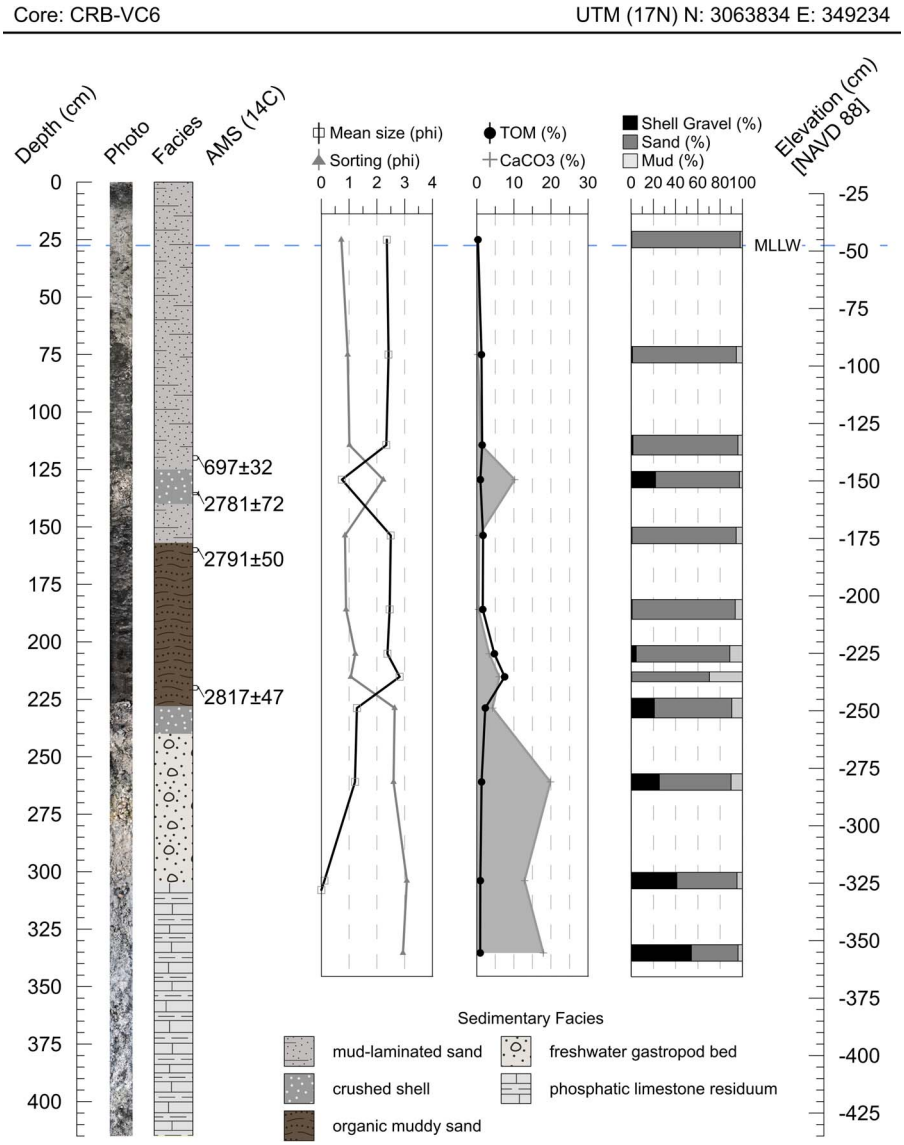

Figure 7A. Core log for CRB-VC6.

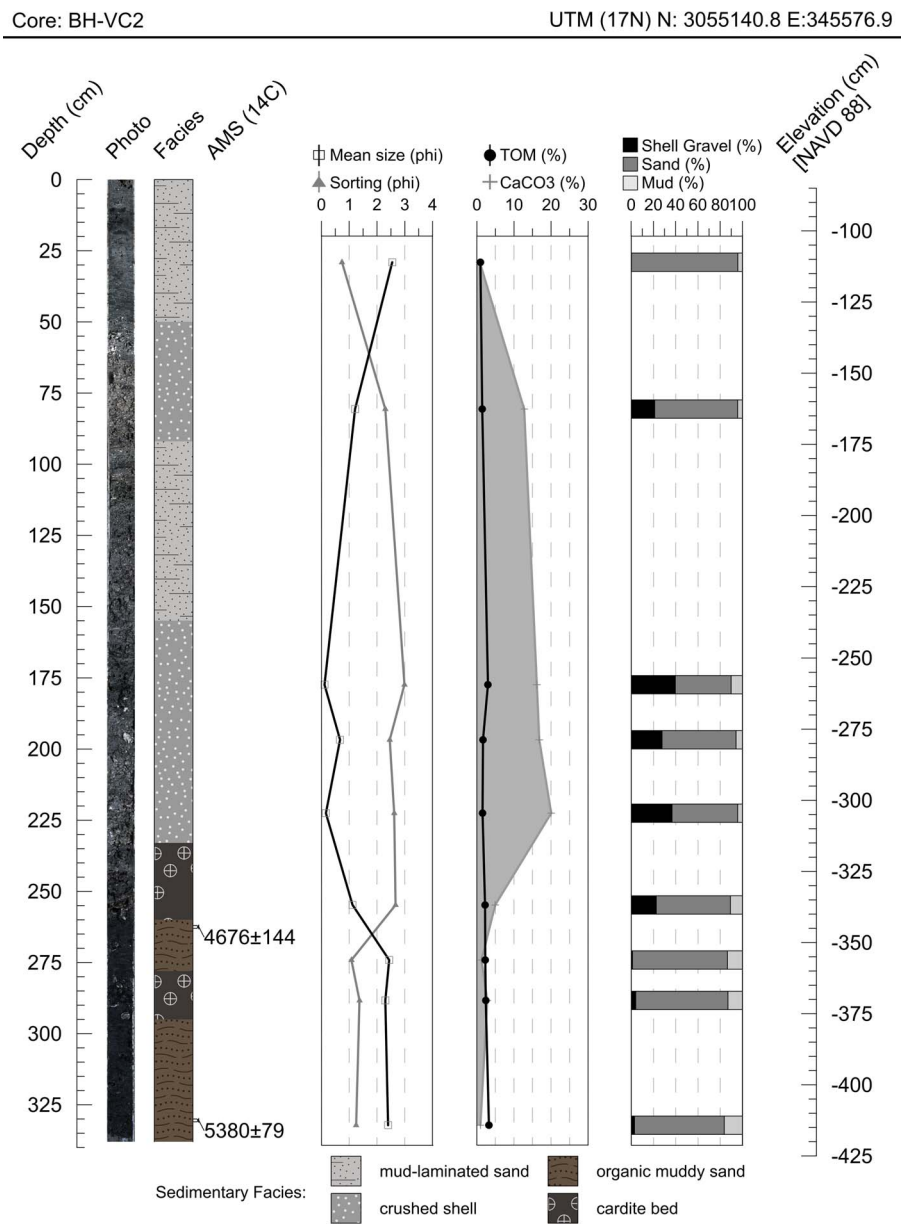

Figure 8A. Core log for BH-VC2.

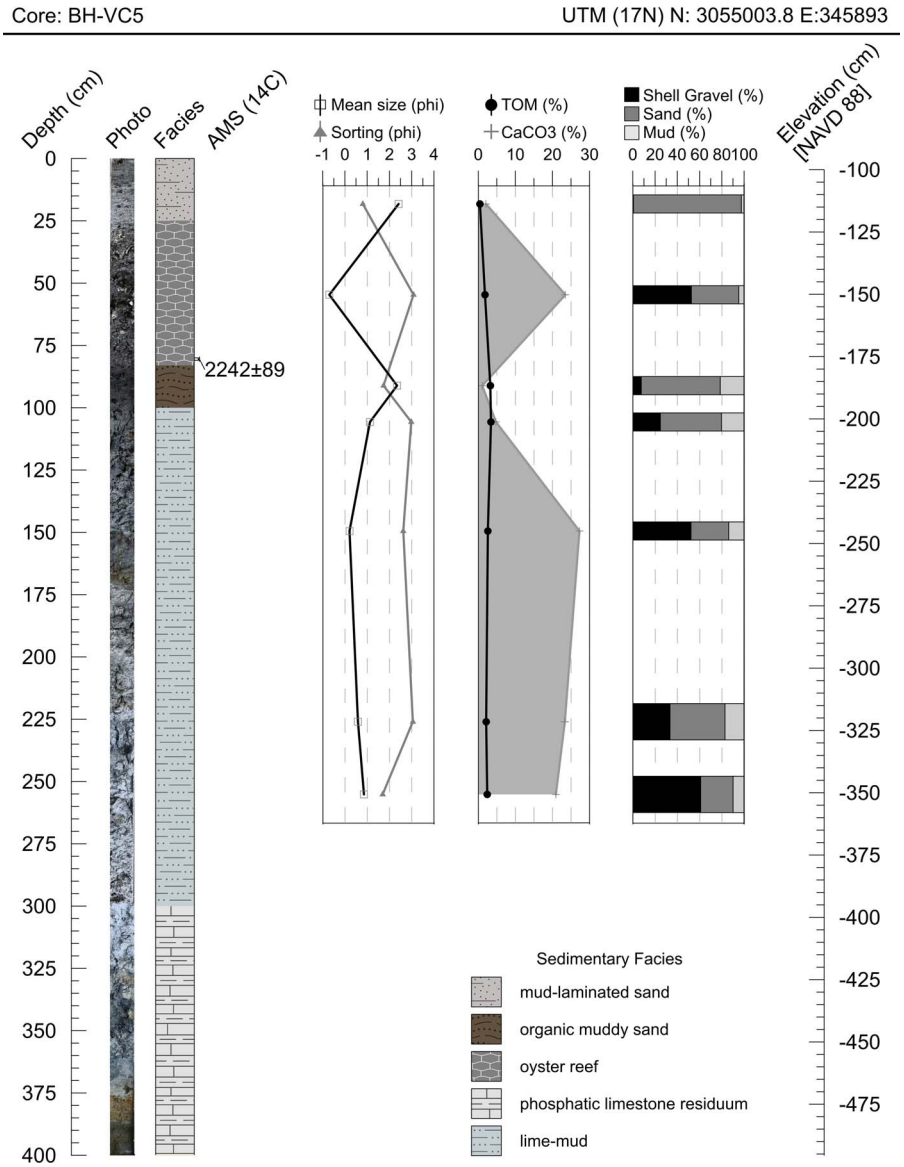

Figure 9A. Core log for BH-VC5.